

Directed Self-Assembly of Tethered Membranes on Nanoparticles

by

Alexander Lee Kelly

A dissertation submitted to the Graduate Faculty of
Auburn University
in partial fulfillment of the
requirements for the Degree of
Doctor of Philosophy

Auburn, Alabama
May 5, 2018

Keywords: Tethered Lipid Bilayers, Nanoparticles, Drug Delivery, Silica

Copyright 2018 by Alexander Lee Kelly

Approved by

Allan E. David, Co-Chair, Assistant Professor of Chemical Engineering
Robert D. Arnold, Co-Chair, Associate Professor of Drug Discovery and Development
Maria Auad, Professor of Chemical Engineering
Elizabeth Lipke, Associate Professor of Chemical Engineering

Abstract

Nanoparticles have demonstrated success in overcoming many barriers of therapeutic delivery. The advantages of these systems include increased drug loading, an ability to package poorly soluble and/or highly toxic drugs, and enhanced biodistribution compared to free drug. However, current nanoparticle-based therapeutics are hampered by low circulation half-life, burst release of drug and/or leakage, and off-target toxicity. A new class of nanocarriers attempts to address these issues by combining the advantages of two traditional systems: inorganic nanoparticles and liposomes. Nanoparticles enveloped in a lipid bilayer combine the monodisperse, pH and thermally stable, and inherent tracking capabilities of inorganic nanoparticles with the biocompatibility, long circulating half-life, and ability to deliver hydrophilic and hydrophobic molecules associated with liposomes. Anchoring the lipid bilayer into the nanoparticle surface further enhances these carriers by increasing membrane compatibility, stability and provides a sub-membrane space for therapeutic loading.

This dissertation involves a detailed discussion on the design and self-assembly of tethered membrane nanoparticles (TMN) and their application within the field of drug delivery. TMN were comprised of a silica nanoparticle core to which lipopolymers were functionalized. The lipopolymers were composed of a polyethylene glycol (PEG) polymer chain and phosphatidylethanolamine lipid. These exterior facing, anchored lipids directed the self-assembly of a lipid bilayer onto the nanoparticle surface with liposomes serving as

the extraneous lipid source. By comparing the lipid concentration, hydrodynamic diameter and zeta potential, the amount of lipid needed to produce a stable, tethered bilayer membrane on the surface of a silica nanoparticle was determined to be a factor of 5:1 with regard to surface area of lipid to surface area of nanoparticle. Use of zwitterionic lipids reduced dependence on electrostatic interactions and membrane assembly formed via hydrophobic interactions and van der Waals attraction forces. Transmission electron microscopy images confirmed the presence of a supported lipid bilayer composed of three separate lipid formulations and encapsulation of 5(6)-carboxyfluorescein indicated a 15-20% release of dye over the course of 6 days depending on bilayer intactness.

Where possible, TMN were compared with the two traditional nanocarriers they were comprised of: silica nanoparticles and liposomes. Stability of each particle type was assessed in serum with TMN exhibiting greater stability over PEGylated silica. Macrophage uptake was used to examine the effect of lipid bilayer composition on expected circulation half-life. A PEGylated exterior was found to reduce TMN uptake by a factor of 13 – indicating the significant role a PEGylated exterior membrane can impart. Finally, TMN and liposomes loaded with doxorubicin were incubated with PC-3 prostate cancer cells. TMN exhibited similar toxicity to liposomal doxorubicin, demonstrating capability of the model system as a drug delivery paradigm.

Next generation delivery vehicles have already begun utilizing cell membrane coats as a way to evade host defense mechanisms, such as the mononuclear phagocyte system, and to increase circulation residence times. However, these systems are currently limited by their simplistic fusion of the membrane onto nanoparticle surfaces. This significantly reduces the array of membranes that can be properly incorporated due to surface

interactions of the interior leaflet. The tethering technique developed herein provides an opportunity to enhance membrane environment recapitulation towards production of biomimetic drug carriers.

This work advances current capabilities of supported membranes on colloidal systems and paves the way for further investigation into the fundamentals controlling bilayer assembly upon tethered nanoparticle cores. The versatility of the developed system is the hallmark of this research, and provides a platform from which to tailor nanoparticle properties for specific disease states, drug loading or release profiles, and unique shapes or porosities. Application of the developed model system has shown efficacy in drug loading and the treatment of prostate cancer. The simplicity in modification of the current platform and the significant potential of tailorable attributes hold promise for the future generation of targeted, biomimetic nanoparticle-based therapies.

Acknowledgements

I would like to thank Dr. Allan E. David and Dr. Robert D. Arnold for their support and guidance throughout the course of this work and my graduate studies. I would like to thank my committee members, Dr. Maria Auad and Dr. Elizabeth Lipke for their knowledge and time in the critical review and preparation of this dissertation. I would also like to thank Dr. Christopher Easley for undertaking the role as the outsider reader for my dissertation. I would like to thank current and past members of the David Lab that include: Dr. Youngsuk Choi, Xin Fan, Prachi Sangle, Richard Cullum, Alan Hanley, Tareq Anani, Barry Yeh, Chelsea Harris, Marjan Azadi, Hunter Rogers, Ricky Whitener, Nayer Sultana and Braden Hahn. Additionally, I would like to thank the members of the Arnold Group: Ben Nie, Matthew Eggert and Lani Jasper for their assistance with many aspects of this work. I would also like to thank the undergrads I had a chance to work with and for the opportunity to mentor: Kyle Paul, Patrick Harris, Gregory Carnes and Robert Price.

I would like to thank Dr. Michael Miller for his help with the transmission electron microscope, Allison Church Bird for her help with the flow cytometer, and Dr. Virginia Davis for use of ATR FT-IR and TGA. Personal gratitude is also extended to Dr. Mario Eden, Dr. Robert Ashurst, Dr. Steve Duke and Dr. Jeffrey Fergus for their guidance unrelated to research. I would also like to thank Karen Cochran, Elaine Jimmerson, Jennifer Harris and Georgetta Dennis for their help in various matters over the years.

I would also like to thank Pranav Vengsarkar, Steven Montgomery, Alexander Haywood, Kyle Stone, Will Hand, Matthew Hilliard, Morgan Ellis and Amanda Gross for being an invaluable support system. There were countless others who made my time at Auburn memorable and I would like to thank them as well for their friendship.

Finally, this work would not have been possible without the continued support from my family. Thank you to my parents, Mary Ann and Thomas J. Kelly, for supporting me throughout my academic career and always encouraging me to be my best. I would like to thank my siblings Kyle Kelly, James, Christina, and Mary Larsen for always trying to understand my research and being as proud of my accomplishments as they are of their own. Thank you to my mother-in-law, Amy Larsen, for her constant support. And finally, I would like to acknowledge and thank my wife, Dr. Jessica Kelly, for her love and support throughout this endeavor.

Table of Contents

Abstract.....	ii
Acknowledgements.....	v
Table of Contents.....	vii
List of Figures.....	x
List of Tables.....	xiii
List of Abbreviations.....	xiv
Chapter 1: Introduction.....	1
1.1 Introduction to Nanotechnology.....	1
1.2 Nanoparticles in Drug Delivery.....	1
1.3 Supported Membranes on Nanoparticles.....	3
1.4 Summary of Chapters.....	5
Chapter 2: Background.....	6
2.1 Production of Silica Nanoparticles.....	6
2.1.1 Sol-gel Synthesis of Silica Nanoparticles.....	8
2.1.2 Theories of Silica Nanoparticle Formation.....	9
2.2 Liposomes.....	11
2.2.1 Phospholipids.....	12
2.2.2 Liposome Classification.....	15
2.2.3 Polymorphic Structure of Liposomes.....	16
2.2.4 Hydrophobic Assembly.....	17
2.3 Supported Lipid Bilayers.....	22
2.3.1 Types of Supported Lipid Bilayers.....	23
2.3.2 Techniques for Supported Bilayer Membrane Formation.....	26
2.3.3 Factors Affecting Supported Bilayer Membrane Formation on Colloidal Particles.....	27

2.3.4 Supported Bilayer Membranes on Nanoparticles for Drug Delivery	32
2.3.5 Commonly Employed Characterization Methods.....	46
Chapter 3: Formation and Characterization of Tethered Bilayer Membranes on Nanoparticles	49
3.1 Introduction.....	49
3.2 Materials and methods	52
3.1 Materials	52
3.2 Surface modification of silica nanoparticles.....	53
3.3 Liposome preparation	54
3.4 Supported lipid bilayer preparation	54
3.5 Nanoparticle sizing	55
3.6 Fourier transform infrared spectroscopy.....	55
3.7 Quantification of reactive surface amine groups	55
3.8 Silica assay.....	56
3.9 Membrane permeability assay	57
3.10 Statistical analysis.....	57
3.3 Results and discussion	58
3.3.1 Physical properties of silica particles, DSPC vesicles and composites	58
3.3.2 DSPC adsorption on silica particles.....	64
3.3.3 Effect of adsorption on hydrodynamic diameter and zeta potential	72
3.3.4 Membrane permeability assessment	78
3.4 Conclusion	81
Chapter 4: Application of Tethered Bilayer Membrane Nanoparticles in the Treatment of Prostate Cancer	83
4.1 Introduction.....	83
4.2 Materials and Methods.....	85
4.2.1 Materials	85
4.2.2 Cell lines	86
4.2.3 Liposome preparation	87
4.2.4 Preparation of doxorubicin liposomes	87
4.2.5 Preparation of doxorubicin composite.....	88

4.2.6 Serum stability	89
4.2.7 Cell staining and fluorescent microscopy	89
4.2.8 Flow cytometry	89
4.2.9 Measurement of MTT staining	90
4.3 Results and Discussion	91
4.3.1 Stability study in serum	91
4.3.2 Effects of composite surface character on macrophage cell uptake	95
4.3.3 Loading of doxorubicin.....	100
4.3.4 In Vitro evaluation of tBLM nanoparticles with PC-3 cells	102
4.4 Conclusions.....	105
Chapter 5: Cytotoxicity of PEG Coated Silica Nanoparticles	106
5.4.1 Silica Nanoparticle Impact on Cell Viability.....	106
5.4.2 Correlating Nanoparticle Uptake with Viability.....	117
Chapter 6: Future Directions.....	110
Chapter 7: Summary and Significance	135
References.....	141
Appendix 1: Silica Particle Production.....	164
3.2.1 Effects of Reagent Concentrations on Size.....	165
3.2.2 Surface Modification	170

List of Figures

Figure 1. Mesoporous (left) and solid (right) silica nanoparticles with common drug delivery modifications.	7
Figure 2. Diagram of a unilamellar liposome and common drug delivery modifications.	11
Figure 3. Phospholipid structure.	13
Figure 4. Liposome size and lamellarity classification.	16
Figure 5. The three most commonly studied types of supported bilayers (left) water, (middle) polymer, and (right) polymer tethered.	23
Figure 6. ATR-FTIR spectra of pure silica nanoparticles, pure PEG ₂₀₀₀ , pure DSPE-PEG ₂₀₀₀ -NHS, PEGylated silica nanoparticles, DSPE-PEG coated silica nanoparticles.	63
Figure 7. Adsorption of DSPC lipid onto aminated, PEGylated and DSPE-PEG2k coated silica particles.	68
Figure 8. Surface morphology of aminated (A), PEGylated (B) and composite (C) nanoparticles visualized with TEM and effect of increased exposure to the electron beam on nanoparticle supported lipid bilayer degradation.	69
Figure 9. Effect of sonication time on amount of PC molecules adsorbed to the nanoparticles for DSPE-PEG2k-Si, PEG2k-Si and NH ₂ -Si (n = 3).	70
Figure 10. Effect of temperature on PC adsorbed with increasing concentration of PC in solution (n = 3).	72
Figure 11. Increasing A_V/A_P ratio leads to a reduction in TMN size (A), decrease in polydispersity (B) and shift of zeta potential towards neutral (C). Error bars represent standard deviation of three separate experiments.	75
Figure 12. Increasing sonication time affects hydrodynamic diameter (A and B), polydispersity (C) and zeta potential of each particle type: liposomes (brown), tethered membrane nanoparticles (blue), amine coated silica (green) and PEG coated silica (yellow). Error bars represent standard deviation of three separate experiments.	78

Figure 13. Release profiles of carboxyfluorescein for DSPC liposomes and TMN produced at different A_V/A_P ratios (connecting lines drawn to guide the reader's eye).	79
Figure 14. Isolated release profiles of carboxyfluorescein from tethered membrane nanoparticles with A_V/A_P ratios of 5:1 and 15:1.	81
Figure 15. Hydrodynamic diameters of DSPC coated TMN with different lipid concentrations incubated in 10% FBS supplemented F12-K media for 8 days. PEG2k coated particles and DSPC liposomes shown as controls.	94
Figure 16. Polydispersity index values of DSPC coated TMN with different lipid concentrations incubated in 10% FBS supplemented F12-K media for 8 days. PEG2k coated particles and DSPC liposomes shown as controls.	95
Figure 17. Dot plot of composite nanoparticle uptake with Raw 264.7 macrophage cells. Particles were coated with DSPC (left) and SSL (right) lipid formulations. Particles were incubated at three concentrations: control (green), 0.001 mg/mL silica (orange), 0.01 mg/mL (blue) and 0.1 mg/mL (red).	97
Figure 18. Median fluorescence intensities of DiD labeled composite nanoparticles and DiD labeled liposomes.	99
Figure 19. Median fluorescence intensities of FITC labeled composite nanoparticles and FITC labeled amine and PEG coated silica particles.	99
Figure 20. Nanoparticle and nanoparticle toxicity papers published over past twenty five years (ISI Web of Science).	107
Figure 21. Surface coverings assessed in toxicity and uptake analysis.	108
Figure 22. Hydrodynamic diameter assessment of PEGylated and aminated silica particles in 10% FBS supplemented F-12K culture medium (connecting lines drawn to guide the reader's eye).	115
Figure 23. Viability profiles of 60 nm silica nanoparticles incubated with CHO cells for 72 hours.	116
Figure 24. Viability profiles of 120 nm silica nanoparticles incubated with CHO cells for 72 hours.	116
Figure 25. Fluorescence microscopy of control CHO cells (top left), cells incubated with PEGylated particles (bottom left) and aminated particles (bottom right) for 24 hours.	117
Figure 26. Mean fluorescence intensity of CHO cells after incubation with Rhodamine B labeled particles.	119

Figure 27. ROS generation in CHO cells with increasing concentration of aminated silica particles: (A) control no DCFDA, (B) control with DCFDA, (C) 0.1, (D) 0.3, (E) 1.0, (F) 3 mg/mL silica.....	120
Figure 28. Median fluorescence intensity of 120 nm silica particles with differing surface characteristics.	122
Figure 29. Effect of ammonium hydroxide concentration on particle size.....	166
Figure 30. Effect of water concentration on particle size.	167
Figure 31. Example of polydispersity obtained while varying water concentration (4 M) and holding NH ₄ OH and TEOS concentration constant (0.5 M).....	168
Figure 32. Effect of TEOS concentration on particle size.	170

List of Tables

Table 1. Abbreviations and phase transition temperatures of commonly used phospholipids. ⁴⁶	14
Table 2. Polymorphic phases, molecular shapes, and molecular packing parameter of phospholipids. Adapted from ref ⁴⁶ and ⁵²	22
Table 3. Intensity-averaged hydrodynamic diameters (HD) and ζ -potential (ZP) values of silica nanoparticles in acetate buffer and PBS, PEG layer thickness, grafting density and conformation of PEG2k and DSPE-PEG2k coated particles.	61
Table 4. Diffusional exponents, n , fitting parameters, k and diffusion mechanisms for non-swellable controlled release systems.	80
Table 5. Intensity-averaged hydrodynamic diameters (HD) and ζ -potential (ZP) values of silica nanoparticles in acetate buffer and PBS, Ham's F-12K basal media stability analysis, PEG layer thickness, grafting density and conformation of PEGylated particles.....	113
Table 6. IC ₅₀ values determined for 60 and 120 nm silica nanoparticles incubated with CHO cells for 72 hours.	116
Table 7. Average size and statistical figures for lab made and purchased silica.	169

List of Abbreviations

AFM	Atomic force microscopy
A_p	Surface area of particles
APTES	(3-aminopropyl)triethoxysilane
ATR-FTIR	Attenuated total reflectance Fourier transform infrared
A_v	Surface area of vesicles
CF	Carboxyfluorescein
CHO	Chinese hamster ovary
CMC	Critical micelle concentration
CTAB	Cetyl trimethylammonium bromide
DCFDA	Dichlorofluorescein
DiD	1,1'-dioctadecyl-3,3,3',3'-tetramethylindodicarbocyanine, 4-chlorobenzenesulfonate salt
DLS	Dynamic light scattering
DLVO	Derjaguin-Landau-Verwey-Overbeek
DMEM	Dulbecco's Modified Eagles Medium
DMPA	1,2-dimyristoyl-sn-glycero-3-phosphate (sodium salt)
DMPC	1,2-dimyristoyl-sn-glycero-3-phosphocholine
DMSO	Dimethyl sulfoxide
DOPC	1,2-Dioleoyl-sn-glycero-3-phosphocholine

DOPS	1,2-dioleoyl-sn-glycero-3-phospho-L-serine
DOTAP	1,2-dioleoyl-3-trimethylammonium-propane
DOX	Doxorubicin
DPPC	1,2-dipalmitoyl-sn-glycero-3-phosphocholine
DSC	Dynamic scanning calorimetry
DSPC	1,2-distearoyl-sn-glycero-3-phosphocholine
DSPE-PEG	1,2-distearoyl-sn-glycero-3-phosphoethanolamine-N-[methoxy(polyethylene glycol)-2000]
EDC	1-Ethyl-3-(3-dimethylaminopropyl)carbodiimide
EPR	Enhanced permeability and retention
FBS	Fetal bovine serum
FDA	Food and Drug Administration
FITC	Fluorescein isothiocyanate
FTIR	Fourier transform infrared spectroscopy
GRAS	Generally recognized as safe
GUV	Giant unilamellar vesicles
HBSS	Hank's balanced salt solution
HCl	Hydrochloric acid
HD	Hydrodynamic diameter
HEPES	4-(2-hydroxyethyl)-1-piperazineethanesulfonic
HUVEC	Human umbilical vein endothelial cells
ITC	Isothermal titration calorimetry
LUV	Large unilamellar vesicles

MFI	Median fluorescence intensity
MLV	Multilamellar vesicles
m-PEG-NHS	Methoxy polyethylene glycol NHS
MRI	Magnetic resonance imaging
MSN	Mesoporous silica nanoparticles
MTT	Thiazoyl blue tetrazolium bromide
MVV	Multivesiclular vesicles
NaOH	Sodium hydroxide
NHS	N-hydroxysuccinimide
PDI	Polydispersity index
PEG	Polyethylene glycol
PLA	Poly(lactic acid)
PLGA	Poly(lactic-co-glycolic acid)
QCM-D	Quartz crystal microbalances with dissipation
RES	Reticuloendothelial system
ROS	Reactive oxygen species
siRNA	Small interfering ribonucleic acid
SLB	Supported lipid bilayer
SUV	Small unilamellar vesicles
tBLM	Tethered bilayer membrane
TEM	Transmission electron microscopy
TEOS	Tetraethyl orthosilicate
TMN	Tethered membrane nanoparticles

tSLB	Tethered supported lipid bilayer
ULV	Unilamellar vesicles
ZP	Zeta potential

Chapter 1: Introduction

1.1 Introduction to Nanotechnology

Nanotechnology is the engineering of functional materials with at least one dimension in the range of 1 to 100 nm, with 1 nm equating to 10^{-9} m.¹ This nanoscale encompasses items that range from elements to bulk materials. In addition, nanotechnology involves the study of the formation of two and three dimensional assemblies of molecular scale building blocks into well-defined nanostructures or nanomaterials.² This control of the fundamental molecular structure of a material yields control of the macroscopic physical and chemical properties of the bulk material.³ Research and application of nanotechnology has gained significant popularity in recent years with the advent of new manufacturing technologies and characterization techniques. Nanotechnology as a science encompasses a variety of fields including applications in energy⁴, catalysis⁵ and medicine^{6,7}.

1.2 Nanoparticles in Drug Delivery

Nanoparticles have been sought after for their unique physical properties that include high surface area-to-volume ratios, quantum properties and their ability to adsorb and carry other compounds. Within the medical field, these properties can be combined to produce drug delivery vehicles. Composition of these vehicles can be of biological origin (e.g., phospholipids, lipids, dextran, chitosan) or more chemical in nature such as polymers (e.g., poly(lactic-co-glycolic acid), polyethylene glycol), metals or silica.⁸

Drug delivery vehicles are comprised of at least two components where one is the active pharmaceutical ingredient and the other augments and facilitates transport/delivery. In general, the primary goals of nanotechnology within drug delivery include (1) increasing specificity of drug targeting, (2) reducing toxicity and improving solubility, (3) increasing safety and biocompatibility, and (4) constant rate therapeutic delivery.^{8,9} Although nanoparticles provide many advantageous properties within drug delivery systems, there are still primary design challenges associated with engineering these carriers. These challenges include (a) drug incorporation and release, (b) formulation stability and circulation half-life, (c) biocompatibility, (d) biodistribution and targeting, and (e) functionality.⁸

The challenges of engineering these carriers are addressed via one of two methods: a “top down” approach where smaller scale details are incorporated within a macroscopic material or a “bottom up” approach where molecular structures are designed and synthesized to produce self-assembling macroscopic materials.³ The top down approach is commonly used within the semiconductor industry through photolithography. This leads to the production of a macroscale material that has had nanostructured functionality added. The bottom up approach utilizes nanostructure building blocks to assemble a final structure. Within the realm of nanoparticles designed for drug delivery, a bottom up approach is typically pursued. Here, nano-sized starting blocks such as phospholipids or molecular species are incorporated to produce a structure capable of delivering therapeutics.

Self-assembly is a large component of the bottom up approach. Self-assembly is defined as “a process in which supramolecular hierarchical organization is established in a

complex system of interlocking components.”¹⁰ This process is composed of competing molecular interactions that include hydrophobic interactions, van der Waals forces, hydrogen bonding and electrostatic interactions. These interactions have been harnessed for the synthesis of solid nanoparticles, assembly of lipid bilayers and the synergism of these two systems towards the production of an enhanced drug delivery vehicle.

1.3 Supported Membranes on Nanoparticles

The application of nanomaterials in medicine first showed great success in the treatment of cancer. One of the reasons for this success was through the manipulation of multiple targeting strategies nanoparticles offer scientists. The first generation of targeting took advantage of the enhanced permeability and retention (EPR) effect to preferentially localize the nanoparticles (and thus the therapeutics) to tumor sites. This passive targeting strategy was later enhanced via the attachment of ligands to the surface of particles that specifically bind to target cells. This active targeting strategy opened the door for nanoparticle delivery to disease states where the EPR effect does not exist.¹¹

One of the challenges of nanoparticle drug delivery remains opsonization and clearance. Many strategies have been explored to overcome this barrier but none has been as successful as the attachment of polymeric materials to the exterior of nanomaterials. This attachment led to greater residence times and biodistribution *in vivo*. Originally, it was believed that this additional polymer layer prevented protein adsorption (a host response) but recently was found to only alter the makeup of the protein corona adsorbed. This understanding has led to attempts at predicting the kinds of protein coronas that form on nanoparticle surfaces upon injection and even utilizing this knowledge to direct delivery.¹²

These targeting strategies represent a broader trend in the field of drug delivery (and others, including tissue engineering, implantable devices, etc.) of attempting to mimic the *in vivo* environment. Supported membranes on nanoparticles represents the next step in this broader, growing trend of taking cues from nature to develop better delivery systems. Revisiting the attachment of polymers to nanomaterial surfaces, Schlenoff¹³ has described a similar (albeit shortsighted) trend as “zwitteration.” Zwitteration refers to the attachment of species that reduce or prevent nonspecific adsorption *in vitro* or *in vivo*. Often, zwitteration is carried out by the attachment of polysaccharides, polymers (PEG), acrylamides and lipid monolayers or bilayers.¹³ These materials all have similar properties in that they are usually neutral or weakly negative in charge and well hydrated. The general idea is to mimic the properties of cellular membranes. Cellular membranes were found to be rich in zwitterion head groups, such as phosphatidylcholine, with the balance made up of neutral and anionic phospholipids.^{14,15} Most of these zwitterionic phospholipids were found to reside on the external leaflet of the lipid bilayer. This unique observation is one that can have dramatic impact on drug delivery systems. For example, a wide variety of synthetic phospholipids are available today. This variety permits investigation of various formulations to produce the most desirable nanoparticle/liposomal delivery system. However, some phospholipids have been found to yield unique results *in vivo*, such as phosphatidylserine. Phosphatidylserine produces an apoptotic “eat me” signal when expressed from a cell.¹⁶ Thus, the inclusion of this lipid within a drug delivery system could lead to deleterious effects. This example highlights the importance in utilizing biological understanding in combination with materials and engineering to develop advanced drug delivery platforms.

Encapsulation of nanoparticles within a membrane bilayer is being investigated as a means to combine the advantages of traditional drug delivery systems as well as address their drawbacks. The solid nanoparticle core provides stability and morphology to the construct, while the membrane bilayer provides biomimetic properties. These biomimetic properties have been shown to enhance stability of the base colloidal particles, prevent nonspecific adsorption to cancer cells and enhance pharmacokinetics and targeting *in vivo*.¹⁷⁻¹⁹ These reports demonstrate the advantages of bilayer membranes on nanoparticles in their most simple configuration and sets the stage for the investigation of tethered bilayer membranes upon nanoparticles.

1.4 Summary of Chapters

The following chapters focus on two primary areas related to tethered bilayer membranes on nanoparticles: a) process development and b) application. Chapter 2 introduces the background knowledge of nanoparticle self-assembly, nanomaterial characteristics and supported lipid bilayers necessary to fully understand the TMN constructed. The development of an experimental method to produce tethered bilayer membranes on nanoparticles is described and characterized extensively within Chapter 3. To our knowledge, this represents the first experimental approach in producing TMN. Chapter 4 focuses on the application of the TMN as a drug delivery vehicle. This application includes characterization of these particles within an *in vitro* environment, the effect of varying surface characteristics on nanoparticle clearance and comparison to liposomal carriers in the delivery of a chemotherapeutic to PC-3 prostate cancer cells. The effect of nanoparticle toxicity is explored in Chapter 5 and future directions of the TMN are developed in Chapter 6.

Chapter 2: Background

2.1 Production of Silica Nanoparticles

Silica nanoparticles have been studied widely as therapeutic delivery vehicles because of their biocompatibility as well as their chemical and thermal stability. In addition, silica nanoparticles have excellent optical properties, very tight size distributions and controllable porosity. Silica nanoparticles can be classified as either porous or nonporous. There have been many studies on the use of both types of particles for drug delivery applications.²⁰ Many of the silica nanoparticle properties can be tailored based off of selection and control of the synthesis technique utilized for manufacture. The diagram in **Figure 1** shows the two types of silica nanoparticles used in drug delivery and some typical modifications.

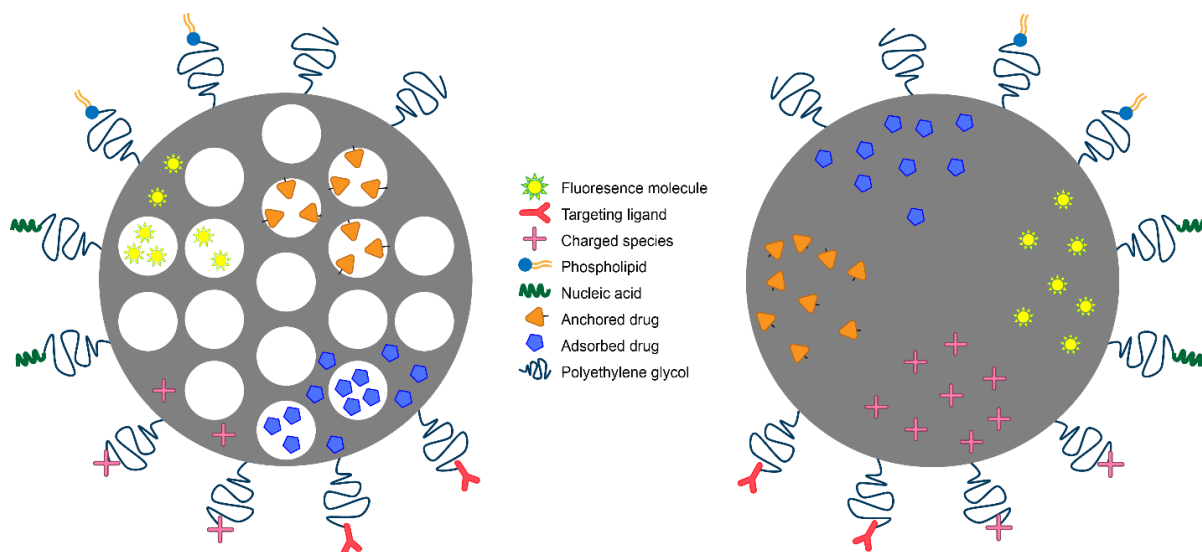


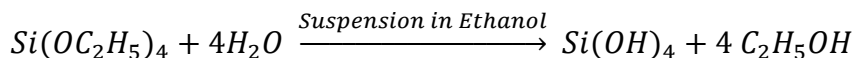
Figure 1. Mesoporous (left) and solid (right) silica nanoparticles with common drug delivery modifications.

Silica nanoparticles can be produced via flame synthesis, chemical vapor deposition, and sol-gel methods.²¹ The sol-gel method can be further subdivided into microemulsion and solution systems. Microemulsion methods utilize surfactant-mediated conditions to control the diffusion rate of reagents into the micron-sized micelle batch reactors. Microemulsion techniques add complexity to the reaction conditions and require further processing steps to remove the surfactants from the final products.²² Solution systems are single, simple mixtures of reagents without additional surfactants. They are a uniform phase of the four commonly used reagents for silica sol-gel production: alkoxysilanes such as tetraethyl orthosilicate (TEOS), a short chained alcohol (e.g., methanol or ethanol), water and an acid/base catalyst. Modulation of these reagents in solution have been found to influence size of the resulting particles.²³

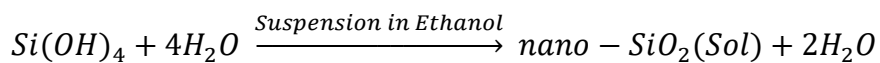
2.1.1 Sol-gel Synthesis of Silica Nanoparticles

The sol-gel method is the most commonly used technique for making nanoparticles for drug delivery applications. Sol-gel processing is a chemical synthesis approach utilizing chemical precursors that form into nanoparticle sols and are arrested before going on to form monolithic gels. It was made famous when Stöber demonstrated production of silica nanoparticles with controlled size in 1968.²⁴ This led to the term “Stöber method” being coined to describe sol-gel synthesis of silica particles. Since then, it has been studied widely, however, an exact understanding of the mechanisms at hand elude development of hard and fast rules of production.²⁰ Nevertheless, general reaction mechanisms are well known and these include the hydrolysis of the alkoxysilanes (TEOS) and the polycondensation of silanol groups to form siloxane bonds (Si-O-Si) that make up the nanoparticles.

Hydrolysis of TOES:



Polycondensation of Si(OH)₄:



In general, the reactions can be acid or base catalyzed. Base catalyzed reactions produce nanoparticles that are considered “Stöber” particles and are stable against transitioning into the gel phase.²⁵ At pH values below 2, condensation of polydisperse higher-order polymer/particles leads to gelation. Base catalysis promotes crosslinking and yields branched polymers which forms mesoporous particles. Whereas, acid catalysis promotes hydrolysis and end-chain condensation which produces microporous gels.²⁶

Additionally, porous particles can be achieved via the introduction of an amphiphilic molecule during reaction such as cetyl trimethylammonium bromide (CTAB).²⁷⁻²⁹

The sol-gel process can be simply described as a colloid with respect to nanoparticle production. A colloid is a suspension in which the suspended phase is dominated by short range forces such as van der Waals and electrostatic interactions and the forces of gravity are considered negligible. Upon mixing, the reagents in solution undergo nucleation following the LaMer theory.³⁰ This leads to the production of very small silica nanoparticles dispersed throughout the solution. A sol is simply a colloidal suspension of nanometer sized particles in a solvent.²⁵ The steps after nucleation are a little less clear with two models proposed: monomer addition and controlled aggregation.

2.1.2 Theories of Silica Nanoparticle Formation

Initially, it was believed that the sol-gel production of silica nanoparticles behaved more like a polymerization reaction after initial nucleation. Under this polymerization theory, silica precursor in the form of TEOS behaves like a monomer that becomes hydrolyzed and is then added to the growing chain via a condensation reaction.²⁵ This monomer addition would continue until the sink of monomer was used up and the resulting solution would be a colloidal suspension of silica nanoparticles. In addition, Ostwald ripening was used to explain the consumption of smaller particles by larger particles, producing more uniform size distributions.³¹

More recently, utilizing state of the art characterization techniques such as cryogenic electron microscopy, the controlled aggregation theory has been formed that perhaps better explains some of the morphological characteristics commonly associated with silica particles including their pores.³¹ This theory suggests that upon addition of silica

precursor to the solution, nucleation occurs as previously believed, producing approximately 2 nm sized “primary” particles. These primary particles go on to associate and aggregate, forming assemblies around the size of 5.1 nm. Upon association, the primary particles compress and are reduced in size to around 1.3 nm. The associated particles (5.1 nm in size) continue to grow with the addition of primary particles until the sink of primary particles is depleted. The sink of primary particles is depleted once the sink of TEOS has been exhausted.

This more recent observation in combination with gas adsorption analysis is believed to have led to a more coherent understanding of where the pores within these particles are derived. As the primary particles continue to build onto the larger, growing particles, attachment of these two species prevents complete association. This incomplete attachment leaves void space between associated particles which produces pores. Processing after production can further enhance access to these pores. Washing steps that include water rather than alcohols can hydrolyze remaining alkoxy groups that would otherwise plug and clog surface access of the pores.^{31,32}

Produced silica nanoparticles are modified easily with more useful surface groups for drug delivery applications. This includes the attachment of surface amine groups via addition of alkoxy silane molecules that contain a primary amine such as (3-aminopropyl)triethoxysilane (APTES).³³ APTES takes advantage of the same base catalyzed hydrolysis and condensation reactions to form siloxane bonds on the surface of the particles. Amine surface coverage permits simple amide bond formation within neutral pH or organic conditions.³⁴ Functionalization of other species such as drug or polyethylene

glycol can be carried out via simple N-hydroxysuccinimide (NHS)/1-Ethyl-3-(3-dimethylaminopropyl)carbodiimide (EDC) chemistry.³⁵⁻³⁷

2.2 Liposomes

Liposomes were first discovered by Alec Bangham in 1964 while examining phospholipids under an electron microscope.³⁸ Since their discovery, liposomes have been highly studied as model biological membranes as well as drug delivery vehicles for both hydrophilic and lipophilic compounds. Liposomes are comprised of phospholipids that self-assemble into lipid bilayers. This self-assembly encapsulates an aqueous volume, providing a lipophilic region within the membrane bilayer and a hydrophilic region within the core of the vesicle. **Figure 2** shows a two-dimensional graphical representation of a liposome in an aqueous environment.

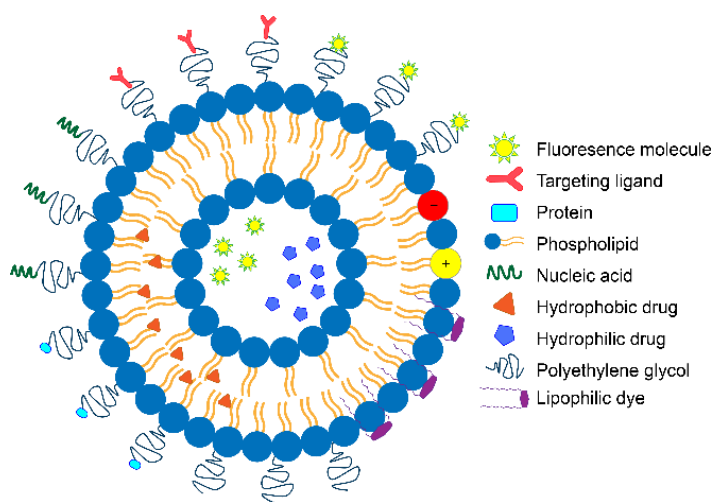


Figure 2. Diagram of a unilamellar liposome and common drug delivery modifications.

Liposomes provide a biocompatible and biodegradable platform that has yielded clinically approved drug formulations in the US and abroad. Doxil (1995), liposomal doxorubicin, was the first clinically approved liposomal formulation for use in treating

Kaposi's sarcoma.³⁹ There have been several other liposome-based drugs approved since Doxil with more in various stages of clinical trials.⁴⁰

2.2.1 Phospholipids

Phospholipids are the main components of cell membranes, allowing them to be found widely throughout animals and plants. Phospholipids are amphiphilic in nature, exhibiting both a hydrophilic head group and a hydrophobic or lipophilic tail. These distinct features are commonly linked via a glycerol backbone. **Figure 3** shows a diagram of a typical phospholipid. Their polar head groups can be zwitterionic, charged (both cationic and anionic), and/or non-charged polyhydroxylated moieties. These polyhydroxylated lipids maintain a polar head group via hydroxyl groups that can form hydrogen bonds with water.⁴¹

Phospholipids can have either one (lysophospholipid, monoglyceride) or two (diglyceride) fatty acid chains attached to the glycerol backbone. These fatty acid chains can range from eight to twenty-four carbons. In addition, they can be fully saturated or unsaturated with one to four double bonds. The most commonly found saturated fatty acids within natural membranes are myristic (C₁₄), palmitic (C₁₆) and stearic (C₁₈), while the most prominent unsaturated fatty acid is oleic acid (often believed to provide health benefits).^{41,42} Unsaturated fatty acids can have either cis or trans double bonds. The cis double bond can produce a bend of up to 30° and the trans configuration has a similar structure to that of saturated fatty acids.

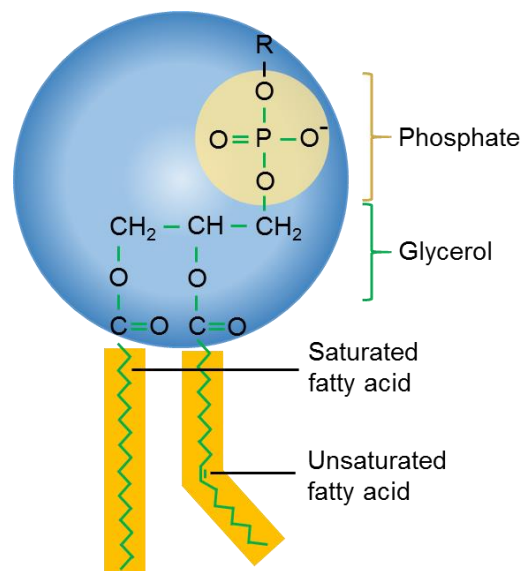


Figure 3. Phospholipid structure.

Phospholipids can be obtained from natural or synthetic origins. Natural phospholipids for production are often obtained from soybean and egg yolk sources, with notable differences in individual phospholipid yield with each source.⁴³ Typically, the cost of natural phospholipids increases with increased purity.⁴⁴ Natural phospholipids have a low inherent toxicity, are biologically inert and weakly immunogenic; however, parenteral and enteral administration requires chemically defined phospholipids for federal regulation reasons.^{43,45} Thus, synthetic phospholipids are often chosen for biomedical applications.

Phospholipids can be synthesized via semisynthetic and fully synthetic methods. Semisynthesis involves the changing of head and/or tail groups from a natural phospholipid precursor.⁴⁶ Total synthesis involves a complete formation from precursor molecules that often produces racemic mixtures that are known to have different physical properties (thermotropic) but have not shown any significant behavioral differences within liposomes.⁴¹ Available methods are able to completely chemically synthesize any

phospholipid; however, the reaction sequences can be quite complex and produce an end result that is rather expensive.⁴³ **Table 1** includes some of the commonly used phospholipids in drug delivery and their abbreviations.⁴⁶

Chemical stability of phospholipids is predominately linked to the fatty acid chain structure. Hydrolysis and oxidation are the most common degradation pathways for phospholipids. Oxidation is typically associated with unsaturated fatty acids, whereas hydrolysis can affect all phospholipids. Hydrolysis results in the breakage of a fatty acid from the glycerol backbone, ultimately leading to two individual fatty acid chains, a polar head group and a free glycerol. The rate of hydrolysis is much slower than that of oxidation and particularly slow at low temperatures while exhibiting a strong pH dependence.

Table 1. Abbreviations and phase transition temperatures (T_c) of commonly used phospholipids.⁴⁶

Phospholipid	Abbreviation	T_c (°C)
Soybean phosphatidylcholine	SPC	-20 to -30
Egg sphingomyelin	HSPC	52
Egg phosphatidylcholine	ESM	37
Dimyristoyl phosphatidylcholine	EPC	-5 to -15
Dipalmitoyl phosphatidylcholine	DMPC	23
Di-oleoyl phosphatidylcholine	DPPC	41
Distearoyl phosphatidylcholine	DOPC	-22
Dimyristoyl phosphatidylglycerol	DSPC	55
Dipalmitoyl phosphatidylglycerol	DMPG	23
Di-oleoyl phosphatidylglycerol	DPPG	41
Distearoyl phosphatidylglycerol	DOPG	-18
Dimyristoyl phosphatidylethanolamine	DSPG	55
Dipalmitoyl phosphatidylethanolamine	DMPE	50
Di-oleoyl phosphatidylethanolamine	DPPE	60
Distearoyl phosphoethanolamine	DOPE	-16
Dimyristoyl phosphatidylserine	DSPE	74
Dipalmitoyl phosphatidylserine	DMPS	38
Di-oleoyl phosphatidylserine	DPPS	51

Oxidation is a radical reaction which results in the breakage of chains or peroxide formation in the presence of adjacent double bonds. Oxidation is often caused by oxidants, sonication and free radicals. Sonication at low temperatures and within an inert environment can often prevent oxidation. Oxidation can also be prevented by forgoing the use of unsaturated lipids, storage within oxygen-free environments, at low temperatures, and shielded from light (photoionization). A yellow color is often observed in formulations containing amine groups in which oxidation has occurred.⁴¹

2.2.2 Liposome Classification

Liposomes are classified based on the number of bilayer membranes they encompass as well as their general size. Liposomes can be classified as multilamellar vesicles (MLV) when they contain more than one bilayer membrane and unilamellar vesicles (ULV) when they are composed of a single membrane. ULVs can be further delineated into small unilamellar vesicles (SUV), large unilamellar vesicles (LUV), and giant unilamellar vesicles (GUV). SUV are typically less than 100 nm while LUV are between 100 and 1000 nm in size. GUV are considered anything greater than 1000 nm. Multivesicular vesicles (MVV) are vesicles in which smaller vesicles are encapsulated.⁴⁷ **Figure 4** shows the common size and lamellarity classification system. Bilayer membrane size is highly dependent upon the state of the lipids but in general can be approximated to around 5 nm in width.⁴⁸

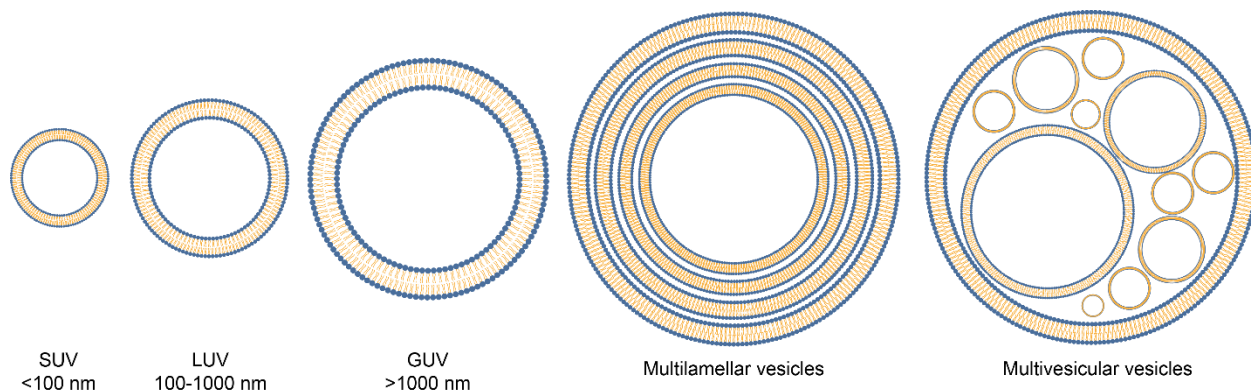


Figure 4. Liposome size and lamellarity classification.

2.2.3 Polymorphic Structure of Liposomes

Phospholipids are amphiphilic in nature, exhibiting both a hydrophilic head group and a hydrophobic or lipophilic tail. These structures self-assemble into lipid bilayers upon introduction to an aqueous environment. Properties of the formed lipid bilayers are functions of temperature, pressure, phospholipid structure, incorporated species (e.g., cholesterol) and buffer conditions.⁴¹ Membrane fluidity is a function of temperature, with the bilayer capable of maintaining three states: a gel phase ($L_{\beta'}$), a ripple phase ($P_{\beta'}$) and a liquid crystalline phase (L_{α}). The temperature at which this change occurs is termed the transition temperature which represents the median between a lipid bilayer gel phase and the fluid phase. In the liquid phase, the phospholipid tails are all disordered and in the gel phase they are all ordered and tilted. The ripple phase is characterized by a microphase separation of domains in which there exists portions of the bilayer that are thick (ordered lipids) and portions where the bilayer is thin (lipids disordered).⁴⁹ The ripple phase is typically associated with the pretransition of phospholipids.⁵⁰

Bilayers within the gel phase are considered solid and less permeable as a result of closely ordered side-to-side packing. This leads to both short-range order and long-range order. Within the liquid crystalline state, there is both long-range order and short-range disorder. These features are associated with the overall bilayer structure being conserved but with movement of the acyl chains. Bilayer thickness in the gel phase is maximal around 5-5.5 nm and phospholipid cross-sectional surface area is minimal around 4-4.5 nm², whereas within the liquid crystalline state the bilayer thickness is minimal around 4-4.5 nm and cross-sectional surface area is maximal at 6-7 nm². This is a result of maximal acyl chain interaction and extension within the gel phase and greater intra- and intermolecular motion in the liquid crystalline state.⁵¹

These interactions can be enhanced or augmented via the inclusion of cholesterol within the liposomal formulation. Cholesterol affects the transition by altering the normal packing of the acyl chains and disrupting the ordered array of hydrocarbon chains in the gel state. The presence of cholesterol inhibits acyl chain motion above the transition temperature and reduces the area per lipid, affecting the liquid crystalline state.⁴⁹ Increasing concentration of cholesterol effectively yields a broadening of the thermotropic transition.^{41,51} It is worth noting that incorporation of hydrophobic drugs within the formulation has a similar effect on the membrane stability and phase behavior.⁴⁸

2.2.4 Hydrophobic Assembly

Phospholipids can exhibit polymorphism in an aqueous environment. The exact phase is dependent on the chemical makeup of the phospholipid (i.e., head group, hydrocarbon chain length and unsaturation) ionic strength of the buffer, pH, temperature, and the presence of divalent cations such as calcium.⁴⁶ To describe the potential structures

that phospholipids can form, it is necessary to develop a thermodynamic background regarding the forces that drive these interactions. To better understand phospholipid interactions it is best to begin with simple lipid structures and move on to amphiphilic molecules.

The major thermodynamic force that stabilizes lipid aggregates is the hydrophobic force.⁵² The hydrophobic force is a result of constraints placed on water molecules as they pack around a nonpolar hydrocarbon. The thermodynamic costs can be used to determine whether specific processes will occur, and can be quantified in terms of free energy, ΔG . In the case of lipid solvation within an aqueous environment, ΔG represents the reversible work for the solvent to reorganize and solvate the solute.⁵³ This reversible work is comprised of enthalpic and entropic components

$$\Delta G = \Delta H - T\Delta S \quad (1)$$

where ΔH represents the average potential energy of interaction between molecules and ΔS is a measure of intermolecular correlations. A system is said to be enthalpically driven if the process involves significant changes in the number of molecular interactions – such as the breaking of hydrogen bonds when forming a liquid-vapor interface. Whereas the system is entropically driven if the process requires significant spatial organization (order) of hydrogen bonding patterns.⁵³

The hydrophobicity of a solute can be enumerated by measuring the equilibrium distribution of the solute within two solvents such as water and hexane. This measure can be expressed as

$$K = \frac{[X]_{H_2O}}{[X]_{HC}} \quad (2)$$

where $[X]_{H_2O}$ is the mole fraction solute in the water and $[X]_{HC}$ is the mole fraction of solute in the hydrocarbon.⁵² In addition, the standard free energy of transfer of a lipid from a hydrocarbon into water is given by

$$\Delta G_{trans}^{\circ} = -RT \ln K = (\mu_{H_2O}^{\circ} - \mu_{HC}^{\circ}) \quad (3)$$

where ΔG_{trans}° is the standard state free energy which can be equated as a measure of hydrophobicity.⁵² Hydrophobicity has been shown to be proportional to the surface area of contact between the nonpolar solute and water⁵², however, this has not always been shown to be experimentally accurate.⁵³ For large molecules, such as long chain alkanes, this hydrophobic effect has been found to be greater. For every increase in chain length of straight chain alkanes with two methylenes, the equilibrium constant has been found to change by a factor of ten in favor of a hydrophobic solvent.^{52,54} Thus, a highly hydrophobic molecule (such as a lipid molecule) has a finite solubility within water, beyond which leads to the production of a second phase.

When examining amphiphilic molecules such as sodium dodecyl sulfate (a common detergent), this secondary “phase” forms as aggregates termed micelles. These micelles are dispersed throughout the solution rather than separating into two distinct phases. The point at which these globular aggregates form is termed the critical micelle concentration (CMC).⁵² This CMC can be thought of as a solubility limit for the monomeric (one unit) form of the molecule. Increases in concentration of the monomer simply leads to an increase in the production of micelles throughout the suspension. Other amphiphilic

molecules such as phospholipids form similar globular structures, where phospholipids form into bilayers.^{54,55} The CMC for phospholipids is less than 10^{-10} M.⁵⁶ This means, for practical purposes, that the concentration of single, monomeric phospholipids in solution is negligible.⁵² It is worth mentioning that the hydrophobic force is not the only force that stabilizes lipid aggregates, but also van der Waals forces (close proximity, weak attractive forces between adjacent carbon chains) and hydrogen bonding (between polar headgroups, such as phosphatidylethanolamine).

At equilibrium, a solution of amphiphilic species may contain a distribution of monomer species and aggregates. This allows the chemical potential for either form to be written as

$$\mu_N = \mu_N^\circ + \frac{kT}{N} \ln\left(\frac{X_N}{N}\right) \quad (4)$$

where X_N is the mole fraction of amphiphile in the aggregated species with N molecules, μ_N° is the standard state chemical potential of species, k is the Boltzmann's constant and T is temperature.^{52,55} This system can be simplified by assuming that there is only one form of aggregated species that can form ($N = M$) in equilibrium with the monomeric species. At equilibrium, the CMC can be equated to $X_{CMC} = X_I = X_M$ ^{52,57}

$$\mu_1 = \mu_M \quad (5)$$

thus

$$\mu_1^\circ + kT \ln(X_{CMC}) = \mu_M^\circ + \frac{kT}{M} \ln\left(\frac{X_{CMC}}{M}\right) \quad (6)$$



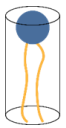
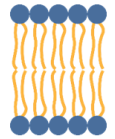

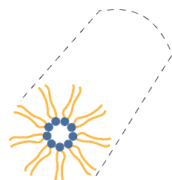
simplifying to

$$\Delta G_{mic}^{\circ} = (\mu_{mic}^{\circ} - \mu_1^{\circ}) = kT \ln X_{CMC} \quad (7)$$

This relationship shows that with a more negative ΔG_{mic}° , the X_{CMC} decreases. This correlates physically with more hydrophobic molecules aggregating at a lower CMC.^{44,52}

Using geometry, it is possible to develop a correlation that relates preferred molecular packing with possible aggregate structure formation. The terms of consideration are the optimal surface area occupied by the polar head group, S_0 ; the maximum length of the acyl chains of the amphiphile, l ; and the molecular volume of the hydrocarbon region of the amphiphile, v . The parameter (v/lS_0) can be used to estimate which micelle formation will be dominant for a particular amphiphile.⁵² The three most common micellar forms are spherical, rods and cylinders, and bilayers. Spherical micelles are predicted when the parameter is less than 1/3, cylinders between 1/3 and 1/2, and bilayers around 1.⁵⁷ Above 1, the polar head groups are small and form what is known as an inverted hexagonal phase, H_{II}. **Table 2** correlates this critical packing parameter with the expected phase behavior of a membrane lipid.^{46,52}

Table 2. Polymorphic phases, molecular shapes, and molecular packing parameter of phospholipids. Adapted from ref ⁴⁶ and ⁵².

Lipid	Molecular Shape	Phase	Critical Packing Parameter ($\frac{v}{l_s a_0}$)
Lysophospholipids	 Inverted Cone	 Micellar	< 1/3 (Sphere) 1/3 to 1/2 (Globular Shapes, Rods)
Phosphatidylcholine Sphingomyelin Phosphatidylserine Phosphatidylinositol Phosphatidylglycerol Phosphatidic Acid Cardiolipin Digalactosyldiglyceride	 Cylindrical	 Bilayer	1/2 to 1 (Spherical) ~1 (Planar)
Phosphatidylethanolamine (Unsaturated) Cardiolipin - Ca ²⁺ Phosphatidic Acid - Ca ²⁺ (pH < 6.0) Phosphatidic Acid (pH < 3.0) Phosphatidylserine (pH < 4.0) Monogalactosyldiglyceride	 Cone	 Hexagonal (H _{II})	>1

2.3 Supported Lipid Bilayers

Scientists have always been intrigued by biological systems given their complexity and efficiency with handling intricate tasks. This fascination has extended to cell membranes. Cell membranes have been recognized for their significant restriction of specific compounds and efficient separations.⁵⁸ Supported phospholipid bilayers have been used as model cell membranes since their discovery in 1965.⁵⁹ These supported membranes have gained significant interest since their inception for their ability to immobilize proteins under non-denaturing conditions, the potential to produce ultrathin high-electric-resistance layers on conductive surfaces and the incorporation of receptors into the insulating layers for the production of biosensors.⁶⁰ In addition, phospholipid bilayer membranes have been the most commonly used cell-surface model and have provided insight into immune

reactions and cell adhesion.⁶¹ The foundation of knowledge and characterization techniques developed for supported lipid bilayers stems from the early work attempting to recapitulate the cellular membrane environment. Scientists today are exploiting the methods and fundamentals from these studies to further understanding of cellular membrane interactions and applying membranes for the production of sensors and drug delivery systems.

2.3.1 Types of Supported Lipid Bilayers

Since their introduction more than 30 years ago,⁵⁹ supported lipid bilayers (SLB) have been of great interest in studying membrane dynamics,⁶² for use as biosensors,⁶³ and more recently as drug delivery vehicles.⁶⁴ Much of the work associated with SLB has been conducted on two-dimensional planar surfaces. Initial focus was on recapitulating the cellular membrane environment to study membrane structure,⁶⁵ membrane dynamics⁶⁶ and lipid-protein interactions.⁶⁷ This initially led to the development of three distinct types of SLB as envisioned by Sackmann⁶⁰ and depicted in **Figure 5**: (i) bilayers where the inner monolayer is covalently or ionically fixed to the substrate, (ii) SLB separated from the substrate by an ultrathin water film or a (iii) polymer cushion. These three categories were later expanded to include a fourth type of SLB where the membrane is separated from the substrate via a tethered polymer-support.⁶⁸

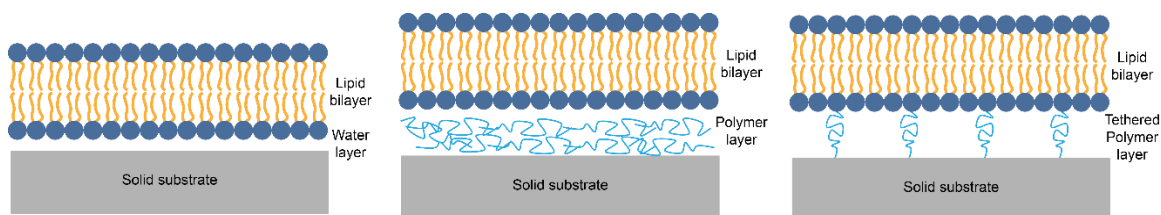


Figure 5. The three most commonly studied types of supported bilayers (left) water, (middle) polymer, and (right) polymer tethered.

Each category of SLB consists of advantages and disadvantages that have been explored. Categories (i) and (ii) provide the simplest mechanism for production, which are often driven by charge-charge interactions between the phospholipid head groups and the substrate. This interaction leads to a water layer separating the bilayer from the solid substrate that is near 30 angstroms in width.⁶⁹ This limited separation between the SLB and the solid substrate is sufficient for mobility of the lipids in both leaflets of the bilayer but the exposed substrate has been found to interact with integral membrane proteins, inhibiting their lateral movement and providing a source for denaturation.^{70,71} Addition of a polymer cushion, category (iii), has been shown to decrease frictional drag between the bilayer and solid substrate^{72,73} and led to a molecular ordering of the lipids identical to multilamellar bilayer vesicles.⁷⁴

Goennenwein *et al.*⁷⁵ found significant differences between human platelet integrin receptors incorporated within supported membranes separated from the solid substrate with water and those on a cellulose film. The study found a 3-10 fold higher adhesion free energy when using the cellulose supported bilayers over the bare substrates.⁷⁵ However, bilayers formed on polymers are often patchy and exhibit numerous defects. To address these defects, an additional category of SLB was formed: (iv) tethered supported lipid bilayers (tSLB), also known as tethered bilayer membranes (tBLM). tSLB utilize an anchor molecule that extends between the substrate and the lipid bilayer. This anchor molecule is often a polymer and is chemically grafted on one end to a phospholipid on the inner leaflet of the bilayer and to the solid substrate on the other. tSLB were found to maintain their fluidity and showed improved homogeneity.⁷⁶ Additionally, tSLB demonstrated an ability

to “heal” small defects more readily than SLB on glass⁷⁷ but were found to exhibit restricted protein diffusion coefficients.^{76,77}

Categories (iii) and (iv), polymer cushions and tethers, are believed to mimic features of the extracellular matrix. This matrix provides support and helps to maintain distance between cells *in vivo* (10-100 nm).⁷⁸ A few properties of polymer cushions have been deemed important in successfully producing polymer supported bilayers and it is believed that similar principles should be extended to tethered systems. First, the polymer chosen should maintain complete wetting between the membrane-polymer interface and the polymer-substrate interface.⁷⁹ This prevents the process of dewetting, where the formation of droplets can lead to destabilization and degradation of the membrane. Dewetting between the polymer and substrate surface can be avoided by grafting the polymer to the solid substrate – an advantage of tethered systems. In addition, the membrane-polymer interaction should be repulsive to prevent any dewetting.^{78,80} This kind of dewetting can lead to areas where the membrane has adhered to the polymer cushion. Areas of adherence cause a decrease in lateral diffusion of lipids and proteins in the membrane as well as decreased overall stability.⁸¹

Tethered systems provide unique control over the substrate-membrane distance and lateral density of functionalized tethers can be used to control viscosity of the polymer cushion. These factors can have a direct impact on the interaction with proteins in the bilayer.⁷⁸ This is unique compared to polymer cushions where the density is simply a function of the polymer support. tBLM can be supported by a variety of polymers that include poly(ethyleneoxide), oligo(ethyleneoxide), or poly(ethylene glycol).⁸² Some studies have utilized block copolymers rather than lipopolymers in order to reduce the

complexity of the system.⁸³ This granular manipulation of the amphiphilic molecule and the macromolecular spacer permits greater control over the system than supported bilayers in categories (i), (ii) or (iii).

2.3.2 Techniques for Supported Bilayer Membrane Formation

The vast amount of knowledge associated with lipid bilayer formation extends from studies conducted in two dimensional planar systems. Their formation has been explored with many different kinds of solid substrates. These surfaces have been characterized as smooth, clean and hydrophilic and include silica, mica, titanium dioxide, gold, silver and platinum.^{84,85} Three traditional methods of formation have seen widespread adoption, while newer techniques remain to be validated. These newer methods include freeze-thawing,⁸⁶ solvent-assisted formation,⁸⁷ peptide-induced vesicle rupture⁸⁸ and detergents.⁸⁹

The first traditional method utilizes the Langmuir-Blodgett technique to deposit a lipid monolayer on the substrate followed by the use of the Langmuir-Schaefer method to add the additional leaflet. The Langmuir-Blodgett technique transfers the initial leaflet from a monolayer formed at the air-water interface in a Langmuir trough. By pulling a substrate vertically through the monolayer, it is deposited onto the surface. The substrate can then be horizontally pushed into the same monolayer (Langmuir-Schaefer) to add the additional leaflet.⁵⁹ The second method is through the adsorption and fusion of vesicles in suspension,⁹⁰ and the third method is a combination of the first two. In the third method, an initial lipid monolayer is developed using the Langmuir-Blodgett technique followed by vesicle fusion to form the exterior leaflet.⁹¹ The Langmuir-Blodgett and Langmuir-Schaefer techniques provide the advantage of being able to form asymmetrical bilayers while vesicle fusion is the easiest and most versatile.⁸⁴

The most recent descriptions of the vesicle fusion method⁹²⁻⁹⁴ suggests that liposomes adsorb to the surface and reach a critical vesicular coverage. This critical coverage induces stress on neighboring vesicles which, in combination with the stress induced from vesicle deformation upon adsorption, initiates rupture. This rupture then leads to the formation of bilayer patches or discs.⁹⁵ These discs contain edges with high surface energy due to the highly curved nature of the lipids. These edges promote interaction with adjacent lipid material, whether its vesicles in suspension or adsorbed, causing further rupture and spreading of the lipid membrane. This propagation has been found to be a function of temperature, where temperatures above the transition state increase the rate of spreading.⁹⁶ In general, SLB are energetically favorable compared to vesicles due to the minimization of the bending energy. This has led to the process being characterized as spontaneous under the right conditions.^{84,95}

2.3.3 Factors Affecting Supported Bilayer Membrane Formation on Colloidal Particles

The vesicle fusion method is the most commonly used procedure in preparation of supported lipid bilayers on colloidal particles.⁹⁷ The factors that impact the rate of bilayer formation on colloidal particles include temperature, pH, ionic strength, ratio of lipid to solid substrate, charge of lipids and substrate surface, as well as the differences in size of the liposomes and solid substrate.⁹⁸⁻¹⁰⁰ DSPC vesicles were found to promote the greatest adsorption when diameters were less than 90 nm. Temperatures above the transition state of DMPC lipid was found to increase the rate of adsorption in comparison to temperatures below, which is likely due to the increased fluidity of the membrane at higher temperatures.⁹⁸ Similar results were obtained for DPPC and DODAB bilayers on silica particles.^{101,102}

The ratio of lipid to solid substrate was one of the first factors recognized as instrumental in the formation of SLB on colloidal particles.¹⁰³ Carmona-Ribeiro *et al.*¹⁰³ utilized adsorption isotherms to discover the deposition of multiple bilayers. This terminology was later refined by Troutier *et al.*⁹⁹ to refer to the ratio between the total surface area provided by the vesicles in suspension (A_V) and the total surface area provided by the particles (A_P). An inflection point is held at an A_V/A_P ratio of 1, where the surface area of lipid vesicles is equal to the surface area of nanoparticles in suspension. At this point, there is theoretically enough lipid in solution to form complete bilayers on the surface of the particles. Below this threshold, there is not enough lipid in solution to form complete bilayers on all of the nanoparticles and a phenomenon known as lipid bridging can occur as demonstrated in **Figure 6**.

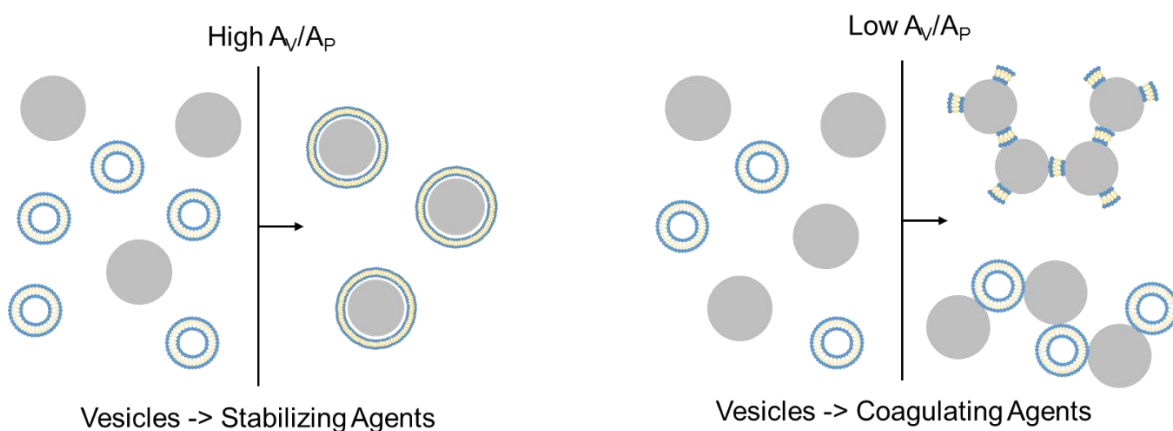


Figure 6. Ratio of vesicle surface area (A_V) to particle surface area (A_P) dictates stability of colloidal systems. Adapted from Troutier *et al.*⁹⁹

pH has been found to influence adsorption to the greatest degree through its impact on surface charge of the lipids and/or nanoparticles. At a pH of 7, the influence of buffer salts (phosphate, boric acid, hepes and tris examined) did not yield dramatic differences from nonbuffered solutions.⁹⁹ Similar results were obtained by Rapuano *et al.*,^{101,102} but

found that tris was the preferred buffer over hepes or water at a pH of 7.4. Tris is believed to adsorb (positively charged amine groups) to the surface of the silica particles whereas hepes does not (negatively charged sulfonic group). This adsorption of tris promotes hydrogen bridges between the phosphate groups on the lipids and the hydroxyl groups from the adsorbed tris molecules. Molecular dynamics simulations of palmitoyl-oleoylphosphatidylcholine (POPC) with silica-type substrates have found a similar effect, where charge densities on the surface (as dictated by solution pH) directly determine the degree of POPC interaction.¹⁰⁴ This interaction is between the phosphate groups on the lipid and the hydroxyl groups on the surface. The degree of interaction correlated with distance between the bilayer and substrate surface, where an increase in hydroxylation yielded reduced distances between the two surfaces (increased interaction/hydrogen bridging). This conclusion is in agreement with the explanation proposed by Rapuano *et al.* for the adsorption of tris molecules to the surface, where 3 hydroxyl moieties would be expressed when the charged amine adsorbs to the silica surface – leading to an increase in hydroxylation.

Nanoparticles and lipids with pH dependence often showed greater association when electrostatic interactions were promoted.^{99,100} The impact of pH on zwitterionic lipids is generally less. However, the degree of ionization of the particle surface can effect these lipids. Thevenot *et al.*¹⁰⁰ found that adsorption of zwitterionic lipids was a function of hydrophobic effects, hydrogen bonding, dipole-dipole interactions and the nature of the spherical solid support. These effects were controlled by changing the pH of the medium. For zwitterionic lipids (DPPC) on poly(lactic acid) (PLA) particles, pH values below 3.5 were found to have a dramatic effect on size, size distribution and number of lipid bilayers

formed.¹⁰⁰ This effect was attributed to an increased ionization of the surface carboxyl groups on the PLA particles. This increased ionization led to the formation of hydrogen bonds between the phosphate groups on DPPC and the particle, as well as increased dipole-dipole interactions – similar to the molecular dynamics simulations previously discussed.

Ionic strength was found to effect bilayer adsorption during formation of the SLB but yielded less of an effect after SLB formation (i.e., increasing ionic strength after formation at lower ionic strength).⁹⁹ Moura *et al.*¹⁰⁵ found that an ionic strength of 10 mM NaCl yielded increased association of phosphatidylcholine lipid with 50 nm silica particles. This greater association was due to increased van der Waals attraction between the lipid and silica particles. Concentrations below this 10 mM required more lipid to garner the same adsorption (did not reach limiting adsorption value) and concentrations above 10 mM yielded high affinity similar to 10 mM but with greater variation in the amounts of lipid adsorbed. A similar trend was observed with DODAB/DPPC vesicle adsorption on silica.¹⁰⁶ Troutier *et al.*⁹⁹ found that ionic strengths greater than 100 mM led to particle agglomeration (DLVO primary minimum) due to significant reductions in charge shielding and also postulated that polyvalent buffers can lead to greater charge shielding compared to monovalent buffers – perhaps compounding effects from ionic strength. This observed effect may help explain the variation in lipid adsorbed at higher ionic strengths observed by Moura *et al.*¹⁰⁵ Calcium has also been implicated to promote SLB formation. This promotion can be observed in two main forms. First, calcium can promote the formation of SLB within systems that otherwise would not readily form (e.g., highly liked-charge vesicles and supports) and, secondly, calcium can reduce the amount of lipid to produce a SLB in similar conditions. This effect is attributed to calcium's bivalent nature, allowing

it to bridge negatively charged entities – such as the phosphate head groups of lipids or negatively charged hydroxyl groups on silica.¹⁰⁷ In the case of zwitterionic lipids, the calcium can convert the headgroup from dipole into a positive monopole, strengthening the interaction with negatively charged substrates.¹⁰⁸ Calcium has also been suggested to initiate flip-flop of phospholipids in the bilayer which leads to greater interaction with solid supports and promotion of rupture.¹⁰⁹ In general, these trends can be summarized by examining thermodynamics of colloidal systems. Conditions where electrostatic interactions, hydrogen bonding, dipole-dipole interactions or hydrophobic effects are promoted lead to increased lipid adsorption. Manipulation of pH and ionic concentrations have been shown to promote or severely limit these effects.

One of the main drawbacks in using vesicle fusion for SLB formation on nanoparticles is the lack of control in phospholipid distribution between the two layers. One study found that electrostatic interactions between the nanoparticle surface and the proximal monolayer (inner leaflet) can direct flip-flop of oppositely charged phospholipids from the distal monolayer (exterior leaflet).¹¹⁰ The resulting inner monolayer consisted of 200% greater cationic lipids in comparison to the exterior monolayer. These results further indicate an important interplay between electrostatic interactions between these surfaces.

Typically, minimal focus has been put on the development of nanoparticle SLB in studies where the particles are ultimately used as a drug delivery vehicle. Often, the development and optimization steps of these particles is obscure or trivialized – perhaps indicating a lack of understanding of the fundamental forces at play. In order to form the SLB, variations of the vesicle fusion method are employed^{12,19,97,111,112} and often sonication is used to increase the rate of vesicle adsorption.^{64,113} It is also common to use the colloidal

particle suspension to hydrate a lipid film, removing the steps necessary for preformed vesicles.^{64,85,114}

2.3.3.1 Thermodynamics of Colloidal Suspensions

The interaction of liposomes and nanoparticles in suspension are regulated by the interdependence of short-range and long-range forces. These same forces govern the formation of liposomes, as previously discussed. The assembly of phospholipids into lipid bilayers is dictated by the intraparticle interactions which are functions of ionic strength, pH, temperature, etc. Interparticle interactions are dictated by the same parameters and determine aggregation states and bilayer formation.

The total interaction energy (W_{total}) between a SLB and nanoparticle surface can be expressed as the summation of the van der Waals interaction (W_{vdW}), double-layer electrostatic interaction (W_{EDL}) and repulsive entropic forces (W_{hyd}):^{57,115}

$$W_{total} = W_{vdW} + W_{EDL} + W_{hyd} \quad (8)$$

van der Waals forces (dispersion forces) are long-range forces between molecules and are caused by fluctuating polarizations of nearby particles with effective distances ranging between 0.2-10 nm. These forces can be attractive or repulsive and tend to align and/or orient molecules in the bilayer. van der Waals forces are always present and influence phenomena such as adsorption, surface tension, wetting and the flocculation of particles in liquids, among others.^{57,116}

If the radius of the nanoparticle is much greater than the thickness of the lipid bilayer and the distance between the nanoparticle and the liposome, the W_{vdW} can be approximated as

$$W_{vdW} = -A_{123} \frac{R_1 R_2}{6(R_1 + R_2)} \left(\frac{1}{d} - \frac{1}{(d+h)} \right) - \frac{A}{6} \ln \left(\frac{d}{d+h} \right) \quad (9)$$

where R_1 is the radius of the nanoparticle, R_2 the outer radius of the liposome with thickness h , at a distance d apart from each other and A_{123} is the Hamaker constant.¹¹⁷ The Hamaker constant can be approximated as a function of the Hamaker constants for the individual species

$$A_{123} \approx (\sqrt{A_{11}} - \sqrt{A_{22}})(\sqrt{A_{33}} - \sqrt{A_{22}}) \quad (10)$$

where A_{xx} is the Hamaker constant between semi-infinite planes of species x in a vacuum.^{108,118}

Electrostatic interactions, or Coulombic interactions, are driven by the accumulation of oppositely charged mobile ions around the nanoparticle surface. This forms the diffusive electric double layer and favors local electroneutrality over the increase in entropy.⁵⁷ Lipid bilayer charge can exist as a result of charged groups located within the membrane (i.e., on the phospholipid or species incorporated within the membrane) or ions from solution can bind to the membrane and impose a charge – making this process highly pH and ionic strength dependent.¹¹⁹ The W_{EDL} of two different nanoparticles with radii R_1 and R_2 can be estimated using Derjaguin's approximation

$$W_{EDL} = \frac{\epsilon R_1 R_2 (\psi_1^2 + \psi_2^2)}{4(R_1 + R_2)} \left[\frac{2\psi_1 \psi_2}{(\psi_1^2 + \psi_2^2)} \ln \left(\frac{1 + e^{-\kappa D}}{1 - e^{-\kappa D}} \right) + \ln(1 - e^{-2\kappa D}) \right] \quad (11)$$

where D is the distance between surfaces and κ is the Debye length.^{108,120} This relationship holds when the double layer thickness is much less than the particle size and the potentials are less than 25 mV.

The first two terms in equation 8 together make up what is commonly referred to as Derjaguin-Landau-Verwey-Overbeek (DLVO) theory, which assumes uniformly distributed surface charges and that the solvent has no structure. These assumptions break down at distances below 1-2 nm and the interactions of separations are further complicated below 3 nm due to the appearance of additional forces.^{57,121} These additional forces include thermal fluctuation and protrusion forces, and steric-hydration forces that have been lumped into the final term, W_{hyd} . Compared with the two DLVO energies, the origin of W_{hyd} is still debated.¹²²

Thermal undulation and protrusion forces contribute to short-range repulsion at distances closer than 1-2 nm for free bilayers, around 1 nm for supported bilayers and ~0.5 nm for gel-state bilayers.^{57,123} In the case of supported bilayers, undulation forces are suppressed by the solid substrate; however, the effect of polymer-coated supports and tethered membranes that maintain the fluidity of the membrane remain to be determined. The undulation force is entropic in nature and emerges when thermally excited waves are confined to a small region of space. This force has been suggested as the mechanism stabilizing zwitterionic bilayers in suspension.¹²⁴ Steric protrusion forces are more localized in comparison to undulation forces and are considered molecular-sized surface fluctuations (e.g., headgroup of phospholipid). In general, the undulation forces are characterized as having larger amplitudes over protrusion forces, while protrusion forces are more numerous.^{57,124}

Tero *et al.*¹²² proposed that the hydration energy, W_{hyd} , between a lipid bilayer and a solid substrate was the average of the hydration energy between a hydrophilic solid and an aqueous solution, W_{solid} , coupled with the hydration repulsion energy between two lipid

bilayer membranes, W_{lipid} . Assuming that W_{solid} and W_{lipid} are independent of each other, Tero *et al.*¹²² suggested that the hydration energy between a lipid bilayer and a solid substrate was the average of each hydration energy at the homogeneous interfaces, such that

$$W_{hyd} = \frac{W_{solid} + W_{lipid}}{2} \quad (12)$$

W_{solid} is a result of tightly bound water molecules at the solid-liquid interface and is represented empirically as an exponential decay^{116,122}

$$W_{solid} = W_0 e^{(-D/\lambda_0)} \quad (13)$$

where W_0 (mJ m^{-2}) and λ_0 (nm) are fitting parameters determined experimentally and D is the distance between surfaces. SLB formation on silica nanoparticles was found to be slower on surfaces with greater hydration (increased presence of hydroxyl groups) and a function of solvent conditions with zwitterionic lipids.¹²⁵ W_{lipid} estimation was based on the types of thermal motion a membrane can experience: protrusion, peristalsis and undulation. Tero *et al.*¹²² has expressed these different motions as

$$W_{protrusion} = 2.7\Gamma kT e^{(-\alpha_p D/kt)} \quad (14)$$

$$W_{peristalsis} = \frac{(kT)^2}{20k_a D^4} \quad (15)$$

$$W_{undulation} = \frac{3\pi^2 (kT)^2}{128k_B D^3} \quad (16)$$

where Γ , α_p , k_a and k_b are the surface density of protruding head groups, protruding energy, area expansion modulus and bending modulus, respectively. The undulation force can be neglected when the membrane exhibits a surface charge, allowing a simplification to¹²²

$$W_{lipid} = W_{protrusion} + W_{peristalsis} \quad (17)$$

For a curved surface, short range interaction (attraction) is typically reduced and long-range van der Waals and electrostatic forces dominate.¹⁰⁸

In general, there are two cases for which SLB can be formed on nanoparticle surfaces. In the first case, adsorption of a liposome onto the nanoparticle surface leads to SLB formation. This occurs when the radius of the nanoparticle is greater than the radius of the vesicle or the surface area of the liposomes is equal to or greater than the surface area of the particles. In the second case, the formation of a SLB on the nanoparticle surface is an intermediate step towards the internalization of the particles. This occurs when the radius of the nanoparticle is much smaller than the radius of the liposome.

Under the vesicle fusion approach, the process of SLB formation is dependent on the ability of a lipid bilayer to curve around the particle and assume the substrate's shape – the adhesion transition. This process has been described as a competition between the adhesion energy between the membrane and substrate and the bending energy (curvature of the membrane) necessary for the bilayer to bend around the particle.^{108,126} This produces a three-state system in which particles are fully enveloped, partially wrapped or freely dispersed.¹⁰⁸ Seifert and Lipowsky¹²⁶ developed a theory to evaluate the binding and stability of surface-bound vesicles, characterizing the transition between the wrapped and

free states with a critical length R_C . R_C is a function of the bilayer bending modulus κ and the adhesion energy per unit area W :

$$R_C = \sqrt{\frac{2\kappa}{W}} \quad (18)$$

This relationship suggests that the critical length is dependent on the liposome-nanoparticle interactions and the bilayer properties. When liposome size is less than the critical length ($R < R_C$), the binding and formation of a SLB is energetically favorable. When liposome size is greater than the critical length ($R > R_C$), the vesicle will unbind as a result of shape fluctuations in the membrane (entropy driven).¹²⁶ It is worth noting that experimental data suggest that this theory alone does not convey the whole answer to vesicle stability and that dynamic distribution of different lipid species and cooperative effects of nearby vesicles need to be taken into account – as previously discussed.¹²⁷

2.3.4 Nanoparticle-Supported Bilayer Membranes for Drug Delivery

There are many benefits associated with applying a lipid layer to a surface, including stabilization, increased solubility and circulation residence times, biodistribution control, protein immobilization, among others. However, the application of a lipid layer is not always best served in the form of a bilayer, which has sparked investigation into the use of lipidic bilayer fragments and/or disks. Additionally, there are many different types of ‘particles’ that have been investigated within the field of drug delivery, such as those constructed from lipid (solid lipid nanoparticles),¹²⁸ viruses or even hydrophobic drug.¹²⁹ These types of associations have been covered by Carmona-Ribeiro⁹⁷ and won’t be

discussed here. This work focused on the use of an inorganic particle core to which a lipid bilayer has been applied, and similar systems will be highlighted.

2.3.4.1 Methods Currently Employed

Despite the utility of silica in biomedical applications, one problem persists – the biocompatibility in comparison to particles composed of naturally occurring materials. A previous report by van Schooneveld *et al.*¹⁸ demonstrated the use of 34 nm silica nanoparticles with a PEGylated/Gd-DTPA lipid monolayer covering. In comparison to the bare silica nanoparticles, the lipid coated particles exhibited a circulation half-life that was 10 times greater. Additionally, it was found that the lipid on the particles did not dissociate from the particles upon administration *in vivo*. This same group later found that the application of a PEGylated/paramagnetic lipid monolayer onto a quantum dot/silica nanoparticle of 31 nm yielded a dual modality imaging agent for MRI and fluorescence imaging.¹³⁰ These particles were targeted to human umbilical vein endothelial cells (HUVEC) with an RGD peptide which produced a ~25-50 fold difference in photon count between targeted and untargeted cell pellets. Wang *et al.*¹⁷ also found that by preparing a hydrophobic surface on silica particles, a PEGylated lipid monolayer was able to improve water suspensibility and greatly reduced nonspecific binding to cancer cells (Hela).

One of the first reports of the use of a lipid bilayer coating to enhance nanoparticle behavior in a biomedical application was a study looking at the transport of polysaccharide nanoparticles through an *in vitro* blood brain barrier model in 1999. Fenart *et al.*¹¹³ found that the application of a 1,2-dipalmitoyl-sn-glycero-3-phosphocholine (DPPC) and cholesterol layer to the outside of the anionic and cationic polysaccharide particles would enhance transport (3-4 fold) through the membrane (transcytosis). It is believed that the

lipid layer provided a shielding effect of the originally highly charged particles since the lipid layer did not enhance transport of the neutrally charged polysaccharide particles. Finally, Fenart *et al.*¹¹³ found that particles were able to increase albumin transport across the barrier 27 fold with the lipid-coated particles.

The initial use of SLB on nanoparticles within the field of delivery were looking for a way to retain drug within pores of mesoporous silica, reduce aggregation under physiological conditions and prevent nonspecific binding in serum.^{17,111,131} The use of mesoporous silica was a likely transition of the technology and provided an easy extension of the methods developed from previous amorphous particle research lead by Carmona-Ribeiro *et al.* and Troutier *et al.* Liu *et al.*¹¹¹ used DOPC liposomes mixed with varying concentrations of anionic (DOPS) and cationic (DOTAP) lipids and found a similar electrostatic driving force for vesicle fusion. It was found that the incorporated bilayer could retain calcein and that release was practically instantaneous if the bilayer was compromised. This work would initiate the focused use of “protocells” by Jeffrey Brinker’s group, leading to several other publications where lipid coated mesoporous particles were used in drug delivery. In a follow up publication, Brinker *et al.*¹³¹ demonstrated an ability to tailor the surface charge of the resulting protocell particle simply by incubating the particles with liposomes of varying electrostatic potential in suspension. This lipid exchange between the suspended protocells and liposomes is believed to have led to a reduction in the defects of the protocell bilayer – a factor important for the containment of drug loaded in mesoporous particles.

Mesoporous silica nanoparticles (MSN) capped with a DMPA/DMPC (10:90, w/w) lipid mixture were explored to deliver hypocrellin B (HB), a photosensitizer, in the

treatment of breast cancer (MCF-7). Yang *et al.*¹³² found that the addition of the lipid bilayer increased the stability of the HB loaded particles and improved cell compatibility. The delivery of HB was successful in reducing the viability of MCF-7 cells with a decrease in viability from 89.6% to 44.6%. Cauda *et al.*¹³³ confirmed a similar stability of MSN after addition of a DOPC/DOTAP coat. Calcein release from the MSN/DOPC/DOTAP particles was found to be 10-fold lower (fluorescence values) than MSN without a lipid coat. Delivery of colchicine to HuH-7 (liver tumor) cells resulted in an enhanced effect over free drug, which was attributed to slow permeation of free colchicine through cell membranes versus the concentrated delivery via the particles.

Brinker's group¹¹² also found that DOPC protocells with SP94 peptides had high specific affinity for Hep3B (live cancer) cells over hepatocytes, which was over 10 times greater than similar DOPC liposomes. Additionally, DOPC ($T_m = -17^\circ\text{C}$) protocells were found to have a 100-fold greater affinity for Hep3B in comparison to DPPC ($T_m = 41^\circ\text{C}$) protocells with SP94. This effect was a result of the recruitment of SP94 peptides to the cancer cell surface when using the DOPC protocells, indicating the importance of membrane fluidity. Overall, Ashley *et al.*¹¹² found that dox loaded DOPC protocells significantly outperformed DSPC liposomes, DOPC liposomes and free dox. The protocells exhibited greater affinity for Hep3B cells with an induced MDR1+ phenotype, less affinity for hepatocytes and greater efficacy in killing Hep3B cells while also maintaining hepatocyte viability. This enhanced efficacy over traditional liposomes was attributed to the 1,000 times higher capacity for drug, enhanced binding affinity and greater long-term stability of the protocells.

Protocells have also been used in the delivery of small interfering RNA (siRNA).¹³⁴ Loading of siRNA into the protocell was facilitated by charge-charge interaction. The negatively charged siRNA associated with the positively charged surface of the primary amine modified MSN. This resulted in a 50- and 10-fold higher loading than DOPC and DOTAP lipid nanoparticles, respectively. The use of a cationic silica particle permits a high loading efficiency of the protocells while also allow the use of zwitterionic lipids in the SLB which helped eliminate cytotoxicity. Overall, the targeted protocells showed greater growth arrest and apoptosis of hepatocellular carcinomas but not control hepatocytes in comparison to similarly loaded lipid nanoparticles. Protocells have also been investigated in the delivery of therapeutics to the spinal cord,¹³⁵ in their uptake mechanism within motoneurons,¹³⁶ proven effective at targeting leukemia cells,¹⁹ and been demonstrated as effective vehicles in a 3D culture model.¹³⁷

Meng *et al.*⁶⁴ demonstrated co-delivery of gemcitabine and, the hydrophobic drug, paclitaxel to human pancreatic cancer in a mouse model, increasing efficacy and had no signs of systemic toxicity. It was also found that the traditional vesicle fusion method of preparation was inefficient for the entrapment of gemcitabine and simultaneous loading of paclitaxel within the membrane. This necessitated the development of modified technique, where paclitaxel was included within the chloroform/lipid film. Following hydration with the gemcitabine loaded MSN, solvent evaporation used to remove the remaining organic solvent.

Several other bilayer-coated, MSN based studies have been conducted.¹³⁸ Zhang *et al.*¹³⁹ found success in applying lipid coated MSN in the treatment of multidrug resistant breast cancer, with increased uptake in cancer cells and enhanced release of irinotecan in

tumor acidity. Han *et al.*¹⁴⁰ found that a soybean lecithin/PEG coating on MSN increased stability, prevented release of loaded dox, and enhanced cell kill of MCF-7 cells when treated with dox loaded particles. A similar report by Mattingly *et al.*⁸⁵ found high toxicity to MCF-7 cells when SLB core-shell silica-iron oxide particles were loaded with doxorubicin. A more recently study by Tu *et al.*¹⁴¹ explored the use of mesoporous silica particles loaded with hemoglobin as an erythrocyte-mimic. Tu and coworkers noted an increased stability of the hemoglobin-loaded particles upon adsorption of the lipid bilayer.

Unique lipid coatings have also begun to gain attention. Application of red blood cell membranes to PLGA nanoparticles has been investigated as a means to increase circulation half-life, finding longer residence times *in vivo* in comparison to PEGylated PLGA nanoparticles and similarly formed RBC-derived liposomes.¹⁴² Platelet coated PLGA nanoparticles have been shown to increase stability, retention of membrane protein content and right-side-out membrane orientation in translocated membranes.¹⁴³ And the formation of a protein corona has been found to be a function of nanoparticle size and surface characteristics (PEGylated versus membrane enveloped), where larger sizes and DPPC/DOPS membrane incorporation resulted in reduced protein adsorption.¹²

2.3.4.2 *Developing a Nanoparticle-Tethered Membrane*

To date, most of the work with these membrane enveloped nanoparticle systems could be compared to the simplest of planar supported membranes. These include the water and polymer supported systems.¹⁴⁴ The reason for this could be linked to the simplicity of previous attempts to drive bilayer assembly/association onto the nanoparticle surface. Often, electrostatic interactions were employed. In this case, the nanoparticle surface maintained an opposite charge (negative) to that of the associating bilayer (positive).¹³¹

Others have chemically rendered the surface of the nanoparticles hydrophobic in order to form a monolayer upon phospholipid addition.¹⁴⁵ Only very recently has a focus developed on the final category of supported lipid bilayers with regard to colloidal systems - tethered lipid bilayers. **Figure 7** provides a schematic outlining the basic makeup of a tethered membrane nanoparticle. Locations for potential drug loadings, fluorescent molecule incorporation and targeting moieties have been indicated – some of which were used in this work.

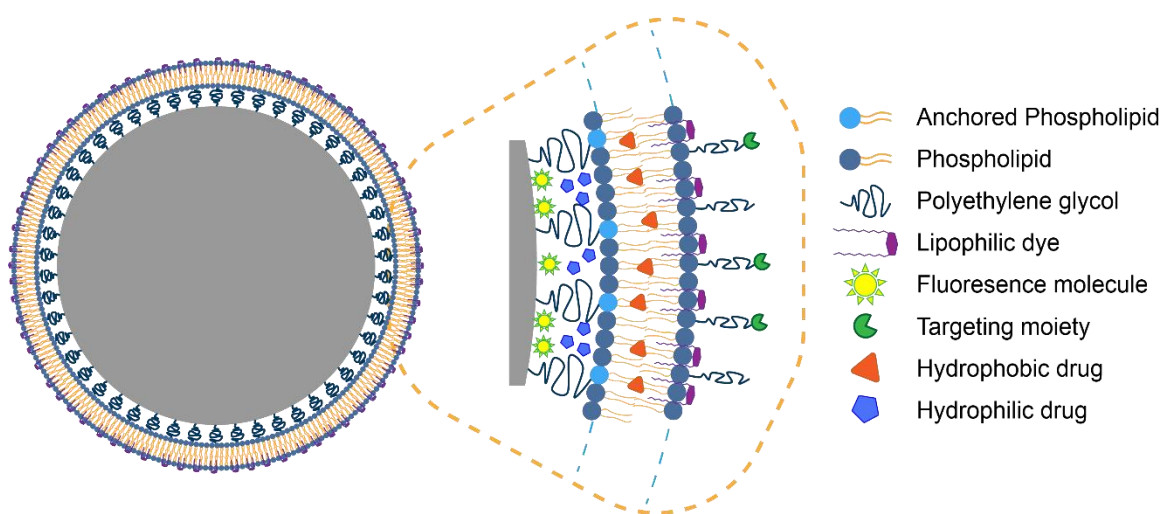


Figure 7. Schematic outlining the basic makeup of tethered membrane nanoparticle with locations of potential drug loadings, fluorescent molecule incorporation and targeting moieties.

Mathematical simulations regarding formation of a tethered lipid bilayer on the surface of a particle found that the production of such a system is theoretically possible and has provided the ground work for further investigation in this area.¹⁴⁶ Fried, *et al.*¹⁴⁷ have successfully produced a tethered lipid bilayer on the surface of a PLGA particle utilizing a peptide as the membrane anchor, however, their particles were on the order of 5 microns or larger with high polydispersity. A similar method was outlined in a recent patent where a nanoparticle is enveloped by a lipid bilayer via tethered proteins.¹⁴⁸ Experimental

investigations into the use of tethered phospholipids (lipopolymers) on nanoparticle surfaces as a means to produce a supported lipid bilayer have not been published.

Tethering provides the advantage of abstracting the supported lipid bilayer away from the surface of the solid nanoparticle. This effect is three-fold, in that provides a submembrane space for drug loading, removes concern for surface porosity or roughness that can impede bilayer spreading and reduces the dependence of bilayer formation on electrostatic interactions. The removal of dependence on electrostatic interactions also reduces the effect of pH and ionic strength on bilayer formation. Tethering also promises increased stability of the lipid bilayer over polymer supported systems where detachment of lipids results in overall lipid loss and can lead to destabilization of the colloid.¹¹⁴ A tethered membrane composite maintains the advantages previously developed for membrane enveloped nanoparticles, including low inherent toxicity and immunogenicity, long circulation half-lives, size and morphology control and increased stabilization.¹¹² pH dependent release strategies have also been explored where the drug cargo is stable at pH 7.4 but releases under endosomal conditions.¹⁹

A great deal of focus within the field of SLB has been on the recapitulation of the cellular membrane environment. Although this work has been instrumental in the development of methodologies for formation and characterization of these types of constructs, this does not necessarily indicate a direct application of similar systems for use as drug delivery vehicles. Where SLB research has particularly focused on the improvement of lateral and rotational diffusion of lipids and proteins within the membrane,⁷⁷ the use of solid-phase lipids such as distearoyl phosphatidylcholine in combination with cholesterol have demonstrated increased blood residence time and

reduced uptake by the reticuloendothelial system (RES) *in vivo*. This enhanced effect was contributed to the rigid bilayer, negative surface charge and the use of carbohydrate-containing lipids.¹⁴⁹ Cholesterol is often included to increase the stability of the liposomes, preventing lipoprotein-induced destabilization.¹⁵⁰ Increasing saturation and length of acyl chains can also yield greater retention of encapsulated drugs.¹⁵¹ There are a variety of methods used to tailor the lipid bilayer towards specific disease states such as the use of synthetic lipids for precise transition states, charge, targeting or release characteristics.¹⁵²

For this work, solid-phase lipids were chosen for their ability to gel and retain drug molecules as well as for direct comparison to clinically approved liposomal formulations. Although the use of solid-phase lipids may be most ideal for the production of a drug delivery system that can withhold its drug payload from systemic circulation, Moura *et al.*¹⁰⁶ found that an increasing structural stability of the liposomes will retard their willingness to disrupt and form SLB on the nanoparticles in suspension. This may be overcome via sonication. Additionally, Ashley and coworkers¹¹² found that a fluid membrane, constructed of low transition temperature lipids, on MSN promoted an avidity effect of incorporated targeting ligands. In this work, a fluid membrane led to recruitment of ligands and greater affinity for cancer cells over the same ligands incorporated within a gelled membrane. Although higher transition temp lipids were utilized in this work, incorporation of lower transition temp lipids provides an easy, informative future study.

Silica nanoparticles were chosen as the ideal core material over traditional solid, spherical nanoparticle systems such as gold or iron oxide given its breadth of study in literature with similar supported lipid bilayer systems and changes in surface characteristics would be easily monitorable, including size and morphology. In addition, silica exhibits

high clarity, showing minor light absorbance over a wide range of wavelengths, chemical stability over a broad range of pH conditions and there are many established bioconjugation strategies. Silica nanoparticles have been used for a variety of biomedical applications including drug delivery,^{26,153,154} controlled release,^{155–157} gene delivery,¹⁵⁸ and even fluorescence imaging¹⁵⁹ and magnetic resonance imaging.^{160,161} The drawbacks of silica particles are that they suffer from limited stability *in vivo* and dose-dependent toxicity. Silica particles often require coatings to shield surface silanol groups that are highly lipophilic and known to promote non-specific binding and uptake by the mononuclear phagocyte system¹⁶² – limitations addressed in this work.

The 100 nanometer size range was chosen to exploit the EPR effect and liposomes of 100 nm have been found to yield greater antitumor activity.¹⁶³ A solid nanoparticle was chosen to provide increased stability to the lipid bilayer, although, porous particle systems have shown success. The understanding gained from using silica will allow easy transition to other nanomaterials that may have inherent advantages such as MRI tracking associated with iron oxide. All of the materials chosen are currently in FDA approved formulations or are generally recognized as safe (GRAS). Silica nanoparticles are also currently being evaluated in a clinical trial¹⁶⁴ and have been found to be biodegradable.¹⁶⁵ Additionally, all of the major component materials used in the synthesis of the TMN are commercially available, addressing issues of rigor and reproducibility found in unique formulations used in the literature.

2.3.5 Commonly Employed Characterization Methods

Transitioning from planar surfaces to colloidal suspensions creates a difficulty in characterization of supported bilayer systems. Where quartz crystal microbalances with

dissipation (QCM-D) and atomic force microscopy (AFM) have become hallmark characterization techniques for planar bilayers,¹⁶⁶ these methods do not readily transition to colloidal systems. New methods of assessment have been explored including adsorption isotherms, dynamic light scattering and laser Doppler electrophoresis. These current methods have been able to provide unique assessments of vesicle fusion in elucidating the mechanism of bilayer formation on colloidal systems. However, there remains potential for additional techniques to answer the fundamental questions regarding thermodynamics of the suspensions including vesicle fusion, bilayer propagation and bilayer stability. Two possible methods of interest are differential scanning calorimetry (DSC) and isothermal titration calorimetry (ITC). DSC provides an opportunity to learn more about bilayer phase transitions and behavior on a nanoparticle surface,^{167–169} while ITC could elucidate biomolecule interaction with nanoparticle-supported lipid bilayers as well as provide a better understanding of the role bilayers play in preventing or initiating agglomeration.^{170–}

¹⁷⁴ Initial studies with DSC have been successful. The phase transition temperature of a DPPC bilayer was found to decrease by 2°C on a silica bead in comparison to corresponding MLVs, believed to be a result of increased lateral stress.¹⁶⁹ Additionally, two unique observations were found. The first was that the particles did not observe the “rippled phase” typically associated with the pretransition of phospholipids.⁵⁰ The second was that both monolayers of the membrane underwent phase transition at the same time, behaving similarly to a liposome suspension. There was no decoupling of the monolayer leaflets as has been observed in planar systems.¹⁷⁵ Similar trends were observed in an investigation of DMPC bilayers on silica nanoparticles with nano-DSC, where the shift in transition temperature was found to be a function of nanoparticle size.¹⁷⁶ Effects of a varied

lipid composition (i.e., cationic and/or anionic lipids and sterols), presence of a polymer support and/or a tethered membrane remain to be explored.

Chapter 3: Formation and Characterization of Tethered Membrane Nanoparticles

3.1 Introduction

Nanotechnology has seen significant adaptation and application within the medical field for use in transporting therapeutics.^{177,178} The field of nanomedicine is focused on developing strategies for targeted drug delivery, increasing potential for previously non-ideal drug candidates (poorly water-soluble drugs, active transport, etc.) and personalized health care. This heightened focus is a result of advantages nanomaterials provide over free drug, including: protection from degradation, control over pharmacokinetics and tissue distribution, and improved intracellular uptake, among others.¹⁷⁸ Several lipid nanoparticle-based drug delivery products have made it to market or are in late-stage clinical trials.⁶

Inorganic nanoparticles have been lauded for their ease of synthesis, monodisperse size ranges, tunable surface properties, and large surface area to volume ratios. Additionally, inorganic nanoparticles often exhibit unique optical or magnetic properties that permit tracking them upon administration *in vivo*.¹⁷⁹ However, upon administration *in vivo*, inorganic nanoparticles are characterized by rapid clearance by the reticuloendothelial system (RES), reducing their overall efficacy. This clearance mechanism has been linked to surface properties of the nanocarriers, and represents one area of intense focus.¹⁷⁹

Provided the success of lipid-based drug delivery systems and the promise of inorganic nanoparticles, recent studies have attempted to combine these traditional

nanoparticle carriers. Nanoparticle supported lipid bilayers (SLB) combine the advantages of lipid bilayers with colloidal cores, providing membrane-like environments for incorporation of targeting strategies while also providing stabilization and morphology control in comparison to traditional liposomes. Much of the work associated with SLB has been conducted on two-dimensional planar surfaces with initial focus on recapitulating the cellular membrane environment to study membrane structure,⁶⁵ membrane dynamics⁶⁶ and lipid-protein interactions.⁶⁷ To date, there are three major categories of SLB as originally envisioned by Sackmann⁶⁰ and later expanded by Wagner *et al.*⁷⁷: (i) bilayers where the inner monolayer is separated from the solid substrate by an ultrathin water film or a (ii) polymer cushion and (iii) SLB separated from the substrate via a tethering anchor.

The first category has seen the most investigation in colloidal systems, where often electrostatic interactions provide the simplest method of forming supported lipid bilayers on colloidal particles. Relatively few studies have examined their use as drug delivery vehicles. Initial reports of phospholipid adsorption onto colloidal particles began in the late 1980's and early 1990's with Cuyper *et al.*¹⁸⁰ forming dimyristoylphosphatidylglycerol-based mangetoliposomes, Carmona-Ribeiro *et al.*^{103,181} exploring polystyrene microspheres and Gilbert *et al.*¹⁸² exploring glass microbeads. Expansion of the field led to investigation of several solid nanoparticle types and lipid combinations as reviewed by Troutier *et al.*¹⁸³

Silica-based mesoporous particles have shown promise in delivering therapeutics¹⁸⁴ and more recent investigations of colloidal SLB have focused on combining these two types of systems. For example, Meng *et al.*⁶⁴ utilized dipalmitoylphosphatidylcholine, cholesterol and 1,2-distearoyl-sn-glycero-3-phosphoethanolamine-N-

[methoxy(polyethylene glycol)-2000] (DSPE-PEG) to produce a SLB on a mesoporous particle for concomitant delivery of gemcitabine and hydrophobic paclitaxel for the treatment of pancreatic cancer. SLB on mesoporous nanoparticles have also been investigated in concept,^{17,185} for the delivery of colchicine,¹³³ as photo-sensitive drug carriers,^{132,186} and for delivery of small interfering RNA.¹³⁴ The amount and success of these studies indicates the value in silica as a nanomaterial core. The second category has gained less traction which is likely due to issues carried over from planar systems in which bilayers formed on polymers are often patchy and exhibit numerous defects – something this manuscript explores. The third category, to our knowledge, has yet to be explored experimentally but has been evaluated computationally by Hu *et al.*¹⁴⁶ with a DOPC membrane tethered with polyethylene glycol (PEG) to a 9 nm solid nanoparticle core.

In the present study, tethered membrane nanoparticles (TMN) comprised of silica nanoparticle tethered bilayer membranes were formed via the directed reassembly of liposomes onto the surface of monodisperse, silica particle scaffolds. Scaffold particles were composed of a silica nanoparticle core to which a DSPE monolayer was anchored into the surface via a PEG brush border. This DSPE monolayer was used to direct the assembly of a lipid bilayer onto the surface of the TMN with zwitterionic DSPC liposomes as the source of additional phospholipid. **Figure 8** provides a graphical outline of the steps taken to produce TMN. The factors affecting bilayer formation on the particles were characterized with adsorption isotherms, FTIR, TEM, dynamic light scattering, laser Doppler electrophoresis and carboxyfluorescein release. We believe this represents the first experimentally produced polymer-tethered bilayer membrane on a nanoparticle surface utilizing commercially available materials. Formation of TMN was found to be a function

of sonication time, bilayer composition, solvent conditions (salt concentration, pH, etc.) and lipid concentration.

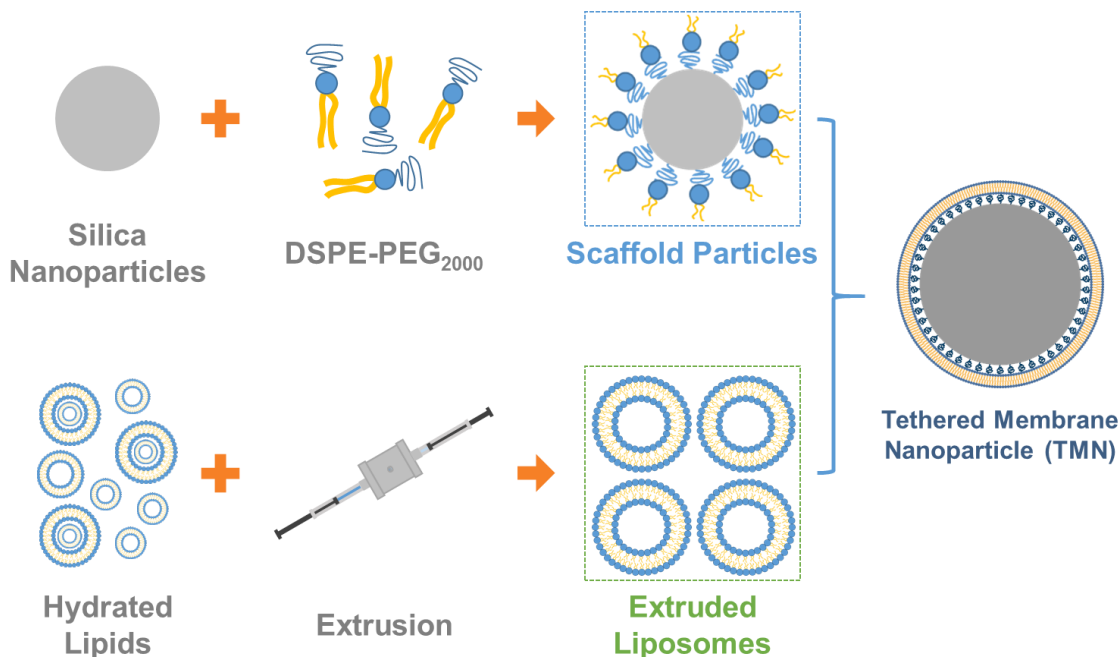


Figure 8. Graphical outline of tethered membrane nanoparticle (TMN) formation process.

3.2 Materials and methods

3.2.1 Materials

All materials were purchased from commercial suppliers and used without further modification, unless noted otherwise. Amine modified (Lot: JEA0116) silica nanoparticles were purchased from nanoComposix (San Diego, CA). N-Hydroxylsuccinimide (NHS) functionalized methoxy polyethylene glycol (m-PEG-NHS) polymer and DSPE-PEG-NHS lipid polymer in 2k Da molecular weight were purchased from Nanocs, Inc. (New York, NY). Fluorescamine, p-methylaminophenol sulfate (99%), ethanolamine (98%), sodium hydroxide (NaOH), oxalic acid anhydrate (98%), ammonium molybdate tetrahydrate

(99%) and 4-(2-hydroxyethyl)-1-piperazineethanesulfonic acid (HEPES, 99%) were purchased from Alfa Aesar (Ward Hill, MA). Silica standard was purchased from Ricca Chemical (Arlington, TX). Dimethyl sulfoxide (DMSO), sulfuric acid, and 37% hydrochloric acid (HCl) were purchased from BDH (VWR, Randor PA). Anhydrous sodium sulfite and tris(hydroxymethyl)aminomethane were purchased from Amresco (Solon, OH). Deionized water used throughout the study was obtained from a Milli-Q Purelab Flex 2 water purification system (ELGA, LLC, Woodridge, Illinois, IL).

3.2.2 Surface Modification of Silica Nanoparticles

PEG molecules were attached to the surface of silica nanoparticles following a modified method of Cole *et al.*¹⁸⁷ Silica nanoparticles were washed two times with 100 mM sodium acetate buffer at pH 4 to remove any ethanol-silanol surface association and one time with 100 mM HEPES buffer at pH 7.5 to deprotonate surface amines prior to reaction. PEGylated silica nanoparticles were prepared by reacting m-PEG₂₀₀₀-NHS at a 2:1 molar excess ratio to reactive amines on the particles. PEG was dissolved in DMSO and then added to silica nanoparticles suspended in HEPES buffer. The reaction mixture was incubated overnight on a RotoFlex tube mixer. Following functionalization, PEGylated particles were washed three times with water to remove unreacted PEG from suspension by centrifuging at 16,000g for 10 minutes and resuspending with a probe tip sonicator (14 W) for 3-5 seconds.

DSPE-PEG₂₀₀₀ functionalized silica nanoparticle scaffolds were prepared similarly but after washing the aminated particles they were resuspended in ethanol. DSPE-PEG₂₀₀₀-NHS was reacted at a 2:1 molar excess ratio to reactive surface amines on the silica particles. DSPE-PEG₂₀₀₀-NHS was dissolved in DMSO prior to mixing with silica

particles. The reaction mixture was incubated overnight (at least 12 hours) with mixing. Following functionalization, the scaffold particles were washed twice with chloroform and once with ethanol before being resuspended in ethanol.

3.2.3 Liposome Preparation

Liposomal formulations were prepared by mixing 1,2-dipalmitoyl-sn-glycero-3-phosphocholine (DSPC) with cholesterol at a 10:5 molar ratio, respectively, in chloroform. Dry lipid films were prepared via evaporation of the chloroform in a Rotavapor R-210/R-215 (Buchi, New Castle, DE, USA) under a constant stream of nitrogen. The thin lipid film was dispersed in 10 mM tris buffer at pH 7.5 and subjected to 7 freeze-thaw cycles before being extruded 7 times through a 0.08 μm double stacked membrane in a high-pressure homogenizer (Lipex, Transferra Nanoscience Inc., Burnaby, B.C., Canada). Final particle size was verified with dynamic light scattering with a mean particle diameter of 117 ± 0.32 nm and a PDI of 0.016. Liposomes were stored at 4°C and used within 3 weeks of formulation. Lipid concentration was determined via quantification of inorganic phosphate following acid hydrolysis.¹⁸⁸

3.2.4 Tethered Membrane Nanoparticle Formation

DSPE-PEG functionalized silica nanoparticle scaffolds were centrifuged at 16,000 g for 10 minutes to remove ethanol solvent. Liposomes were added to the scaffold particle pellet and the mixture was diluted to 500 μL with Tris buffer. The liposome/scaffold particle mixture was sonicated to produce tethered membrane nanoparticles (TMN). TMN were separated from extraneous liposomes via centrifugation with the pellet resuspended by sonication.

3.2.5 Nanoparticle Sizing

Nanoparticle diameter, polydispersity index (PDI) and surface charge (zeta potential) were determined by dynamic light scattering and laser Doppler electrophoresis using a Zetasizer Nano ZS (Malvern Instruments, Inc., Westborough, MA). Measurements were performed with nanoparticles dispersed in 10 mM tris buffer at a pH of 7.5. Nanoparticle morphology was characterized using transmission electron microscopy (TEM) on a Zeiss EM10. TEM samples were prepared by depositing a drop of nanoparticle suspension onto a Formvar/carbon coated copper TEM grid (Electron Microscopy Sciences, Hatfield, PA). The drop was removed with filter paper after 15 minutes and the grid was dried overnight at room temperature. Aminated silica nanoparticle diameter was determined to be 113 ± 13 nm after sizing approximately 400 particles. Nanoparticle diameter was determined using the nanoparticle sizing tool within the ImageJ software developed at the National Institutes of Health, USA.¹⁸⁹

3.2.6 Fourier Transform Infrared Spectroscopy

Successful attachment of DSPE-PEG to the surface of silica nanoparticles was determined with attenuated total reflectance Fourier transform infrared (ATR-FTIR) spectroscopy. Samples were prepared by centrifuging to form a pellet by adding analyte to potassium bromide, forming a pellet and placing the pellet and applying the dried sample to a diamond crystal. A Nicolet 6700 was used for analysis with 64 scans of each sample. Data was converted to percentage absorbance for analysis.

3.2.7 Quantification of Reactive Surface Amine Groups

Silica nanoparticle surface amine groups were quantified using a fluorescamine fluorescence based assay.¹⁹⁰ Silica nanoparticle suspensions were diluted in water. 150 μ L

of particle suspension was pipetted into a 96 well plate. 50 μL of fluorescamine dissolved in DMSO (3 mg/mL) was added to each well and allowed to react for 10 minutes shielded from light. Samples were excited at 400 nm and their emission measured at 475 nm with a FlexStation 3 (Molecular Devices, Sunnyvale, CA). Known concentrations of ethanalamine were used as a standard. Surface amine concentration was found to be $0.48 \pm 0.14 \mu\text{mol amine/mg silica}$.

3.2.8 Silica Assay

Silica nanoparticle concentration was determined using a modified blue silicomolybdic assay.¹⁹¹ The assay was comprised of two working solutions. Briefly, acidified ammonium molybdate was prepared by adding 0.3 mL of concentrated HCl to 10 mL of 1% (w/v) ammonium molybdate. Reducing reagent was prepared by mixing 0.12 g anhydrous sodium sulfite, 0.4 g p-methylaminophenol sulfate in 10 mL water with 6 mL oxalic acid (10% w/v), 6 mL 50% (v/v) sulfuric acid and 8 mL water. Silica nanoparticle samples were dissolved in 1 M NaOH overnight and diluted with water before analysis. 200 μL of acidified ammonium molybdate reagent was mixed with 500 μL of sample and allowed react for 10 minutes at room temperature. Finally, 300 μL of reducing reagent was added and the mixture and incubated at room temperature for 2.5 hours before reading the absorbance at a wavelength of 810 nm using a SpectraMax i3 (Molecular Devices, Sunnyvale, CA). A standard solution of silica was used to determine nanoparticle concentration. Final concentration of the silica particle suspensions was found to be $12.94 \pm 0.13 \text{ g L}^{-1}$.

3.2.9 Membrane Permeability Assay

Membrane permeability analysis was conducted according to Mock *et al.*¹⁹² Carboxyfluorescein was prepared at a concentration of 100 mM by dissolving 37.63 mg CF in 737 μ L of 10 mM Tris buffer (pH = 7.5) and 263 μ L 1M NaOH.¹⁹³ Leakage experiments were performed with a SpectraMax M5e (Molecular Devices, Sunnyvale, CA). Excitation and emission wavelengths of 492 and 517, respectively, were used. Samples were incubated in a 96-well plate at 37°C and the fluorescence signal of CF monitored. The maximum amount of encapsulated CF was measured by adding 1% Triton-X 100, an amount found to ensure complete release of CF.¹⁹⁴

TMN were loaded with CF by adding 100 mM CF stock solution to the lipid-scaffold particle mixture before sonication. Excess CF was removed from solution via centrifuge. Liposomes were prepared as previously described but hydrated with 100 mM CF solution. Excess CF was removed from liposome solutions with a disposable HiTrap desalting column (GE Healthcare, Chicago, IL). The eluate containing CF liposomes was diluted 100 times for leakage measurements. Percentage leakage was determined as

$$\% \text{ Leakage} = (F_t - F_0) / (F_f - F_0) * 100 \quad (19)$$

where F_t was the fluorescence intensity at time t , F_0 the initial intensity at 0 hours and F_f the fluorescence intensity after disruption of the vesicles by detergent.

3.10 Statistical Analysis

All experiments were completed in triplicate (n =3). Results are shown as the average of all replicates \pm standard deviation. Results were compared using Student's T-test or one-way ANOVA, where applicable, and considered significant with p values less than 0.05.

3.3 Results and Discussion

3.3.1 Physical Properties of Silica Particles, DSPC Vesicles and TMN

Hydrodynamic diameter and zeta potential values of aminated silica, PEGylated silica and DSPC liposomes varied with surface coating and solvent conditions. Aminated silica nanoparticles were found to be 113 ± 13 nm with TEM. The aminated silica nanoparticles had a highly positive zeta potential which is a result of the presence of primary amines. Following PEGylation, the zeta potential shifted towards neutral, indicative of the shielding effect provided via the attachment of PEG. DSPC liposomes remained relatively neutral in the solvents tested, which is attributed to the zwitterionic nature of DSPC. **Table 3** summarizes this information for each particle type.

The conformation of PEG chains on the surface of the nanoparticles was assessed by calculating the Flory radius, R_F , of the PEG molecules and distance, D , between attachment points of PEG on the surface. When $R_F > D$, adjacent PEG chains overlap and stretch away from the surface yielding a brush conformation. When $R_F < D$, the polymer chains are not overlapped and form a ‘mushroom’ conformation. The Flory radius is described in eq 20 where a is the length of one monomer in Angstroms (3.5 \AA) and N is the degree of polymerization.^{195,196} D can be calculated using eq 21, where M is the PEG Dalton weight, N_A is Avogadro’s number ($6.022 \times 10^{23} \text{ mol}^{-1}$) and Γ is the surface concentration of PEG (g/nm^2) as determined in eq 22. Here, t is the PEG layer thickness (nm) determined from DLS.¹⁹⁶ Finally, the grafting density, σ , can be calculated from eq 23.^{196,197} Given that the scaffold nanoparticles are unstable in suspension provided their hydrophobic exterior, density of PEG chains on the surface were calculated by quantifying

DSPE-PEG grafted to the surface with the inorganic phosphate assay. The conformation and PEG grafting densities are shown in **Table 3**.

$$R_F = aN^{3/5} \quad (20)$$

$$D = \left(\frac{M}{\Gamma N_A} \right)^{0.5} \quad (21)$$

$$\Gamma = \rho t \quad (22)$$

$$\sigma = \left(\frac{a}{D} \right)^2 \quad (23)$$

Theoretical calculations indicated that the PEG layers on PEG2k-Si and DSPE-PEG2k-Si particle surfaces were in the brush conformation. Grafting densities of DSPE-PEG2k on silica nanoparticles was varied by controlling the molar ratio of DSPE-PEG2k to reactive surface amine groups on the silica particles. As grafting density values increase, there is an increase in the compression of neighboring PEG chains which correlates with greater stretching of the polymer brush and subsequently a larger hydrodynamic diameter.¹⁹⁸

Hu *et al.*¹⁴⁶ proposed a lower bound for the grafting density to ensure that a tBLM is firmly tethered to the substrate

$$\sigma = \frac{\Phi}{a} \left(\frac{R_{ves}}{R_{core}} \right)^2 \quad (24)$$

where Φ is the anchor to lipid ratio which should not drop below 10% according to planar tBLM studies, R_{ves} is the radius of the supported vesicles and R_{core} is the radius of the solid nanoparticle core. The lower bound grafting density for the particle in this work estimates to 0.273 chains/nm² which is near that determined experimentally of 0.25 chains/nm²,

achieved when functionalizing at a 2:1 molar ratio of DSPE-PEG2k to surface amines. Although the experimental value is lower than the theoretical value predicted, experimental results indicate that the achieved grafting density is sufficient in producing tBLM nanoparticles. Additionally, we have demonstrated an ability to control this density by varying reaction quantities. It is believed that the use of cryo-electron microscopy could result in a more accurate estimation of the experimental construct.

Table 3. Intensity-averaged hydrodynamic diameters (HD) and ζ -potential (ZP) values of silica nanoparticles in acetate buffer and PBS, PEG layer thickness, grafting density and conformation of PEG2k and DSPE-PEG2k coated particles.

	Buffer	Amine	PEG-2k	DSPE-PEG2k	DSPC Liposomes
HD (nm)	Acetate, 10 mM, pH 4	138 ± 0.4	148 ± 0.8		104 ± 3.9
PdI		0.03 ± 0.01	0.03 ± 0.2		0.072 ± 0.01
ZP (mV)		+56.8 ± 0.9	+8.9 ± 0.2	Not Stable	+9.11 ± 0.95
HD (nm)	PBS, 1X, pH 7.4	Not Stable	141 ± 5.8		102 ± 6.3
PdI			0.02 ± 0.01		0.137 ± 0.01
ZP (mV)			-0.8 ± 0.3		-1 ± 0.32
PEG Layer Thickness (nm)		-	10.8 ± 0.8	-	-
Molar Ratio of DSPE-PEG2k to Surface Amines			2:1	2:1	4:1
Grafting Density (no. of chains/nm ²)			0.61 ± 0.14	0.25 ± 0.04	0.63 ± 0.04
Distance Between Attachment Points, <i>D</i>			0.45 ± 0.05	1.99 ± 0.16	1.26 ± 0.04
Conformation			Brush (RF > D)		-

HD: hydrodynamic diameter (nm); ZP: ζ -potential (mV); PdI: Polydispersity index; Results shown as mean ± standard deviation

Successful formation of the scaffold particles via attachment of DSPE-PEG2k to the particle surfaces was characterized by their behavior in suspension and with ATR-FTIR. Aminated particles exhibited stability within an acidic acetate buffer due to charge-charge separation, however, the scaffold particles remained unstable. The presence of the PEG layer on the scaffold particles traditionally would have provided steric stabilization within an aqueous solvent as shown with the PEG coated particles. However, the addition of the DSPE molecule to the exterior introduces a hydrophobic element that leads to aggregation of nearby particles.

Infrared absorptions were used to monitor functionalization of the constituent species. Component materials and scaffold nanoparticles were analyzed with ATR-FTIR. The aminated silica nanoparticles displayed characteristic peaks at 789, 948, 1051, 1634, 1700 and 3400 cm^{-1} . The IR absorption band around 1110 cm^{-1} is typical of asymmetric stretching vibrations associated with siloxane (Si-O-Si) bonds¹⁹⁹ and the broad peak between 3100 and 3600 cm^{-1} indicates the presence of exchangeable protons most likely from remaining hydroxyl groups on the surface of the particles.²⁰⁰ The DSPE-PEG₂₀₀₀-NHS compound used to form the scaffold nanoparticle exhibited peaks resulting from the DSPE, PEG₂₀₀₀ and NHS components. Both the DSPE and PEG components contributed to peaks around 2900 cm^{-1} (~2930 and 2970 cm^{-1}) which correlate with the asymmetric and symmetric stretching vibrations of CH₂ and CH₃ groups. Additionally, the PEG component contributed IR bands associated with the CH₂ wagging vibration (~1350 cm^{-1}) and C-O-C stretching vibrations (~1190 cm^{-1}). The IR absorption for DSPE around 1348 cm^{-1} is believed to be undetectable.²⁰¹ The peak around 1700 cm^{-1} is a contribution from the NHS ester used to form the amide bond during reaction with the aminated particles.²⁰² The

spectrum of PEGylated silica nanoparticles exhibited peaks at 2930 cm^{-1} and 2985 cm^{-1} which correlate with the asymmetric and symmetric stretching vibrations of CH_2 and CH_3 groups. Additionally, the same peaks can be found on the DSPE-PEG coated silica along with a peak around 1130 cm^{-1} which is likely from the C-O-C stretching vibrations of the PEG molecule. The presence of the characteristic peaks of silica and those from DSPE and PEG moieties after addition of the reactive species indicates proper functionalization. The reduced presence of these peaks in the spectra of **Figure 9** is likely a result of the low concentrations with which they are present on the surface of the particles. Note, following attachment of each moiety, the nanoparticles were washed multiple times with water and/or chloroform before measuring and component species should not remain.

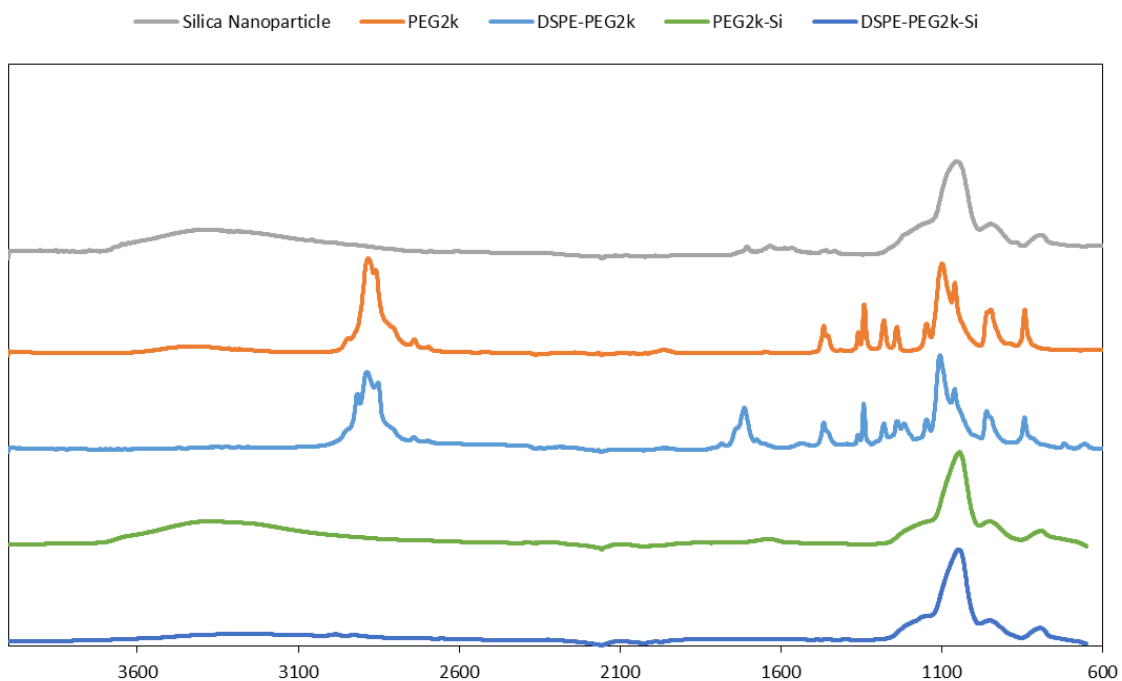


Figure 9. ATR-FTIR spectra of pure silica nanoparticles, pure PEG₂₀₀₀, pure DSPE-PEG₂₀₀₀-NHS, PEGylated silica nanoparticles, DSPE-PEG coated silica nanoparticles.

3.3.2 DSPC Adsorption on Silica Particles

When mixing phospholipid with silica nanoparticles, it is important to note there exists a maximum concentration of lipid that can exist on the particle surface in forming a single lipid bilayer. This maximum can be approximated using simple geometry of spheres and an estimation for the bilayer thickness. The length of the saturated and fully extended hydrocarbon chain can be estimated from

$$l[\text{\AA}] = 1.5 + 1.265n_c \quad (25)$$

where n_c is the number of carbon atoms.⁴¹ For DSPC, l approximates to 2.43 nm. Using this value, the membrane thickness can be approximated to 4.8 nm. This estimated thickness is similar to the 4.2 nm reported by Kucerka *et al.* at 60°C²⁰³ and 4.05 nm reported by Lewis *et al.* at 60°C²⁰⁴ and is a function of temperature. Using this value, the number of total phospholipids per liposome can be estimated. The outer layer surface area, A_{outer} in nm², can be approximated via the surface area of a simple sphere

$$A_{outer} = 4\pi r^2 \quad (26)$$

where r is the radius in nm. Assigning the bilayer a thickness of b in nm, the inner bilayer surface area, A_{inner} in nm², can be approximated via

$$A_{inner} = 4\pi(r - b)^2 \quad (27)$$

Adding equations [2] and [3] and dividing by the total surface area of a phospholipid head group, a in nm², we arrive at N_{tot} which is the total number of phospholipids within a liposome

$$N_{tot} = \frac{4\pi[r^2 + (r - b)^2]}{a} \quad (28)$$

If the concentration of lipid in solution is known, M_{lipid} in mol/L, the total number of liposomal particles can be calculated as N_{lipo} , where a has been found to be 0.43 nm² for DSPC²⁰⁵ and impact from cholesterol was ignored

$$N_{lipo} = \frac{(M_{lipid})(N_a)}{(N_{tot})(1000)} \quad (29)$$

where N_a is Avagadro's number. Along these lines, it makes sense to describe the amount of lipid added during composite formation in terms of surface area needed to produce a complete bilayer on the silica particle. This naming convention was described by Carmona-Ribeiro *et al.*,²⁰⁶ where A_V is the total surface area of vesicles in solution and A_P is the total surface area of silica particles in suspension as calculated from the number of particles and their mean diameter measured by TEM. In this sense, an A_V/A_P ratio equal to 1 would describe a situation where there was just enough lipid in suspension to cover the surface of the silica nanoparticle.

A_V/A_P ratios of 1, less than 1 and greater than 1 (correlating with fractions or multiples of this concentration) were explored to determine the influence of vesicle concentration on adsorption behavior of DSPC for aminated, PEGylated and scaffold nanoparticle types. The effect of varying lipid concentration on total lipid adsorbed is shown in **Figure 10**. The total amount of lipid adsorbed was found to be highly dependent on the surface characteristics of each nanoparticle type. The aminated particles showed an immediate increase to 4.35 ± 0.30 molecules of PC adsorbed/nm² at an A_V/A_P ratio of 1:1. This amount of lipid is near the theoretical maximum of a complete lipid bilayer encasing

the particles. This was followed by a slight decrease in concentration to 3.11 ± 0.25 PC adsorbed/nm² and subsequent linear rebound ($R^2 = 0.988$) toward the theoretical maximum concentration (~ 5.04 molecules of PC adsorbed/nm²). The increasing adsorption of DSPC onto the aminated particles is a function of the electrostatic interaction between the -P=O moiety of DSPC and primary amine on the surface of the particles.

The PEGylated particles showed a linear ($R^2 = 0.979$) increase of PC molecules adsorbed with increasing concentration of lipid added, never reaching the theoretical maximum over the concentration range explored. This behavior indicates that the PEGylated particles show less association of the lipid in solution and is in agreement with Ross *et al.*¹¹⁴ who found that bilayer assembly was not formed on PEGylated silica particles by vesicle fusion. This is further substantiated by PEG-modified planar substrates where hydrophobic modification is necessary to ensure vesicle adsorption and spreading.²⁰⁷

The scaffold nanoparticles exhibited similar behavior to aminated particles, indicating greater association of the lipid with the surface of the particle as free lipid concentration increased. The scaffold nanoparticles showed a greater concentration of lipid on their surface in comparison to PEGylated nanoparticles at an A_V/A_P ratio of 1:1 (0.424 μ mol lipid added) or greater. This increased association of lipid with the surface of the composite scaffold over the PEGylated particle indicates an increase in the affinity of the lipids for the surface of the scaffold particle. The presence of the tethered DSPE phospholipid on the surface of the scaffold particle enhances the interaction of free phospholipid added. These tethered DSPE phospholipids direct additional lipid onto the surface due to van der Waals attraction between the aliphatic chains and hydrophobic interactions. The scaffold particles had statistically significant differences in lipid

adsorption when compared to the aminated particles at 15:1 ($p = 1.6 \times 10^{-4}$) and 20:1 ($p = 3.7 \times 10^{-7}$) as well as at every concentration greater than 0.25:1 (0.106 μmol) in comparison to the PEGylated particles. For the scaffold particles, it was found that A_V/A_P ratios below 1 resulted in destabilization of the particles. This is believed to result from the formation of lipid bridges among the particles rather than complete bilayer formation.²⁰⁸ Both Troutier *et al.*⁹⁹ and Carmona-Ribeiro *et al.*¹⁸¹ report a similar trend but for the adsorption of dioctadecyldimethylammonium chloride and dipalmitoylphosphatidylcholine onto anionic poly(styrene) particles, respectively.

It has been suggested that the process of phospholipid vesicle fusion with glass supports is governed by Derjaguin-Landau-Verwey-Overbeek (DLVO).¹⁹ This is the same theory that is commonly used to describe colloid aggregation, making it a fitting model to describe the population of liposome and scaffold particles in suspension. DLVO theory is comprised of two forces, those of electrostatic repulsion and van der Waals attraction. Given that salt concentration can reduce the Debye length and decrease the overall electrostatic repulsion, it would be expected that ionic strength of the buffers used to form the particles would have a dramatic effect on interaction. Indeed, this same behavior was observed by Troutier *et al.*⁹⁹ with cationic lipids, where they found that stability of their bilayer encapsulated particles were a function of pH and ion concentration. For this reason, the pH and salt concentration were maintained at 7.5 and 10 mM, respectively, with monovalent tris buffer.

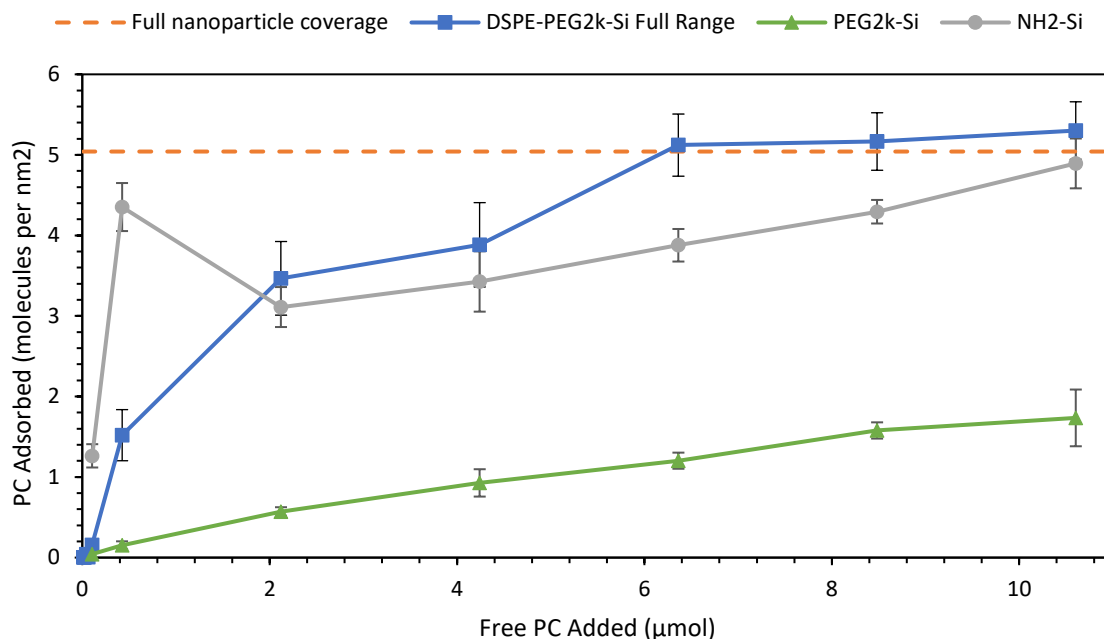


Figure 10. Adsorption of DSPC lipid onto aminated, PEGylated and DSPE-PEG2k coated silica particles.

The formation of supported lipid bilayers on the surface of the silica particles was observed with transmission electron microscopy (TEM). The aminated nanoparticles exhibited a smooth surface that is characteristic of silica. The PEGylated particle surface appeared the same as PEG itself is not viewable under the TEM and disintegrates under the electron beam. Although, its presence has been visualized with the help of a background stain.¹⁹⁶ Composite nanoparticles displayed a rough, undulating outer surface which is in stark contrast to the aminated and PEGylated particle surfaces. This surface morphology is characteristic of lipid coated nanoparticles and is believed to be an artifact of the drying step required for TEM.^{64,208,209} It is worth noting that the deposited lipid bilayer is susceptible to degradation by the electron beam. Extended exposure to the beam did result in the loss of the bilayer from the surface of the silica particles as shown in **Figure 11**.

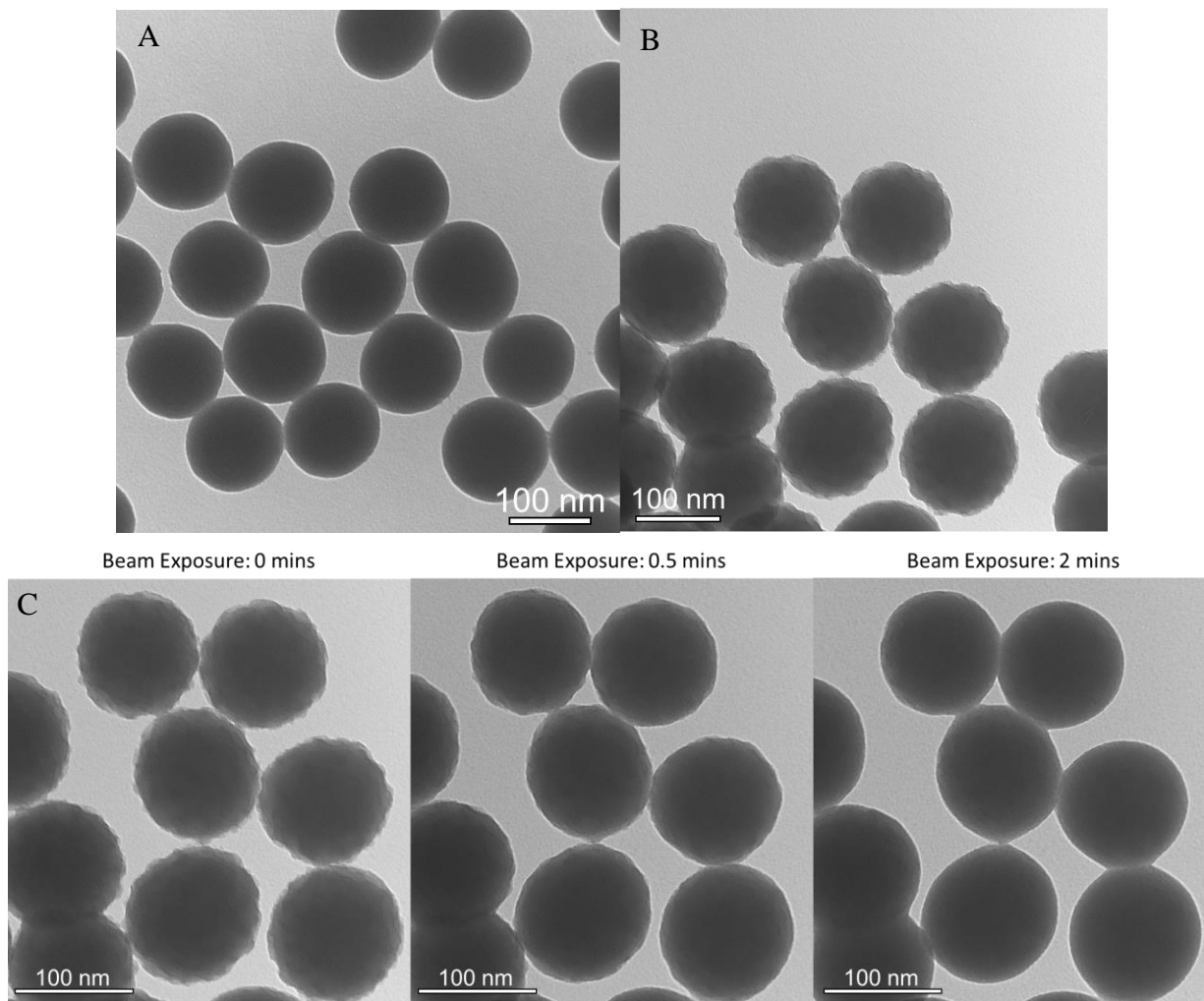


Figure 11. Surface morphology of aminated (A), PEGylated (B) and composite (C) nanoparticles visualized with TEM and effect of increased exposure to the electron beam on nanoparticle supported lipid bilayer degradation.

Sonication of lipid-particle suspensions has shown success producing lipid-coated mesoporous silica particles⁶⁴ and was implemented in this study to reduce the amount of time necessary to produce TMN. Sonication time was explored between 0 and 60 minutes at 15-minute intervals at an A_V/A_P ratio of 5:1. The amount of adsorbed lipid was quantified and the effect on hydrodynamic diameter and polydispersity observed. The amount of lipid detected on the PEGylated particles remained consistent regardless of sonication time,

while the scaffold particles showed an increase from 0.43 to 3 PC molecules adsorbed/nm² after 15 minutes and remained consistent at the 30, 45 and 60-minute timepoints. Following 15 minutes of sonication, significant differences in the amount of lipid adsorbed onto the particles were not found. The aminated particles actually exhibited a decrease in the amount of lipid adsorbed with sonication. At 0 minutes of sonication, the amount of lipid on the particles was found to be more than double that theoretically necessary to produce a complete bilayer on the particle. Following the vesicle fusion method of bilayer formation, this is likely a result of either a multilamellar structure encasing the silica particle or perhaps the adsorption of intact liposomes that refuse to disrupt according to the traditional vesicle fusion pathway.⁹⁵ Following 15 minutes of sonication, the concentration of lipid adsorbed decreased to 3.47 ± 0.63 PC molecules/nm² (similar to the scaffold nanoparticle) and remained consistent throughout the time span studied.

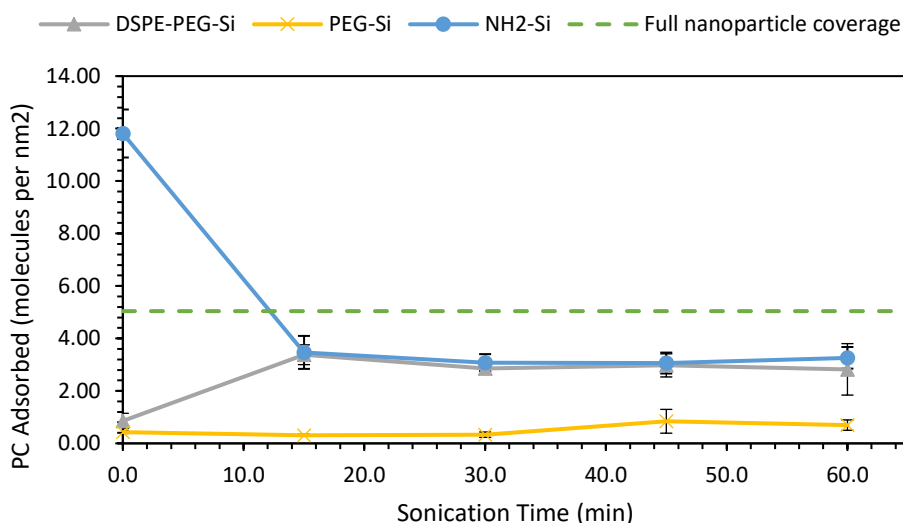


Figure 12. Effect of sonication time on amount of PC molecules adsorbed to the nanoparticles for DSPE-PEG2k-Si, PEG2k-Si and NH2-Si (n = 3).

Provided that membrane fluidity is a function of temperature, the bilayer is capable of maintaining two states: a gel phase and a liquid crystalline phase. The temperature at which this change occurs is termed the transition temperature and represents the median between a lipid bilayer gel phase and the liquid crystalline state (55°C for DSPC). To investigate the effect of DSPC membrane fluidity on bilayer formation, two temperatures were chosen: 4 and 65°C. TMN were mixed a 5:1 A_V/A_P ratio with liposomes and sonicated for 10 seconds. The particles were then incubated at their respective temperatures with continuous mixing. **Figure 13** displays the effects of temperature on the amount of lipid adsorbed onto the particles. The concentrations were statistically different at 0.424 (1:1, $p = 0.009$), 6.36 (15:1, $p = 0.041$) and 10.6 (25:1, $p = 0.004$) μmol of PC added. These results indicate that at the concentrations necessary to produce a complete bilayer on the particles, greater than 15:1, temperature has a significant effect. These results are consistent with those seen from Jing *et al.*²¹⁰ who found that vesicle fusion was a function of both liposome size and temperature. Above the transition temperature, DPPC liposomes 90 nm in size spontaneously ruptured on silica in a manner consistent with previous vesicle fusion descriptions.²¹⁰ However, at 160 nm the liposomes were found to adsorb but not rupture regardless of temperature, even at saturation. As a temperature gradient was imposed from 22°C to above the transition temperature (41°C), the 160 nm liposomes became more flexible and flattened until a complete bilayer was formed. It was hypothesized that below the transition temperature, the liposomes are more rigid and the activation energy for rupture at the point of minimum curvature is greater for the 160 nm liposomes in comparison to the 90 nm liposomes, indicating both a size and temperature dependence on forming an SLB. Noting the results of Jing *et al.*²¹⁰, it is believed that increased temperature

would lead to increased lipid adsorption at all sonication intervals if combined with the sonication method utilized in this study.

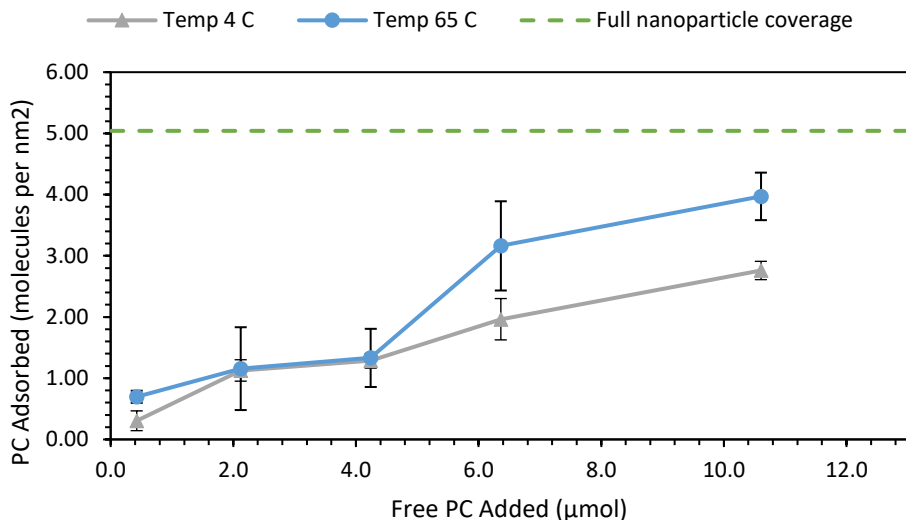


Figure 13. Effect of temperature on PC adsorbed with increasing concentration of PC in solution (n = 3).

3.3.3 Effect of Adsorption on Hydrodynamic Diameter and Zeta Potential

Quantifying the amount of lipid on the surface of the particles is useful for determining adsorption of the lipid in solution but it does not infer the behavior of the particles in solution. Thus, the hydrodynamic diameter (HD), polydispersity index and zeta potentials were determined via DLS. The HD of suspended nanoparticles represents the size of a hypothetical hard sphere diffusing in the solution.²¹¹ For silica nanoparticles this definition is apt, and as moieties are grafted to the surface of the particle an increase in the hydrodynamic diameter would be expected. The bare, aminated silica particles exhibited a HD of 138 ± 0.4 nm. This size rose to 148 ± 0.8 nm following attachment with PEG2k. It was not possible to measure the change in HD upon attachment of DSPE-PEG2k as the

particles were not stable in buffers nor a variety of organic solutions (e.g., chloroform, ethanol) given the hydrophobic character of the DSPE-facing exterior. However, it is believed that this size is relatively that of PEG2k given the grafting densities were similar (**Table 3**). Following adsorption of the DSPC bilayer to the particle, the HD varied depending on amount of lipid added during formation. Panel A of **Figure 14** displays the change in HD and polydispersity index (PdI) with increase in A_V/A_P ratio. Only ratios ≥ 1 were explored provided that ratios less than 1 were known to result in aggregation. The HD decreased as the concentration of lipid added increased, beginning at 245 ± 5.3 nm and decreasing to ~ 155 nm. Although there is theoretically enough lipid in solution at a 1:1 A_V/A_P ratio to encapsulate the particle in a lipid bilayer, it appears that defects in the bilayers may result in agglomeration. Additionally, the amounts of lipid are based on a simplistic geometrical model for surface area and inherently contains error. A plateau was quickly reached above an A_V/A_P ratio of 2.5:1 (1.06 μmol lipid), where increasing lipid concentration resulted in only minor differences in intensity-averaged diameters observed.

Examining the polydispersity indices for the same concentrations a similar trend is discovered. The PdI begins around 0.2 ± 0.02 for a 2:1 A_V/A_P ratio and decreases to ~ 0.1 , nearing that of the silica particle, as shown in Panel B of **Figure 15**. Note, the PdI for the bare silica particles was found to be ~ 0.03 . The rate of change is less than that of the hydrodynamic diameter, where lipid concentrations of 5:1 and greater displayed only minor changes among polydispersity. This data suggests that the concentration of lipid in solution can dictate the size and polydispersity of the TMN that is ultimately formed, with concentrations greater than 5:1 showing little to no difference among these two parameters.

The zeta potential of the TMN was determined at the same concentrations. Zeta potential values provide a measure of the electric potential at the slipping plane of the electric double layer and are often used to assess the stability of the particles in a suspension. For this study, the zeta potential was used to assess the change in surface potential with increasing lipid concentration on the TMN. As the amount of lipid incubated with the scaffold particles increased, the zeta potential values shifted towards neutral from their largely negative origin. At a 1:1 A_V/A_P ratio, the zeta potential was found to be -31.9 ± 0.7 mV. This value is likely a result of the externally grafted DSPE groups on the exterior. When the primary amine group of DSPE is synthetically grafted to the PEG2k molecule, this leaves the phosphate group as the sole charge in the otherwise zwitterionic species. As the concentration of lipid in solution increased, and consequently that on the particle, the zeta potential decreased to -21.7 ± 1.1 mV at 2.5:1, -14.8 ± 1.4 mV at 5:1 and finally levelling out at around -9.9 ± 1.6 mV at 15:1. This trend indicates a shift in the surface characteristics of the particles towards that of the DSPC liposomes, ~ -4 mV. Correlating this data with the increasing concentration of lipid that was found on the surface suggests that the adsorption of DSPC is reducing the overall zeta potential of the particles, and the surface is becoming more like that of DSPC liposomes.

Total energy input into the system was the final parameter investigated in producing TMN. The amount of energy was managed by changing the length of time the lipid-scaffold particle suspension was subjected to sonication. Sonication time was varied between 0 and 60 minutes at a fixed rate of 14 W. Note, rate increases to 28 and 42 W at similar time intervals did not show appreciable differences in lipid adsorbed (data not shown). Previous reports by Meng *et al.*⁶⁴ utilized 32.5 W for 20 minutes. At a 14 W input, this would amount

to 46.4 minutes – or approximately the 45-minute time point in this study. An A_V/A_P ratio of 5:1 was used in this study as it fell on the slope of the adsorption curve for both the TMN and aminated particles - where the greatest differences were expected to arise.

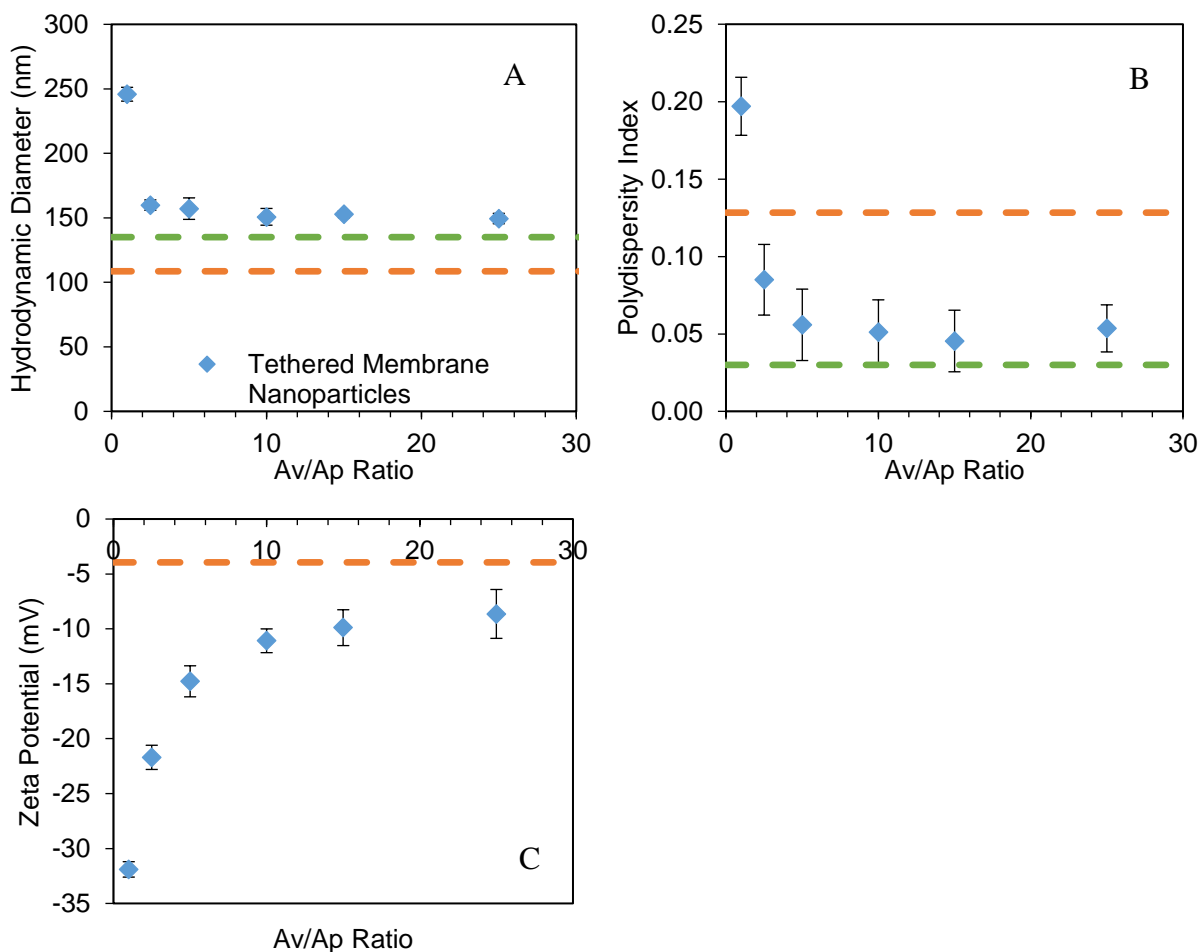


Figure 14. Increasing A_V/A_P ratio leads to a reduction in TMN size (A), decrease in polydispersity (B) and shift of zeta potential towards neutral (C). Orange line represents DSPC liposome properties and green line represents aminated silica nanoparticle properties. Error bars represent standard deviation of three separate experiments.

The HD of the TMN decreased from its initial starting position of 244.8 ± 20.3 nm at 0 minutes to 161.3 ± 5.9 nm at 30 minutes and 160.5 ± 5.7 nm at 60 minutes of sonication. There were not large differences among the 30, 45 and 60-minute time points. The

PEGylated nanoparticles increased in HD with increasing sonication time, beginning at 217.8 ± 24.6 nm in size and reaching 431.4 ± 176.6 nm after 60 minutes. Additionally, the variation among samples generally increased with sonication time as observed in the standard deviation increase. The DSPC liposomes decreased from 108.4 ± 1 nm to 76.4 ± 2.8 nm after 60 minutes of sonication. This decrease was expected as sonication of liposomes has long been used to decrease the overall size of a liposome suspension.²¹² The aminated particles exhibited aggregation at all time points as indicated by a HD above 1300 nm at each time point with great variability among the samples. This data is shown in Panel B of **Figure 15**. This behavior is likely a result of lipid bridging among the nanoparticles even though there is excess lipid in solution.²⁰⁸

The polydispersity of the aminated particles remained consistent at ~ 0.4 throughout all sonication time periods. The PEGylated particles increased in polydispersity from 0.34 ± 0.1 to 0.55 ± 0.3 and the DSPC liposomes increased from 0.02 ± 0.01 to 0.177 ± 0.01 after 60 minutes of sonication. The TMN were the only particles to show a decrease in polydispersity with increasing sonication time. Initially upon mixing the liposome suspension with the scaffold particles, the scaffold particles remain unstable due to the highly hydrophobic exterior presented by the DSPE moieties with a PdI of 0.442 ± 0.1 . After 15 minutes of sonication, this value decreases to 0.143 ± 0.04 before further decreasing to 0.10 ± 0.03 after 60 minutes of sonication indicating stabilization of the particles from adsorption of lipid to their surface. This character of stabilization was not observed by any other particle type.

The zeta potential of the aminated particles remained slightly positive (~ 5 mV) throughout the sonication time frame but dipped down to 0.1 ± 2.1 mV at the 60-minute

point. The PEGylated particles decreased in from -5.7 ± 1.3 mV to -8.1 ± 0.4 mV and the DSPC liposomes remained consistently at ~ -2 mV. The scaffold particle showed the greatest change, beginning at -26.3 ± 0.9 mV and became more neutral with increased sonication time to -11 ± 0.7 mV at 60 minutes. This shift towards neutral, and towards that of pure DSPC liposomes, is an indication of the surface being covered with additional lipids. As previously mentioned, the DSPE-PEG2k molecules decrease the zeta potential with their negative phosphate groups, but as these are covered up by the forming bilayer and zwitterionic DSPC molecules, the charge shifts neutrally.

These differences in HD, PdI and zeta potential among the scaffold, PEGylated and aminated particles indicate a direct effect of surface properties on the formation of a supported lipid bilayer under the conditions explored. The presence of DSPE-PEG2k on the surface of the nanoparticle has demonstrated a clear advantage in the predictability of size, dispersity, stability and surface charge. Monitoring of the zeta potential also demonstrates an effective way of characterizing the transition of the scaffold particle from its initial state (highly negatively charged) towards that of the zwitterionic DSPC liposomes (more neutrally charged) as the lipids associate with the surface.

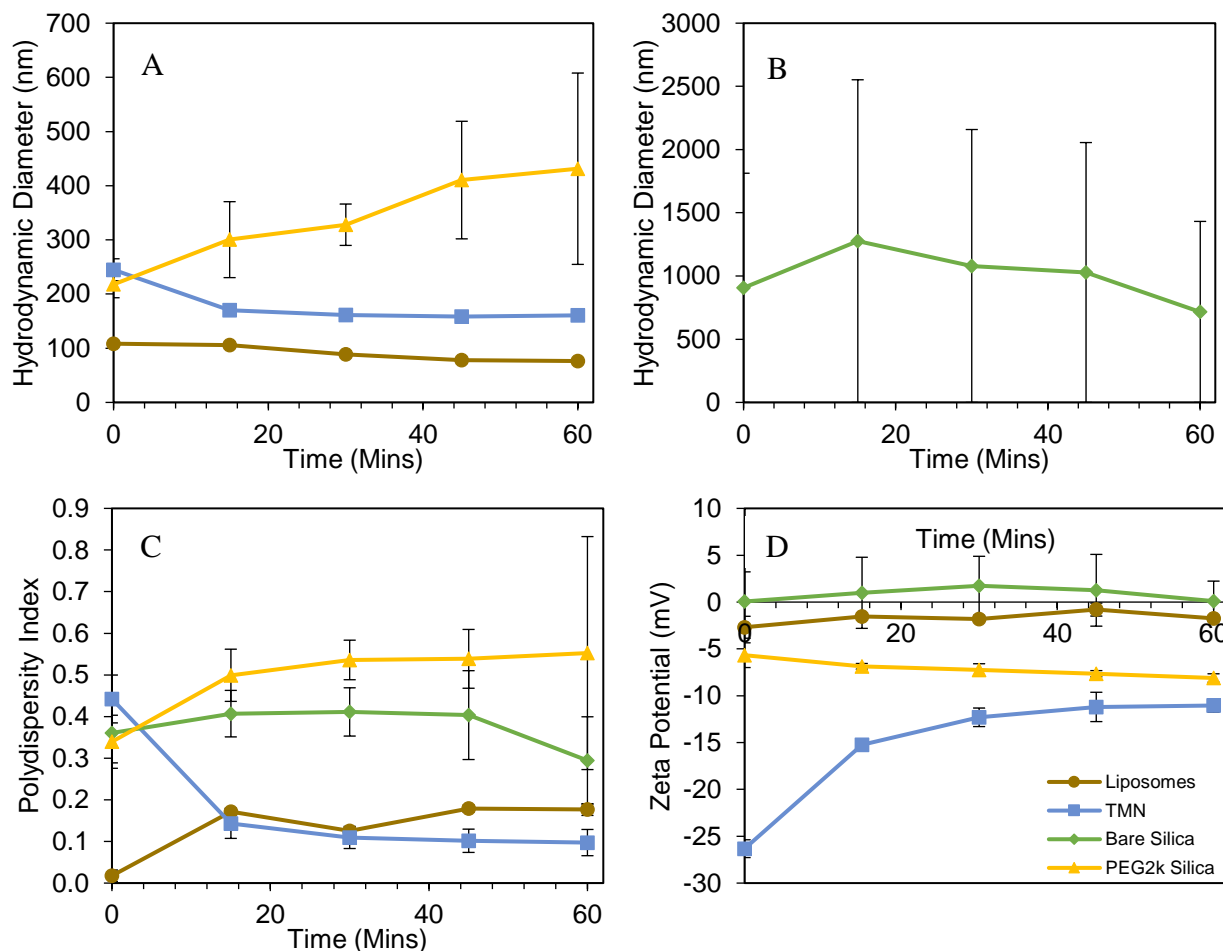


Figure 15. Increasing sonication time affects hydrodynamic diameter (A and B), polydispersity (C) and zeta potential of each particle type: liposomes (brown), tethered membrane nanoparticles (blue), amine coated silica (green) and PEG coated silica (yellow). Error bars represent standard deviation of three separate experiments.

3.3.4 Membrane permeability assessment

Our lab has previously used carboxyfluorescein (CF) as a model to measure the release of intraluminal contents.^{192,213} Release of CF from the TMN was compared with DSPC liposomes prepared via extrusion. TMN constructed from four different A_V/A_P ratios were compared, two on the slope of the adsorption curve and two at the plateau. TMN formed at 10, 15 and 25:1 ratios were found to release CF at a slower rate than the TMN constructed at a 5:1 ratio. The 5:1 TMN quickly released $20 \pm 7.5\%$ of its loading after

three days of incubation while the 10:1 TMN released $12.8 \pm 4.1\%$ and the other two ratios were less than 10%. After six days of incubation, all four TMN converged with release between 15 and 20%. It should be noted that this release may be an artifact of the washing procedure, where the dye that is “releasing” is actually only adsorbed to the exterior of the particles. An extended release profile over a longer period of time should clarify these results.

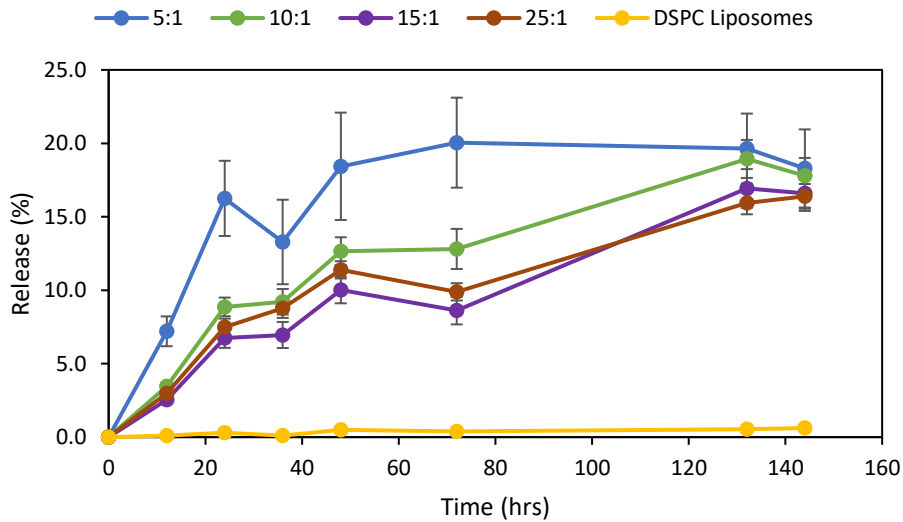


Figure 16. Release profiles of carboxyfluorescein for DSPC liposomes and TMN produced at different A_V/A_P ratios (connecting lines drawn to guide the reader’s eye).

This data was fit to a commonly used solute release model to help identify the mechanism of release. Peppas and coworkers^{214,215} have developed a simplification of the Higuchi model²¹⁶ for solute release

$$\frac{M_t}{M_\infty} = kt^n \quad (30)$$

where k represents an experimental constant and n is the diffusional exponent that describes the release mechanism. This model has previously been applied to

polymersomes.²¹⁷ The data for 5:1 and 15:1 A_V/A_P ratios were selected to model as they exhibited the greatest overall difference. The model parameters are enumerated in **Table 4** and the results of the fit are shown in **Figure 17**. The 5:1 and 15:1 release profiles yielded exponents of 0.33 and 0.68, respectively. The 0.33 value of 5:1 is closer to Fickian release than zero-order but still falls below the model's threshold of 0.43. The model does hold a better fit (R^2 of 0.80 versus 0.66 when linearized) for the data collected at 72 hours and before. It is known that one of the limitations of this model is that it only applies to the initial 60% of release.²¹⁵ An extended release study that examines full release of CF may help characterize this behavior to a greater extent. The exponential parameter for 15:1 was 0.68 which correlates with anomalous release, or non-Fickian release. It is worth noting that this release profile also had a linear fit with an R^2 value of 0.92, perhaps indicating a more zero-order like character – or concentration-independent release.

Table 4. Diffusional exponents, n , fitting parameters, k and diffusion mechanisms for non-swelling controlled release systems.

Mechanism/Sample	Exponent (n)	k
Fickian diffusion	0.43	-
Anomalous (non-Fickian)	$0.43 < n < 1.0$	-
Zero-order release	1.00	-
5:1	0.33	4.30
15:1	0.68	0.591

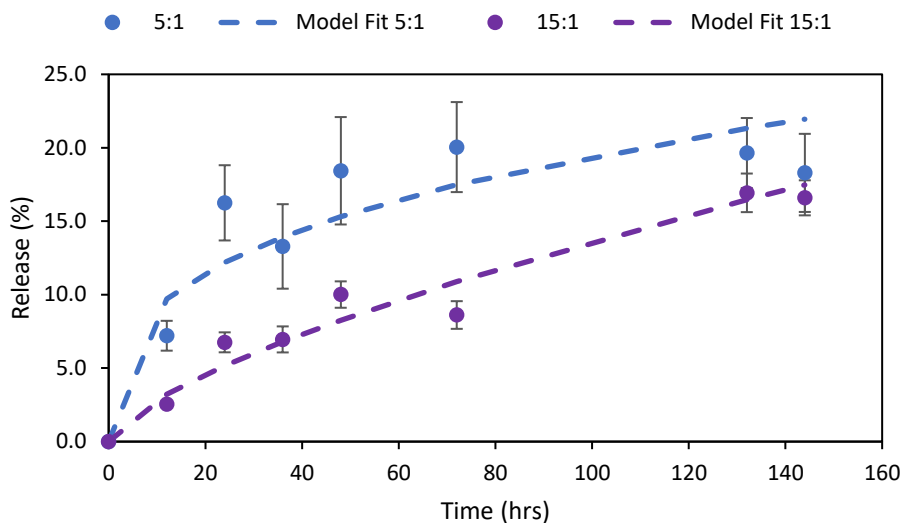


Figure 17. Isolated release profiles of carboxyfluorescein from tethered membrane nanoparticles with A_V/A_P ratios of 5:1 and 15:1.

From these release profiles it is clear that the amount of lipid introduced into solution when forming the TMN does have an effect on the release of CF. This is likely a result of the array of bilayer intactness achieved while varying A_V/A_P ratio. These release profiles contrast to the DSPC liposome controls which released less than 1% of CF over the same period, which is consistent with our previous reports.^{192,213} Although there is a significant difference between the release from the TMN and the liposomes, it should be noted that no optimization was conducted on the lipid formulation for the TMN. An optimal lipid coating likely exists that enhances the entrapment of CF and further prevents release until desired.

3.4 Conclusion

Deposition of lipid bilayers onto silica nanoparticles with a tethered inner monolayer has been demonstrated. TMN formation was found to be a function of sonication time, temperature and ratio of lipid to nanoparticle surface area. The TMN

formed associate the advantages of nanoparticles and lipids. These include a solid core that acts as a scaffold, providing mechanical stability, morphology and a narrow size distribution. The advantages of a lipid coating have been previously outlined and include biocompatibility and biomimetic behavior. We believe this nanoparticle system has broad potentialities for use as a therapeutic vector and drug delivery reservoir, model membrane systems, or as a support for biomolecule screening.

Chapter 4: Application of Tethered Membrane Nanoparticles in the Treatment of Prostate Cancer

4.1 Introduction

Prostate cancer is the third most common type of cancer and ranks 6th among the estimated number of deaths expected from cancer for 2018. Prostate cancer (PCa) is the most common type of cancer among men, affecting about 1 in every 7, and accounts for 1 in every 5 new cancer diagnoses.²¹⁸ PCa presents as a solid tumor, making the use of nanoparticle formulations an adept choice for taking advantage of the enhanced permeability and retention effect (EPR).^{219,220} Chronic inflammation combined with reactive oxygen species (ROS) generation are putative risk factors for PCa development.²²¹ Nanoparticles have been explored to deliver both chemoprevention agents and traditional chemotherapeutics.²²² Chemoprevention agent delivery have included the use of natural antioxidants such as those found in green tea polyphenols.²²³ These polyphenols possess antioxidant properties that protect cells against the damaging effects of reactive oxygen species.²²⁴

Nanoscale drug delivery systems such as liposomes and nanoparticles have received tremendous attention and focus within the scientific community towards the development of treatments for cancer.⁹ This focus is a result of the unique properties nanoscale materials provide, including high surface area-to-volume ratios that permit decoration with drug, polyethylene glycol and targeting agents; as well as a size range that

promotes extravasation into the tumor microenvironment. Attachment and/or incorporation of drugs within nanoparticle scaffolds has been used to control drug release profiles. Nanoparticles also provide an opportunity to deliver therapeutic agents alongside diagnostic probes, useful in determining disease state and progression. Liposomal formulations offer the ability to encapsulate both hydrophilic and hydrophobic drugs, often with unfavorable pharmacokinetic properties, and PEGylated liposomes have seen significant increases in circulation residence times. Through the manipulation of these material properties, there have been significant advances and even approval of nanoscale formulations.³⁹

Lipid composition is an important metric in developing effective and stable drug delivery platforms. Additionally, composition can be used to anticipate the behavior of lipid-based drug delivery systems *in vivo*. Factors that are often focused on include blood clearance and distribution. It has been found that the use of solid-phase lipids such as distearoyl phosphatidylcholine in combination with cholesterol have demonstrated increased blood residence time and reduced uptake by the RES. This enhanced effect was attributed to the rigid bilayer, negative surface charge and the use of carbohydrate-containing lipids.¹⁴⁹ Additionally, the inclusion of cholesterol has been shown to increase stability, preventing lipoprotein-induced destabilization. The unique properties of lipids provide an ability to design a delivery system with specific release and stability characteristics in mind.

Nanoparticles provide a capability in overcoming the dose-limiting side effects typically associated with chemotherapeutics. However, solid nanoparticles often exhibit rapid clearance upon administration *in vivo*, leading to poor residence times. PEGylated

liposomes, on the other hand, have been associated with long circulation times and increased pharmacokinetics of drug. Combination of these two delivery systems provides the opportunity to create a composite nanoparticle system exhibiting the long residence times associated with liposomes and the potential for tailorable release profiles and/or use as a theranostic agent.

Here we present the development of a tethered membrane nanoparticles (TMN) for use as a drug delivery vehicle. Stability of the TMN was determined in serum and the effect of lipid bilayer composition on expected circulation half-life was determined via incubation with macrophage cells. Finally, TMN and liposomes were remote loaded with doxorubicin (DOX) and administered *in vitro* to PC-3 prostate cancer cells.

4.2 Materials and Methods

Materials and methods were the same as Chapter 2 except where indicated.

4.2.1 Materials

All materials were purchased from commercial suppliers and used without further modification, unless noted otherwise. Amine modified (Lot: JEA0116) silica nanoparticles were purchased from nanoComposix (San Diego, CA). N-Hydroxysuccinimide (NHS) functionalized methoxy polyethylene glycol (m-PEG-NHS) polymer and 1,2-distearoyl-sn-glycero-3-phosphoethanolamine bonded to polyethylene glycol (DSPE-PEG-NHS) lipid polymer in 2k Da molecular weight were purchased from Nanocs, Inc. (New York, NY). 1,2-distearoyl-sn-glycero-3-phosphocholine (DSPC) and 1,2-distearoyl-sn-glycero-3-phosphoethanolamine-N-[methoxy(polyethylene glycol)-2000] (ammonium salt) (mPEG2k-DSPE) were purchased from Avanti Polar Lipids (Alabaster, AL). 1,1'-

dioctadecyl-3,3,3',3'-tetramethylindodicarbocyanine, 4-chlorobenzenesulfonate salt (DiD) was purchased from Invitrogen (Carlsbad, CA). Fluorescamine, p-methylaminophenol sulfate (99%), ethanolamine (98%), sodium hydroxide (NaOH), oxalic acid anhydrate (98%), ammonium molybdate tetrahydrate (99%) and 4-(2-hydroxyethyl)-1-piperazineethanesulfonic acid (HEPES, 99%) were purchased from Alfa Aesar (Ward Hill, MA). Silica standard was purchased from Ricca Chemical (Arlington, TX). Dimethyl sulfoxide (DMSO), sulfuric acid, and 37% hydrochloric acid (HCl) were purchased from BDH (VWR, Randor PA). Anhydrous sodium sulfite, sucrose, cholesterol, fluorescein isothiocyanate (FTIC), thiazoyl blue tetrazolium bromide (MTT) and tris(hydroxymethyl)aminomethane were purchased from AMRESCO, Inc. (Solon, OH). Carboxyfluorescein was purchased from Acros (New Jersey, USA). Doxorubicin was purchased from TCI America (Portland, OR). Deionized water used throughout the study was obtained from a Milli-Q Purelab Flex 2 water purification system (ELGA, LLC, Woodridge, Illinois, IL).

4.2.2 Cell Lines

Authentication of cell lines was confirmed by the National Institute of Standards and Technology, using a multiplex PCR assay. Cells were maintained in Ham's F-12K (Kaighn's) nutrient mixture with L-glutamine (Corning cellgro, Manassas, VA), supplemented with 10% fetal bovine serum (FBS) from VWR Life Science Seradigm (Radnor, PA) and 1% penicillin/streptomycin purchased from (Corning cellgro, Manassas, VA). RAW cells were maintained in Dulbecco's Modified Eagles Medium (DMEM)/High Glucose (HyClone, GE Healthcare Life Sciences), supplemented with 10% FBS and 1% antibiotics. Both cell lines were incubated at 37°C in 5% CO₂.

4.2.3 Liposome Preparation

Liposomal formulations were prepared by mixing 1,2-distearoyl-sn-glycero-3-phosphocholine (DSPC) with cholesterol at a 10:5 molar ratio for, respectively, in chloroform for DSPC liposomes and a 9:5:1 molar ratio of DSPC, cholesterol, mPEG₂₀₀₀-DSPE for sterically stabilized liposomes. Dry lipid films were prepared via evaporation of the chloroform in a Rotavapor R-210/R-215 (Buchi, New Castle, DE, USA) under a constant stream of nitrogen. The thin lipid film was dispersed in 10 mM tris buffer at pH 7.5 and subjected to 7 freeze-thaw cycles before being extruded 7 times through a 0.08 μm double stacked polycarbonate membrane in a high-pressure homogenizer (Lipex, Transferra Nanoscience Inc., Burnaby, B.C., Canada). Final particle size was verified with dynamic light scattering with a mean particle diameter of 117 ± 0.32 nm and a PDI of 0.016. Liposomes were stored at 4°C and used within 3 weeks of formulation. Lipid concentration was determined via quantification of inorganic phosphate following acid hydrolysis.¹⁸⁸

Fluorescent DiD-labeled liposomes were prepared according to Kamps *et al.*²²⁵ with slight modifications. Briefly, 1 mol% DiD was added to a mixture of lipids and cholesterol in chloroform. DiD was added before the solution was evaporated and a lipid film produced. The lipid film was rehydrated in tris buffer or ammonium sulfate depending on whether the liposomes were to be loaded with doxorubicin. The remaining portion of the procedure was the same as above.

4.2.4 Preparation of Doxorubicin Liposomes

Doxorubicin loaded liposomes were prepared by remote loading with an ammonium sulfate gradient as described previously.^{226,227} Briefly, lipids and cholesterol

dissolved in chloroform were mixed and dried using a rotary evaporator. The formed thin lipid film was hydrated with 250 mM ammonium sulfate (pH 5.0) and subjected to 7 freeze-thaw cycles before being extruded 10 times through a 0.08 micron double stacked membrane in a high-pressure homogenizer (Lipex, Transferra Nanoscience Inc., Burnaby, B.C., Canada). Following extrusion, the liposomes were placed in a water bath at 4°C for ten minutes to gel the membrane and then dialyzed overnight in an isotonic 10% (w/v) sucrose solution at 4°C to remove excess ammonium sulfate. Doxorubicin was then added to the liposomes at a 0.2:1 molar ratio and incubated at 65°C for 1 hour with mixing every 15 minutes. The loaded liposomes were dialyzed overnight with a 10% (w/v) sucrose solution. Doxorubicin loading was quantified spectroscopically in acidified ethanol.²²⁸

4.2.5 Preparation of Doxorubicin TMN

TMN were prepared as previously mentioned in Chapter 3. In order to load doxorubicin, liposomes were mixed with scaffold nanoparticles but in the presence of ammonium sulfate rather than tris buffer. 500 mM ammonium sulfate was used to dilute the scaffold particle-lipid mixture to arrive at final concentration of 250 mM. Upon formation, the TMN were separated from excess lipid via centrifugation and resuspended via pipetting into isotonic 10% (w/v) sucrose. Doxorubicin was then added to the composites at a 1:1 molar ratio and incubated at 65°C for 1 hour with mixing every 15 minutes. The loaded composites were incubated in a refrigerated water bath for 10 minutes before centrifuging to remove excess doxorubicin. Doxorubicin loading was quantified spectroscopically in acidified ethanol.²²⁸

4.2.6 Serum Stability

Nanoparticles, whether liposomes, TMN or silica particles, were added to phenol free F-12K basal media supplemented with 10% fetal bovine serum. Particle suspensions were analyzed with dynamic light scattering at 0, 24, 48, 72, 96, 144 and 184 hours and then 1 and 2 month intervals to observe changes in hydrodynamic diameter and polydispersity.

4.2.7 Cell Staining and Fluorescent Microscopy

RAW 264.7 cells were plated in a 24 well plate and/or chamber slide at a concentration of 50,000 cells per well. After 24 hours of equilibration time, culture media was removed and treated with media containing FITC-stained TMN or DiD liposomes at 1, 0.1, 0.01, 0.001 mg/mL. Particles were incubated with the cells for 4 hours. Following treatment, cells were washed once with PBS and fixed with 10% neutral buffered formalin. They were then permeabilized with 0.1% Triton X-100 and incubated with blocking buffer (1% BSA in PBS) before addition of cellular stains. Cell processes were stained with Alexa Fluor 488 Phalloidin and nuclei with Hoechst 33342. Fluorescent images were captured with an EVOS cell imaging system (ThermoFischer Scientific, Waltham, MA, USA).

4.2.8 Flow Cytometry

Nanoparticle samples were analyzed with a BD Accuri C6 flow cytometer (BD Biosciences, San Jose, CA, USA) containing two lasers (488 and 635 nm). The instrument was set up with a 533/30 band pass filter to examine fluorescence emitted by 488 nm laser excitation and a 675/25 band pass filter was used to examine fluorescence emitted by 635 nm laser excitation. A threshold of 10,000 on FSC was set, with a flow rate of 12 μ L/min and data recorded for 2 minutes. The cytometer was flushed with DI water until the events/s

were less than 100. Fluorescein isothiocyanate (Ex/Em: 490/525) was used to label silica nanoparticles. Fluorescein isothiocyanate (FITC) was reacted with nanoparticle surface amines at a 2:1 molar ratio in a 50% dimethyl sulfoxide-ethanol mixture. DiD (Ex/Em: 644/665) was used to label lipid bilayers and was incorporated within the liposomal formulation at 1% of the total lipid concentration (e.g., 0.1 μmol in a 10 μmol prep).

4.2.9 Measurement of MTT Staining

The ability of cells to metabolize 3-(4,5-dimethylthiazol-2-yl)-2,5-diphenyltetrazolium bromide (MTT) into insoluble formazan crystals was used as an indicator of toxicity.²²⁹ Results were corroborated with phase contrast microscopy. Cells were seeded in 96 well plates at 1×10^4 cells per well. After 24 hours of equilibration time, culture media was removed and cells were treated with media containing nanoparticle formulations. Doxorubicin concentrations in the range of 1 to 10 μM were used. This range bookended the as the dose, 2.5 μM , that resulted in ~50% cell kill after 72 hours in the PC-3 cell line. After 24, 48 and 72 hours 50 μL of 2 mg/mL of MTT was added to each well and incubated for 4 hours. The media containing particles and MTT reagent was aspirated and 150 μL of dimethyl sulfoxide (DMSO) was applied to the cells to solubilize formed formazan crystals. Plates were shaken vigorously for 5 minutes and then the absorbance measured at 540 nm using a SpectraMax i3 (Molecular Devices, Sunnyvale, CA). The data were ratioed to an untreated control and the values plotted against the concentration of doxorubicin incubated.

4.3 Results and Discussion

4.3.1 Stability Study in Serum

Within biological fluids, proteins bind to the surface of nanoparticles and form what is referred to as the protein corona. This protein corona can influence the interaction nanoparticles have with a biological system.²³⁰ Serum incubation studies provide a measure with which to assess particle stability upon administration *in vivo* and has recently been used to evaluate the kind of protein coats formed on the surface of nanoparticles.²³¹ Although particles may be engineered to be inherently stable, it is possible that changes to the surface can occur as proteins adsorb, leading to instability and aggregation.²³² These protein coats have been found to form within minutes of incubation and to be a function of nanoparticle size, surface charge, surface energy and roughness.²³³ Employing the understanding of protein coat formation, some researchers are even looking at developing methods to target specific nanoparticle-protein complexes with the goal of better predicting and controlling circulation residence times and biodistribution.²³⁴ These studies have examined formation of protein coats with differing particle surface characteristics in serum conditions and identified the proteins adsorbed. Similar studies have identified a link between nanoparticle surface characteristics and macrophage uptake.²³⁵ Our lab has previously demonstrated a correlation between *in vitro* macrophage uptake and clearance *in vivo*,¹⁸⁷ making serum stability assessment an apt estimation of nanoparticle behavior *in vitro* and *in vivo*.

TMN were formed in the presence of varying concentrations of DSPC liposomes. It was recognized that concentrations below an A_V/A_P ratio of 1 would result in agglomeration. TMN were formed with A_V/A_P ratios of 1, 2.5, 5, 10, 15, and 25:1. These

particles were incubated in culture medium containing 10% FBS and changes to their HD and PdI monitored with DLS. **Figure 18** and **Figure 19** display the results recorded over an 8 day period. There appears to be a lower bound for A_V/A_P ratio in producing the TMN. It was found that the 1 and 2.5:1 ratios produced the greatest variability in HD and PdI. At a 2:1 ratio, the HD of the particles began at 300 nm and showed greater sizes throughout the course of study. All other lipid ratios hovered around 160-180 nm depending on the time point.

A similar trend was observed with the PdI values. Lipid ratios of 1 and 2.5:1 showed the greatest variation with TMN formed at 10:1 and above exhibiting more consistent PdI values. A_V/A_P ratios of 5, 10, 15 and 25:1 yielded PdI values below 0.2, indicating monodisperse samples, at all time points and varied between 0.12 and 0.18 depending on lipid ratio and time point. Particles formed with a 1:1 ratio consistently exhibited PdI values greater than 0.3, indicating greater polydispersity, and had the greatest amount of variation among data points. This variability in PdI can also explain the fluctuation in HD, where the z-average values recorded are simply an average of the intensity-weighted peaks in the samples and doesn't represent a true diameter distribution of the particles in suspension. Visual observation of the samples also support the conclusion that these particles were less stable and agglomerated. Initially, the particles produced with a 5:1 A_V/A_P ratio yielded PdI values similar to the higher ratios but over time, showed increasing polydispersity. Similar stability of the particles at the 30 and 60 day time points was observed for the 5, 10, 15 and 25:1 A_V/A_P ratios. These results suggest that upon initial formation of the protein corona on the nanoparticle surface, additional incubation in the serum environment has no effect on the stability of the particles, for a given SLB covering.

The lack of significant differences among particles with A_V/A_P ratios greater than 5:1 is likely a result of the polymer layer. Proteins in solution have been shown to nonspecifically adsorb at defect sites on solid supported bilayers lacking a polymer cushion. These kinds of defects have been found to have a detrimental impact on biosensor design.²³⁶ It is believed that the presence of the PEG polymer cushion reduces nonspecific adsorption of proteins from suspension and yields stable particles over the time span investigated. Additionally, the higher concentrations of lipid in suspension would prevent agglomeration of the particles due to lipid bridging.²⁰⁸

The two controls used in this study were PEGylated silica particles and DSPC liposomes. The PEGylated silica particles were stable in suspension for the first 6 hours. At the 6-hour time point the particles began to agglomerate considerably, and variation among samples became substantial. These particles' PDI value was initial below 0.1, indicating highly monodisperse distributions, but quickly ballooned to greater than 0.4 with variability at each time point (error bars were removed for clarity). The DSPC liposome control showed consistent diameters around 120 nm throughout the study and PDI values around or below 0.2 throughout. This indicates an influence from the chemical nature of the nanoparticle surface (compare PEGylated with SLB-NP) on protein adsorption and stability, which is consistent with previous studies.¹²

The application of the tethered lipid bilayer to the surface of the silica particles demonstrates enhanced stability of the silica particles in compete culture media over PEGylated particles. This behavior is similar to that of the liposome control, where HD and PDI remain consistent at the same time intervals. This effect on stability is similar to that reported by Moura *et al.*, who found enhanced colloidal stability of silica particles at

high ionic strengths as a result of an applied phosphatidylcholine membrane.¹⁰⁵ This is further supported by Durfee *et al.*¹⁹ who postulated that the stability in serum of a zwitterionic lipid coated mesoporous silica particles was due to the zwitterionic nature of the membrane and less with the attached PEG. These results suggest an intense effect of incorporating the SLB on nanoparticle stability and suggest its use as a drug delivery vehicle may be dramatically impacted, perhaps with greater residence times *in vivo*.

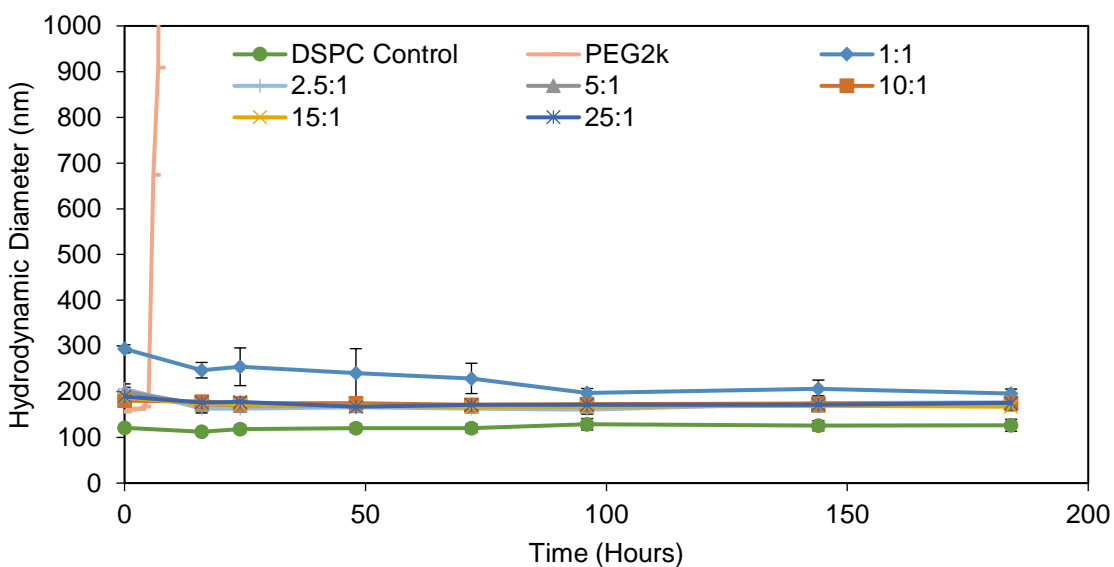


Figure 18. Hydrodynamic diameters of DSPC coated TMN with different lipid concentrations incubated in 10% FBS supplemented F12-K media for 8 days. PEG2k coated particles and DSPC liposomes shown as controls. Error bars represent standard deviation (n=3). PEG2k error bars removed for clarity.

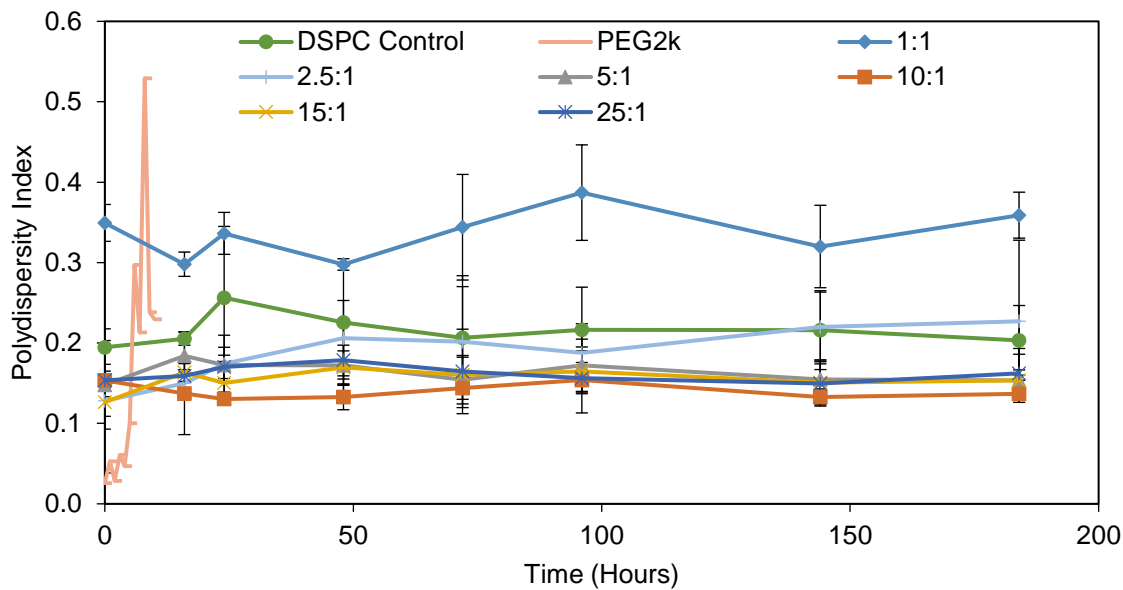


Figure 19. Polydispersity index values of DSPC coated TMN with different lipid concentrations incubated in 10% FBS supplemented F12-K media for 8 days. PEG2k coated particles and DSPC liposomes shown as controls. Error bars represent standard deviation (n=3). PEG2k error bars removed for clarity.

4.3.2 Effects of TMN Surface Character on Macrophage Cell Uptake

The application of a lipid bilayer to nanoparticle surfaces has been proposed as a way to enhance the biomimetic nature of the encapsulated particles.⁹⁷ To this end, an *in vitro* simulation was conducted that mimics the RES process found *in vivo*. Uptake studies were performed with RAW 264.7 cells, which have been used to correlate *in vivo* macrophage uptake.¹⁸⁷ The TMN were incubated with RAW264.7 cells for four hours and the nanoparticle uptake assessed via flow cytometry. The TMN were tagged with two separate fluorescent dyes to facilitate comparisons among liposomes and silica nanoparticles. FITC was used to tag the silica nanoparticle core and DiD was used to label the lipid bilayer as shown in **Figure 20**. TMN were incubated at three different concentrations. Silica particle concentrations of 0.001, 0.01 and 0.1 mg/mL were chosen

for comparison. Liposomes were administered at the same particle number concentrations. For 0.001, 0.01 and 0.1 mg/mL this correlated with 5.6×10^8 , 5.6×10^9 and 5.6×10^{10} particles/mL, respectively.

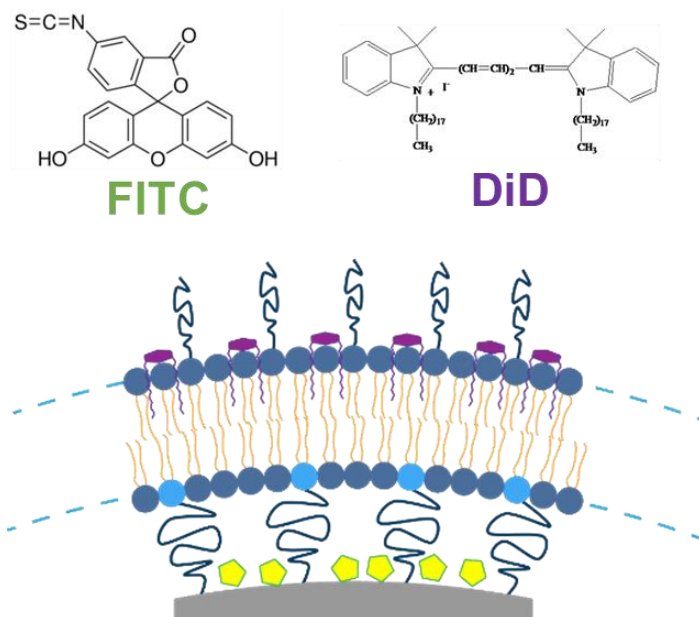


Figure 20. Pictorial representation of FITC and DiD fluorescent labels incorporated within tethered membrane nanoparticles.

Figure 21 shows the dot plot of the labeled TMN in comparison to the control. As particle concentration increased, the population of cells on the dot plot moved up and to the right. This indicated an increase in fluorescence intensity of DiD (up) and FITC (right). The RAW 264.7 cells were incubated with TMN with two different surface coatings, DSPC (left plot) and SSL (right plot), to examine the effect of incorporating a PEG brush border on the surface of the particles. The plot on the left of DSPC coated composites shows a significant increase in uptake in comparison to the plot on the right of SSL coated particles. In general, the SSL particles lag behind DSPC in uptake as would be expected with a PEGylated nanoparticle. FITC displayed lower overall fluorescence intensity in

comparison to DiD. This is believed to result from a shielding effect from its incorporation within the lipid bilayer, on the particle surface and its relative intensity compared with DiD.

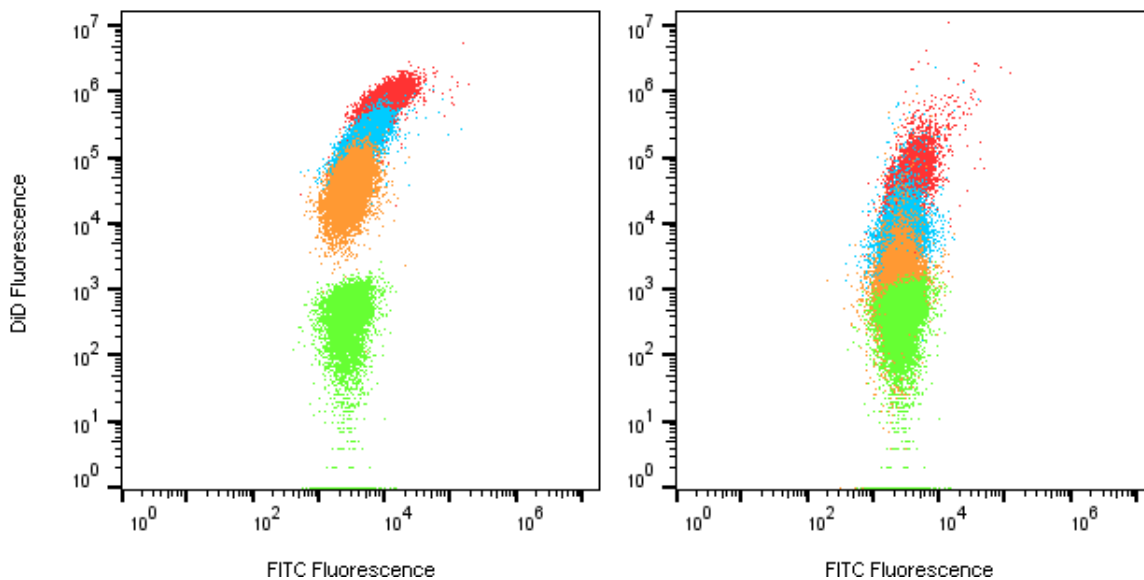


Figure 21. Dot plot of composite nanoparticle uptake with Raw 264.7 macrophage cells. Particles were coated with DSPC (left) and SSL (right) lipid formulations. Particles were incubated at three concentrations: control (green), 0.001 mg/mL silica (orange), 0.01 mg/mL (blue) and 0.1 mg/mL (red).

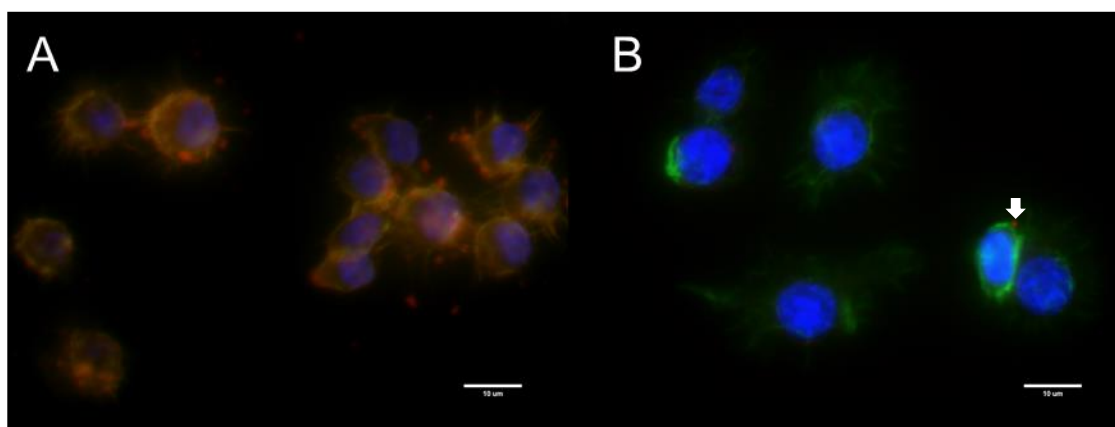


Figure 22. Composite fluorescent microscope images of macrophage cells incubated with 0.01 mg/mL of tethered membrane nanoparticles coated with DSPC (A) and SSL (B) formulations. Blue = DAPI, Green = phalloidin, and Cy5 = DiD. Scale bars represent 10 microns.

Fluorescent microscope images were used to visually compare uptake of TMN coated with DSPC and SSL formulations. Composite fluorescent microscope images of macrophage cells incubated with 0.01 mg/mL of TMN are shown in **Figure 22**. The DSPC coated particles showed greater uptake as indicated by the greater amount of Cy5 color in Panel A over that observed with the SSL coated particles in Panel B. Panel B does have a couple, less observable punctate regions of Cy5 indicating association of the particles with the macrophage cells (indicated via the arrow). These results correlate with the trend observed via flow cytometry.

Figure 23 and **Figure 24** display the median fluorescence intensities of the DiD labeled particles and FITC labeled particles, respectively. In general, the TMN showed greater uptake in comparison to the liposome controls. The SSL coating on the TMN reduced uptake over DSPC coated particles by a factor of 13 at 0.1 mg/mL and showed a statistical difference at each concentration (0.001 mg/mL, $p = 0.0006$; 0.01 mg/mL, $p = 0.0038$; 0.1 mg/mL, $p = 0.0005$). The results of the TMN follow the same trend as DSPC and SSL formulated liposomes, with statistical differences at each concentration and a near 30 times difference at the highest concentration (0.001 mg/mL, $p = 0.0009$; 0.01 mg/mL, $p = 0.0001$; 0.1 mg/mL, $p = 0.0027$). DSPC coated composites showed the greatest uptake at each concentration and DSPC liposomes showed the second highest uptake followed by SSL coated composites and then SSL liposomes.

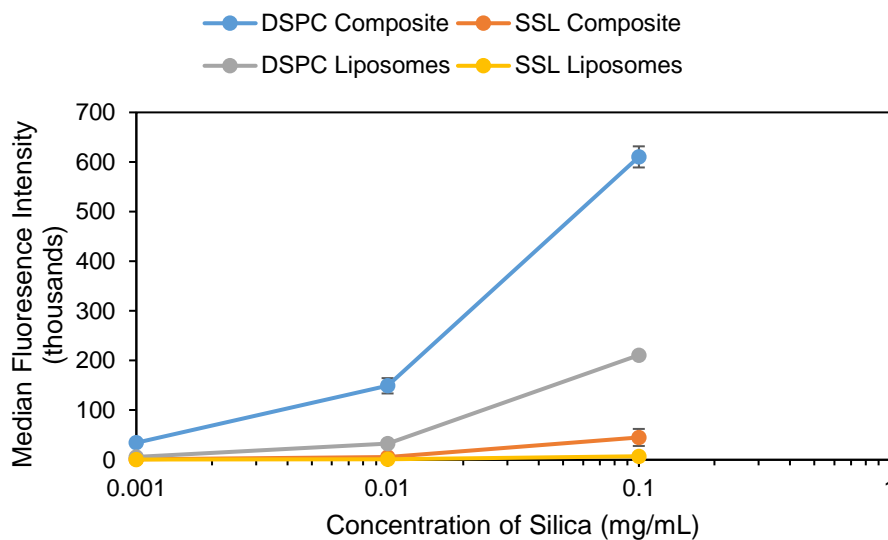


Figure 23. Median fluorescence intensities of DiD labeled composite nanoparticles and DiD labeled liposomes.

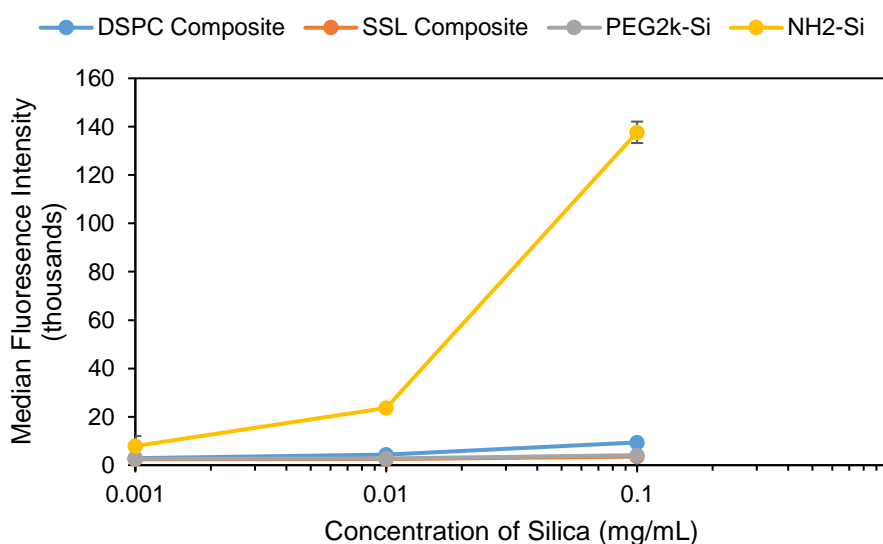


Figure 24. Median fluorescence intensities of FITC labeled composite nanoparticles and FITC labeled amine and PEG coated silica particles.

Aminated particles showed the greatest uptake among silica particle comparisons (**Figure 24**). This greater uptake is believed to be a result of the highly positive surface charge. DSPC, SSL and PEGylated silica all showed similar uptake. However, it is likely that the overall reduced fluorescence intensity of the FITC fluorophore bound to TMN

impacted the overall comparison among silica particles. These trends indicate an ability to tailor RES clearance by controlling surface characteristics of the TMN. It is expected that inclusion of a PEG brush border would significantly reduce clearance as seen with other, traditional nanoparticle systems.

The TMN showed a greater uptake in comparison to traditional liposomes at each concentration examined. Given that the particles were found to be stable in cell culture medium, this greater uptake is likely a result of gravitational settling and not agglomeration. Settling of silica particles is very common in suspensions and has been found to dramatically impact particle effects on cells.²³⁷ This settling effectively increases the concentration of particles available for uptake at the cell interface.²³⁸ In some cases, particle agglomeration significantly increases local concentration near the cells as is likely for the aminated particles. Whereas, liposomes remain in suspension and maintain a lower relative concentration of particles available for uptake. Inclusion of PEG brush borders likely has a two-fold effect, increasing stabilization of the particles in suspension while also reducing protein adsorption.

4.3.3 Loading of Doxorubicin

Liposomes have been studied extensively as delivery vehicles for doxorubicin and have seen success as a possible treatment for prostate cancer.²³⁹ Thus, doxorubicin serves as a unique model in developing the capabilities of our nanoparticle tBLM composites. Moreover, remote loading of doxorubicin provides an opportunity to demonstrate the usefulness of these composites without concern about membrane leakage of the encapsulated drug. Provided dox precipitates upon crossing the bilayer membrane, its

release rate is expected to be less than that of the previously explored carboxyfluorescein molecule.²²⁷

Encapsulation efficiency of doxorubicin in liposomes is commonly achieved at 95% or higher when using an ammonium sulfate gradient when using a DOX to dry lipid ratio of 0.2:1.²⁴⁰ For this work, a similar encapsulation efficiency was achieved at around 80-95%. The loading efficiency was found to be highly dependent on pH of the exterior DOX solution. A pH of 8-8.5 was targeted with pH's of 8.41, 8.15 and 8.09 achieved. This led to appreciable differences in DOX loading as illustrated in **Figure 25**. A pH of 8.09 lead to an entrapment efficiency of $85 \pm 0.1\%$, which increased to $92 \pm 0.2\%$ at a pH of 8.41. This

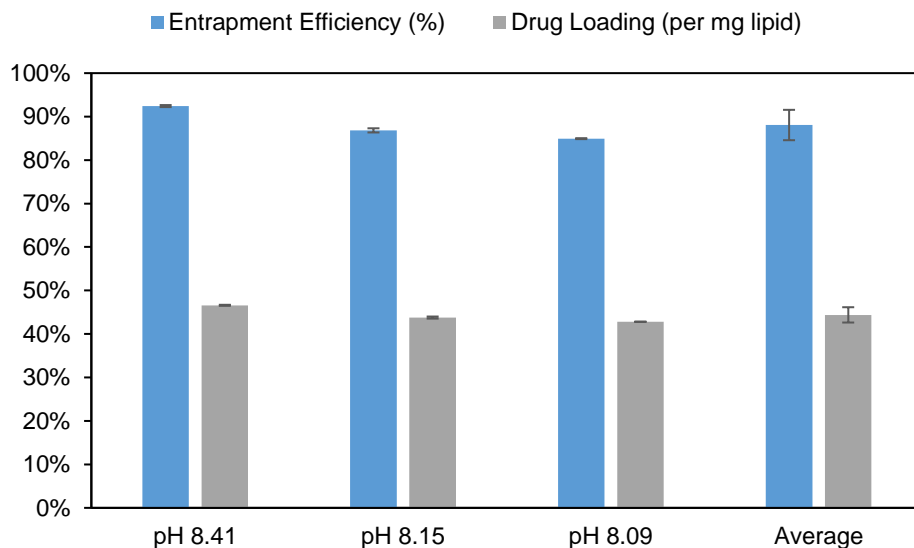


Figure 25. Loading efficiency of doxorubicin within tethered membrane nanoparticles was found to be highly pH dependent utilizing an ammonium sulfate gradient.

The presence of the silica nanoparticles within the lumen of the lipid bilayer also presented a unique situation. The silica particles were found to interact with the loaded doxorubicin, making direct assessment of loaded DOX inaccurate. This was alleviated via

quantification of the wash supernatant rather than the particles themselves. This DOX association was the result of remaining primary amines and hydroxyl moieties on the surface of the silica particle that were not functionalized with DSPE-PEG2k. DOX molecules have been found to form hydrogen bonds with both hydroxyl and amine groups,²⁴¹ which explains the association of DOX with the surface of the silica particle. It is also believed that the primary amines provide another reservoir of protons useful when loading. This increased interaction may also serve as a pH-dependent release mechanism *in vivo*, providing a controlled release off the surface of the particle upon entrapment within the endosome.

4.3.4 *In vitro* Evaluation of Tethered Membrane Nanoparticles with PC-3 Cells

Human PC-3 cells were chosen to examine the effects of doxorubicin loaded TMN on anti-tumor activity. PC-3 is known to readily form tumors in athymic mice,²⁴² ensuring the data collected will be relevant for comparison with future *in vivo* experiments. It was found that free doxorubicin induced a concentration and time-dependent decrease in MTT staining with an IC₅₀ value around 1.5 μ M after 72 hours of incubation. At the 24 and 48 hour time points, DOX was found to reduce MTT staining by roughly 20 and 35%, respectively.

TMN and SSL liposomes loaded with doxorubicin were incubated with PC-3 cells for 24, 48 and 72 hours. Concentrations of 1, 3, 5 and 10 μ M were chosen to incubate with the PC-3 cells to determine concentration dependent effects. Panel C of **Figure 26** shows the resulting MTT staining of PC-3 cells after incubation for 72 hours with DOX loaded TMN and DOX loaded liposomes with their respective controls. Both particle types displayed similar MTT staining to their controls at the lowest concentration, 1 μ M. As

DOX concentration increased, TMN and liposomes performed similarly. Both particle types yielded higher levels of MTT staining in comparison to free DOX. At 10 μM , the decrease in MTT staining was statistically similar (liposomes, $p = 0.058$; TMN, $p = 0.252$) to free DOX for both the TMN and liposomes. Similar trends were observed at the 24 and 48 hour time points as shown in Panel B and C of **Figure 26**, respectively.

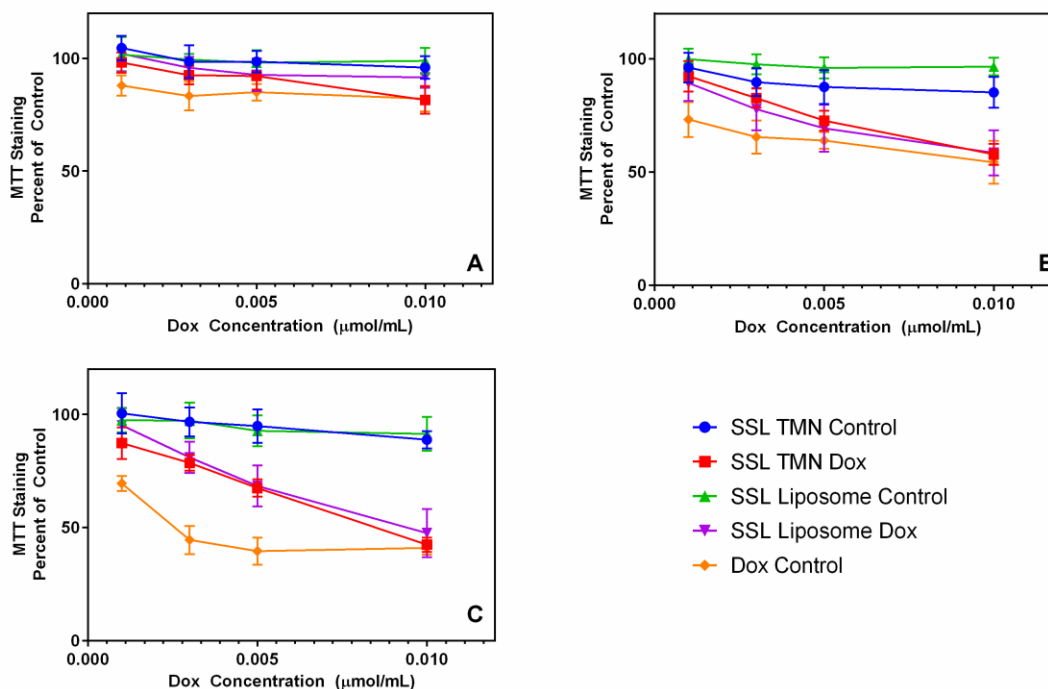


Figure 26. Concentration-dependent effects of doxorubicin loaded SSL liposomes and SSL tethered membrane nanoparticles on MTT staining in human prostate cancer cells after 24 (A), 48 (B) and 72 (C) hours of incubation.

The time-dependent effects on MTT staining were also examined and are shown in **Figure 27**. Panel C displays the time-dependent MTT staining of particles loaded with 5 μM dox and their controls at 24, 48 and 72-hour time points. Free dox reduced MTT staining from $85 \pm 4\%$ at 24 hours to $64 \pm 4\%$ at 48 and $40 \pm 6\%$ at 72 hours. Dox loaded liposomes and TMN performed similarly, with reductions in MTT staining to approximately 92%, 70% and 67% at 24, 48 and 72 hours, respectively. Similar trends

between the two DOX loaded particles were observed at the other concentrations examined, as shown in **Figure 27**.

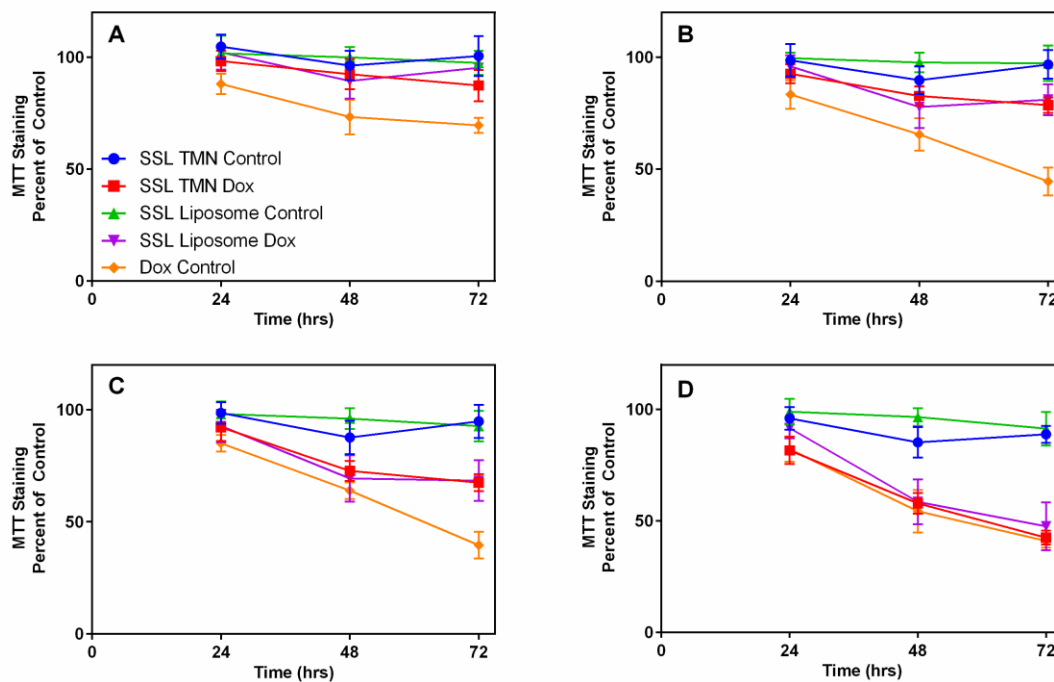


Figure 27. Time-dependent effects of doxorubicin loaded SSL liposomes and SSL tethered membrane nanoparticles on MTT staining in human prostate cancer cells after 72 hours of incubation at 1 (A), 3 (B), 5 (C) and 10 (D) μM .

These results suggest that the TMN loaded with doxorubicin yields a similar effect on MTT staining when compared with DOX loaded liposomes. At each concentration and time point, the TMN performed comparably to liposomes. Both particle types deviated from free DOX at concentrations lower than 10 μM . These results were expected, as encapsulated drug must first be released from the nanoparticles. However, at the higher concentration the similar toxicities among the particles and free dox suggest there is an enhanced release and/or uptake mechanism. Our previous work indicates that this is a cell mediated effect.²⁴² These results are encouraging and demonstrate the TMN as an effective drug delivery vehicle, with results comparable to traditional liposomes.

4.4 Conclusions

Production of silica nanoparticle tethered bilayer membranes have been demonstrated with two separate surface characteristics. Bilayers comprised entire of zwitterionic DSPC and DSPC with an exterior PEG layer have been assembled. The effect of this exterior PEG layer on macrophage uptake has been compared with the DSPC bilayer. Remote loading of doxorubicin was employed and the loaded particles administered to a PC-3 prostate cancer cell line. Comparisons among the TMN, free DOX and sterically stabilized liposomes found that both nanoparticles yielded similar cell kill results. Future studies may include examining modifications in the formulation of lipid used to coat the TMN. Secretory phospholipase A₂ (sPLA₂) is overexpressed in prostate cancer and our lab has developed an sPLA₂ responsive lipid formulation.²⁴² This formulation led to increased efficacy *in vivo* and was linked with greater uptake *in vitro*. The versatility of the TMN system has been demonstrated and the ability to alter the composition of the tethered membrane provides many avenues of optimization for the disease of interest, such as cancer.

Chapter 5: Cytotoxicity of PEG Coated Silica Nanoparticles

5.1 Introduction

Silica nanoparticles present a robust, biocompatible and stable nanoparticle platform from which to build a drug delivery vehicle. Silica particles have excellent optical properties, monodisperse size distributions and controllable porosity. Porous and nonporous particles have been explored extensively as a drug delivery system.^{20,26} These particles can be easily formed via flame synthesis, chemical vapor deposition, and sol-gel methods.²¹ Many of the silica nanoparticle properties can be tailored during synthesis. The simplicity of formation and ease of modification make silica an apt material for use as a drug delivery platform, however, the field of nanoparticle-based drug delivery is lacking in assessment of toxicity of these materials.

Nanoparticle toxicity is an ever-increasing issue that has lacked sufficient attention over the past three decades. This trend is clearly shown in **Figure 28**. This ISI Web of Science search enumerates the published papers regarding nanoparticles (nano or ultrafine) and those that include some focus on toxicity. Nanoparticles are often made of nontoxic materials, however, they have very different physiochemical properties due to their size.²⁴³ These properties are often what make nanoparticles advantageous for drug delivery applications, however, their ability to accumulate within biological systems appears to produce toxic effects.²⁴⁴ Often, toxicology studies are conducted on lung tissue as the lungs are believed to be one of the most common routes of nanoparticle exposure. Inhalation of

silica has been associated with the development of silicosis, a severe respiratory disease.²⁴⁵ Studies have examined silica nanoparticles interaction with the skin barrier and found that the surface characteristics of the particle were significant factors in particle penetration.^{245,246} Silica nanoparticle size has also been found to be a factor in cytotoxicity.²⁴⁷

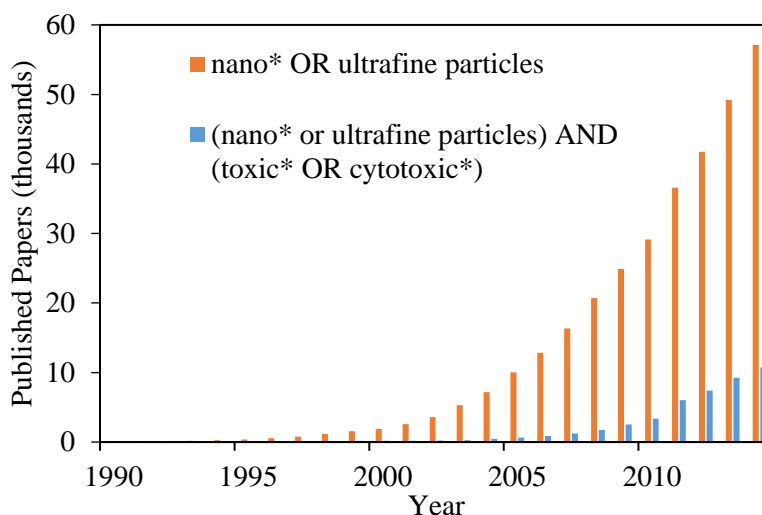


Figure 28. Nanoparticle and nanoparticle toxicity papers published over past twenty five years (ISI Web of Science).

With the growing interest in nanoparticle toxicity, researchers have begun conducting many *in vitro* studies. Evaluation has been conducted with a variety of cell lines and a single cell line has not been standardized given the plethora of uses of nanoparticles. In some cases, *in vitro* studies have been shown to correlate well with expected *in vivo* results when examining drug compounds.²⁴⁸ Thus, it serves that similar results should be attainable for nanoparticles. Chinese hamster ovary (CHO) cells provide a commonly used cell line for toxicity studies. Our lab²⁴⁹ has recently evaluated the toxicity of different surface coverings of iron oxide nanoparticles with CHO cells and Awasthi *et al.*²⁵⁰ have performed a similar analysis with silver nanoparticles, giving a basis for comparison.

The CHO cell was chosen to serve as an *in vitro* model with which to compare the effect of nanoparticle surface covering on toxicity. In order to elucidate these effects, silica nanoparticles of two different sizes (120 and 60 nm) were analyzed with four different surface properties: amine, PEG2k, PEG5k and PEG20k. PEG2k and 5k are commonly used in drug delivery applications while PEG 20k provided a significant size difference from which to draw comparisons. Additionally, these studies provide an assessment of the building blocks from which the tethered membrane nanoparticles (TMN) were constructed. Evaluation of these building blocks may serve to elucidate possible components of toxicity within the more complex construct of TMN. **Figure 29** provides a graphical summary of the factors considered. Properties of the silica particles were assessed via a serum stability study, cell viability assessment via a mitochondrial function (MTT assay), reactive oxygen species generation, and nanoparticle uptake was assessed with flow cytometry.

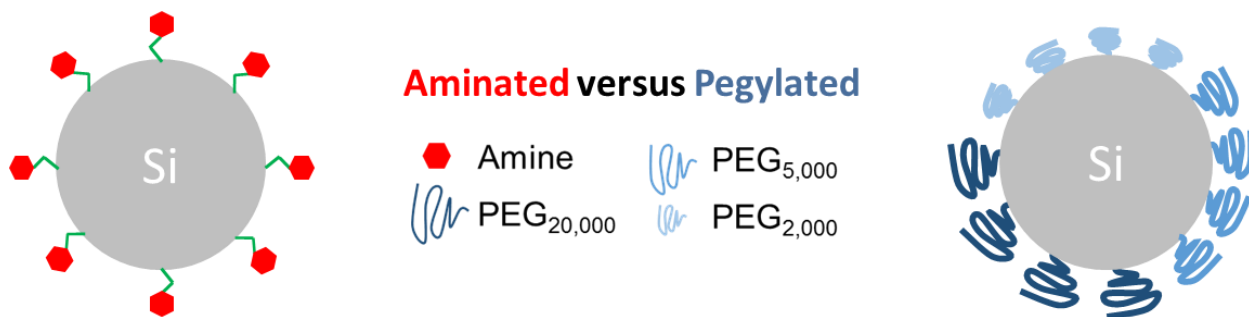


Figure 29. Surface coverings assessed in toxicity and uptake analysis.

5.2 Materials and Methods

Materials and methods were the same as in previous chapters except where indicated.

5.2.1 Materials

All materials were purchased from commercial suppliers and used without further modification, unless noted otherwise. Amine modified (Lot: JEA0152) silica nanoparticles were purchased from nanoComposix (San Diego, CA). N-Hydroxylsuccinimide (NHS)

functionalized methoxy polyethylene glycol (m-PEG-NHS) polymer in 2k, 5k and 20k Da molecular weight were purchased from Nanocs, Inc. (New York, NY). Fluorescamine, p-methylaminophenol sulfate (99%), ethanolamine (98%), sodium hydroxide (NaOH), oxalic acid anhydrate (98%), ammonium molybdate tetrahydrate (99%) and 4-(2-hydroxyethyl)-1-piperazineethanesulfonic acid (HEPES, 99%) were purchased from Alfa Aesar (Ward Hill, MA). Silica standard was purchased from Ricca Chemical (Arlington, TX). Dimethyl sulfoxide (DMSO), sulfuric acid, and 37% hydrochloric acid (HCl) were purchased from BDH (VWR, Randor PA). Anhydrous sodium sulfite, sucrose, cholesterol, fluorescein isothiocyanate (FTIC), thiazoyl blue tetrazolium bromide (MTT) and tris(hydroxymethyl)aminomethane were purchased from AMRESCO, Inc. (Solon, OH). Deionized water used throughout the study was obtained from a Milli-Q Purelab Flex 2 water purification system (ELGA, LLC, Woodridge, Illinois, IL). Carboxy-DCFDA was purchased from Chemodex (Gallen, Switzerland).

5.2.2 Cell lines

The Chinese Hamster Ovary (CHO-K1) cell line was obtained from Rajesh Amin, Department of Drug Discovery and Development, Auburn University, Auburn, AL. Authentication of all cell lines was confirmed by the National Institute of Standards and Technology, using a multiplex PCR assay. CHO cells were maintained in Ham's F-12K (Kaighn's) nutrient mixture with L-glutamine (Corning cellgro, Manassas, VA), supplemented with 10% fetal bovine serum (FBS) from VWR Life Science Seradigm (Radnor, PA) and 1% penicillin/streptomycin purchased from (Corning cellgro, Manassas, VA). RAW cells were maintained in Dulbecco's Modified Eagles Medium (DMEM)/High Glucose (HyClone, GE Healthcare Life Sciences), supplemented with 10% FBS and 1% antibiotics. Both cell lines were incubated at 37°C in 5% CO₂.

5.2.3 Preparation of Silica Nanoparticles

Silica particles were modified as previously mentioned in Chapter 3 and confirmation of silica nanoparticle modification was confirmed in Chapter 4 via DLS and ATR-FITR.

5.2.3 ROS Assay

The production of ROS was measured following the protocol of Wu *et al.*²⁵¹ using carboxy-DCFDA. DCFDA is known to passively enter the cells where it reacts with ROS to form a fluorescent compound, dichlorofluorescein. Briefly, DCFDA was dissolved in dimethylsulfoxide (DMSO) at a concentration of 1 μM . Particles were incubated with cells for 24 hours. Following incubation, the cells were washed two times with HBSS and incubated with DCFDA at 37°C for 30 minutes. Remaining DCFDA was removed and HBSS added. Cells were analyzed with fluorescence microscopy and flow cytometry.

5.3 Results and Discussion

5.3.1 Silica Particle Characterization and Serum Stability

Nanoparticle suspensions received from nanoComposix were analyzed with a fluorescamine assay to determine reactive surface amine concentration on the particles. Fluorescamine is nonfluorescent until bound with a primary amine, which permits quantification of surface amine groups that are available for functionalization.¹⁹⁰ Amine concentration was determined to be 0.48 ± 0.14 $\mu\text{mol amine/mg silica}$. Additionally, a modified blue silicomolybdic assay was used to determine silica concentration. As received silica suspensions were found to be 12.94 ± 0.13 mg/mL . This suspension was diluted to 10 mg/mL for all experimental purposes. PEG molecules were reacted with primary surface amine groups to form PEGylated nanoparticles.

Silica particles were characterized with TEM and DLS. TEM analysis yielded a mean nanoparticle diameter of 113 ± 13 nm and 119 ± 17 nm for the amine and hydroxyl coated particles, respectively. Hydrodynamic diameter and zeta potential varied with surface coating. **Table 5** shows the hydrodynamic diameter and zeta potential of the nanoparticles tested in 10 mM acetate buffer and 1X phosphate buffered saline (PBS). The aminated particles were unstable in PBS and displayed visible flocculation upon mixing. This behavior is a result of crosslinking caused by the polyvalent phosphate ion and its interaction with the surface amine groups. PEGylated particles had a larger hydrodynamic diameter than the amine particles and a neutral zeta potential, indicating successful PEG attachment. Additionally, polydispersity index (PdI) values were low in all samples indicating monodisperse suspensions.

The conformation of PEG chains on the surface of the nanoparticles was assessed following the same method outlined in Chapter 3. The conformation and PEG grafting densities are shown in **Table 5**. Theoretical calculations indicated that the PEG layers on each particle surface were in the brush conformation. As grafting density values increase, there is an increase in the compression of neighboring PEG chains which correlates with a larger hydrodynamic diameter.¹⁹⁸ This phenomenon is demonstrated in the data collected in **Table 5**, where the grafting density of the PEG-5k is greater than PEG-2k or PEG-20k and as such exhibits a greater hydrodynamic diameter. The calculated PEG grafting densities suggest higher degrees of functionalization for PEG-2k and PEG-5k particles in comparison to PEG-20k particles. Higher grafting densities on silica nanoparticles have been associated with lower cell toxicity and decreased protein adsorption.²⁵²⁻²⁵⁴ In each case, it has been suggested that lower grafting densities permitted greater availability of

the silica nanoparticle core for interactions with proteins and/or cells. Additionally, Kingshott, *et al.*²⁵⁴ and Pasche, *et al.*²⁵⁵ propose that there is an interplay between PEG length, grafting density and surface charge on the effect of protein adsorption.²⁵⁴ These studies suggest that for greater Dalton weight PEGs, less grafting density is needed to ensure the same stability of a lower Dalton weight PEG at a higher density.

Table 5. Intensity-averaged hydrodynamic diameters (HD) and ζ -potential (ZP) values of silica nanoparticles in acetate buffer and PBS, Ham's F-12K basal media stability analysis, PEG layer thickness, grafting density and conformation of PEGylated particles.

	Buffer	Hydroxyl	Amine	2k-PEG	5k-PEG	20k-PEG
HD (nm)	Acetate, 10 mM, pH 4	145 \pm 2.3	138 \pm 0.4	148 \pm 0.8	191 \pm 2.5	183 \pm 5.7
PdI		0.13 \pm 0.01	0.03 \pm 0.01	0.03 \pm 0.2	0.02 \pm 0.01	0.06 \pm 0.02
ZP (mV)		-5.3 \pm 0.1	+56.8 \pm 0.9	+8.9 \pm 0.2	+5.9 \pm 2.3	+1.3 \pm 1
HD (nm)	PBS, 1X, pH 7.4	146 \pm 1.8	Not Stable	141 \pm 5.8	173 \pm 13	169 \pm 3
PdI		0.08 \pm 0.02	Not Stable	0.02 \pm 0.01	0.03 \pm 0.01	0.05 \pm 0.02
ZP (mV)		-22.7 \pm 0.5	Not Stable	-0.8 \pm 0.3	-0.9 \pm 0.1	-0.7 \pm 0.2
Stability (hrs)		> 24	< 1	6	5	2
PEG Layer Thickness (nm)				10.8 \pm 0.8	53.7 \pm 2.5	45.6 \pm 5.7
Grafting Density (no. of chains/nm ²)				0.43 \pm 0.03	0.86 \pm 0.04	0.18 \pm 0.02
Conformation				Brush ($R_F > D$)		

HD: hydrodynamic diameter (nm); ZP: ζ -potential (mV); PdI: Polydispersity index; Results shown as mean \pm standard error of mean

The stabilities of the particles in cell culture medium were evaluated through changes in hydrodynamic diameter, with instability noted upon major changes in size. For this study, 25 uL of particles (10 mg/mL) were suspended in Ham's F-12K cell culture medium and incubated at 37°C with hydrodynamic diameter measurements taken every hour for 10 hours, or until the particle settled out, with a final measurement taken at 24 hours. The results are shown in **Figure 30**. The amine-coated particles showed a substantial agglomeration tendency. Their size increased within the first hour of incubation and displayed visible settling. The hydroxyl particles remained stable throughout the 24 hour time period of analysis as confirmed by no significant changes in hydrodynamic diameter. The PEG-coated silica particles showed varying degrees of stability. PEG-2k coated particles remained stable up until 6 hours of incubation. PEG-5k particles began to agglomerate at the 5 hour mark and PEG-20k particles showed instability after only 2 hours of incubation. It is believed that these variations in particle stability are a function of PEG densities, PEG Dalton weight and the availability of the nanoparticle core to interact with the cell culture medium as previously discussed.²⁵²⁻²⁵⁶ PEG-2k and PEG-5k particles have lower Dalton weight coverings and greater grafting densities in comparison to PEG-20k particles. Following the trends previously outlined, these properties suggest that the surface of the PEG-2k and PEG-5k particles are more shielded, imparting greater stability, and that PEG-20k particles may exhibit greater stability with a higher grafting density.

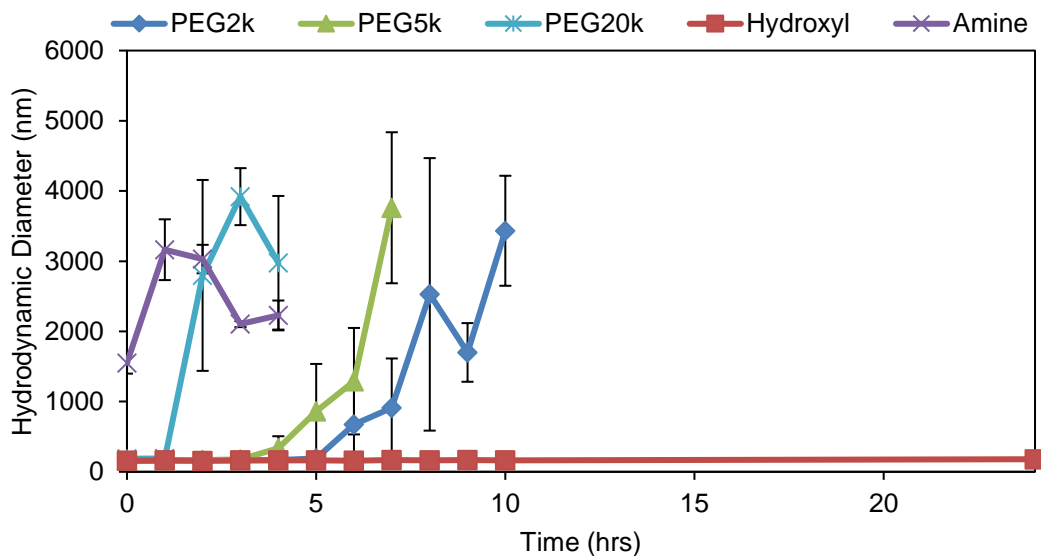


Figure 30. Hydrodynamic diameter assessment of PEGylated and aminated silica particles in 10% FBS supplemented F-12K culture medium (connecting lines drawn to guide the reader's eye).

5.3.2 Silica Nanoparticle Impact on Cell Viability

Silica particles were functionalized with three differing PEG groups and incubated with CHO cells for 72 hours. An MTT assay was conducted to determine cytotoxicity and predict half maximal inhibitory concentrations (IC_{50}) for each particle surface covering. **Figure 32** and **Figure 31** show the viability profiles for the 60 and 120 nm silica particles, respectively. It is clear from the that the aminated silica showed the greatest effect on viability while the differing PEG Dalton weights did not differ greatly. **Table 6** provides the IC_{50} values for all four surface coverings on both particle sizes. At both sizes, the aminated particles showed the lowest IC_{50} values. The 120 nm PEGylated particles had IC_{50} values all hovering around 1.5 mg/mL while the smaller sized particles had greater variability among PEG coatings.

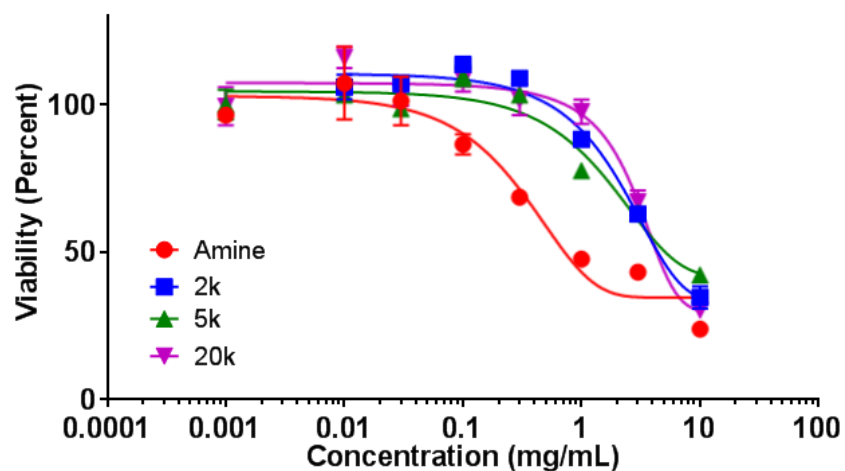


Figure 31. Viability profiles of 60 nm silica nanoparticles incubated with CHO cells for 72 hours.

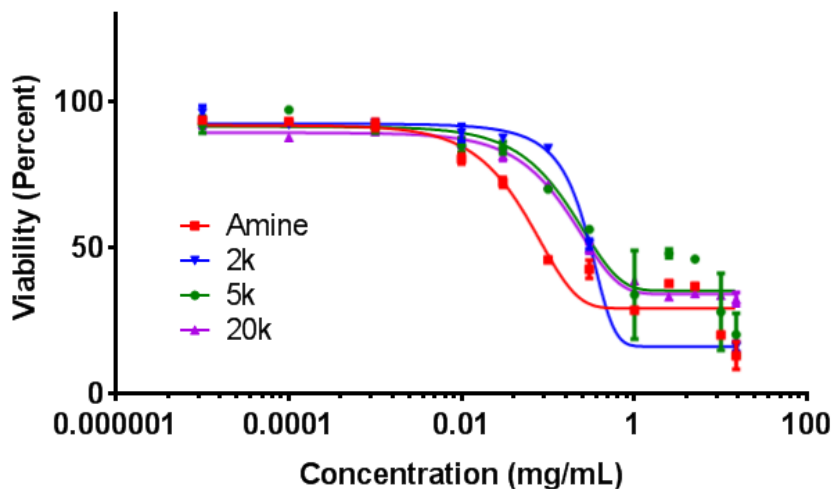


Figure 32. Viability profiles of 120 nm silica nanoparticles incubated with CHO cells for 72 hours.

Table 6. IC₅₀ values determined for 60 and 120 nm silica nanoparticles incubated with CHO cells for 72 hours.

	60 nm (mg/mL)	120 nm (mg/mL)
Amine	0.416 ± 0.176	0.591 ± 0.053
PEG 2k	2.583 ± 0.090	1.435 ± 0.134
PEG 5k	1.746 ± 0.106	1.566 ± 0.125
PEG 20k	3.535 ± 0.153	1.333 ± 0.169

5.3.3 Correlating Nanoparticle Uptake with MTT Staining

Particle uptake was analyzed in order to correlate the inhibition of CHO cell growth with increased particle association. Fluorescence microscopy provided a bulk assessment of particle interaction with the CHO cells. **Figure 33** shows a comparison of control cells with PEG2k coated and aminated particles incubated with CHO cells for 24 hours. The particles were labeled with rhodamine b isothiocyanate before incubation. The PEGylated particles can be seen interspersed between the cells and less localized on or within the cells. The aminated particle image shows clear punctate regions on or within the cells. This is a clear difference between the two different particle types and correlates with the MTT staining data collected, where greater association of the aminated particles would suggest a greater effect on viability.

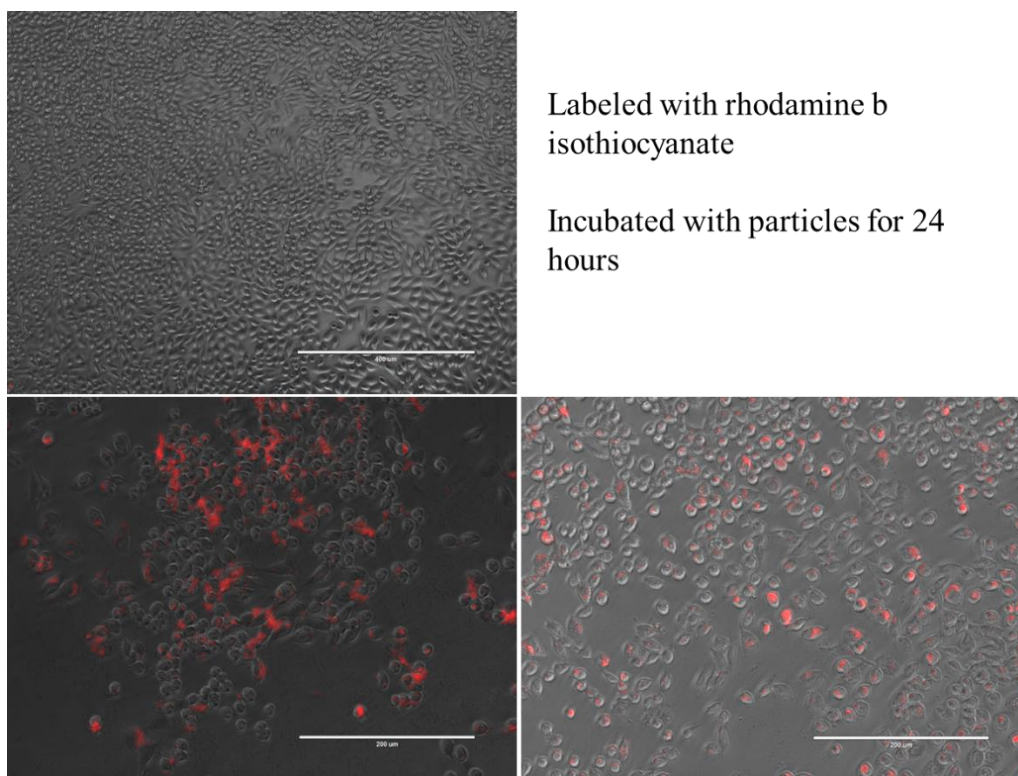


Figure 33. Fluorescence microscopy of control CHO cells (top left), cells incubated with PEGylated particles (bottom left) and aminated particles (bottom right) for 24 hours.

In addition to the gross assessment provided by fluorescence microscopy, flow cytometry data was collected to correlate particle association with viability. Particles were again labeled with rhodamine and incubated with the CHO cells for 24 hours before flow analysis. Two regions of interest were gated – a live and dead region. The mean fluorescence intensity was plotted against the particle concentration and is shown in **Figure 34**. It was expected that with increasing concentration of particles there would be an increase in mean fluorescence intensity, regardless of surface coating. The majority of particles followed this trend up to 0.5 mg/mL but not at the higher concentration of 1 mg/mL. The aminated particles showed a dose dependent response throughout the concentration range examined. Aminated particles also yielded one of the greatest fluorescence intensities at all concentrations. PEG 20k had the greatest fluorescence intensity of any sample which is believed to be an error within the experiment that could be corrected by using median fluorescence intensity values instead of mean. The collected flow data does not provide the best support for the fluorescent microscopy or viability data collected. This is likely because this data represents a single experimental run – a proof of concept. Further validation of these results is required.

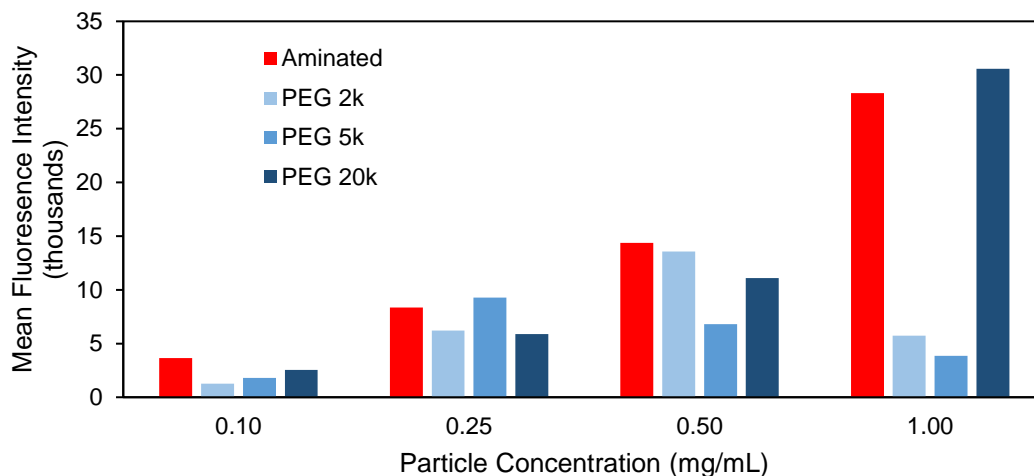


Figure 34. Mean fluorescence intensity of CHO cells after incubation with Rhodamine B labeled particles.

5.3.4 Evaluation of ROS Generation

To date, a method for the proper evaluation of nanoparticle toxicity has not been developed. Although a gold standard does not yet exist, several parameters have been recognized to affect toxicity evaluations such as size, surface area and solubility.²⁵⁷ One important mechanism of nanotoxicity has been identified – oxidative potential. Oxidative potential is an intrinsic property of materials to oxidize components in the immediate environment.²⁵⁷ This leads to the production of reactive oxygen species (ROS). This increase in ROS leads to an imbalance in cellular redox homeostasis and physiological function. ROS generation has been linked to mitochondrial damage,²⁵⁸ DNA damage, morphological transformations in cells and lung injury.²⁵⁹ Additionally, chronic inflammation combined with reactive oxygen species (ROS) generation are putative risk factors for PCa development.²²¹ Regardless of the prevalence of ROS studies in literature and its role in cellular toxicity, the effect of PEG Dalton weight remains to be studied.

ROS generation was studied with fluorescence microscopy. Amine coated particles were incubated with CHO cells at 0.1, 0.3, 1 and 3 mg/mL. Observation of the CHO cells after application of DCFDA resulted in a fluorescence signal. **Figure 35** displays the effect of increasing concentration of aminated particles on CHO cell ROS production. As the concentration increased, an increase in fluorescence intensity was observed. In addition to an overall increase in fluorescence intensity, a greater population of cells with very high DCFDA activity was detected at the higher concentrations. This correlates with the decrease in cell count observed in the wells. These two results together suggest that with increasing concentration of particles, the CHO cells exhibited greater ROS production and greater cytotoxicity. It is worth noting that the specificity of DCFDA and other ROS measuring probes have been called into question.²⁶⁰ By maintaining strict controls, it is believed that the trends developed herein are representative of nanoparticle effects on the cells.

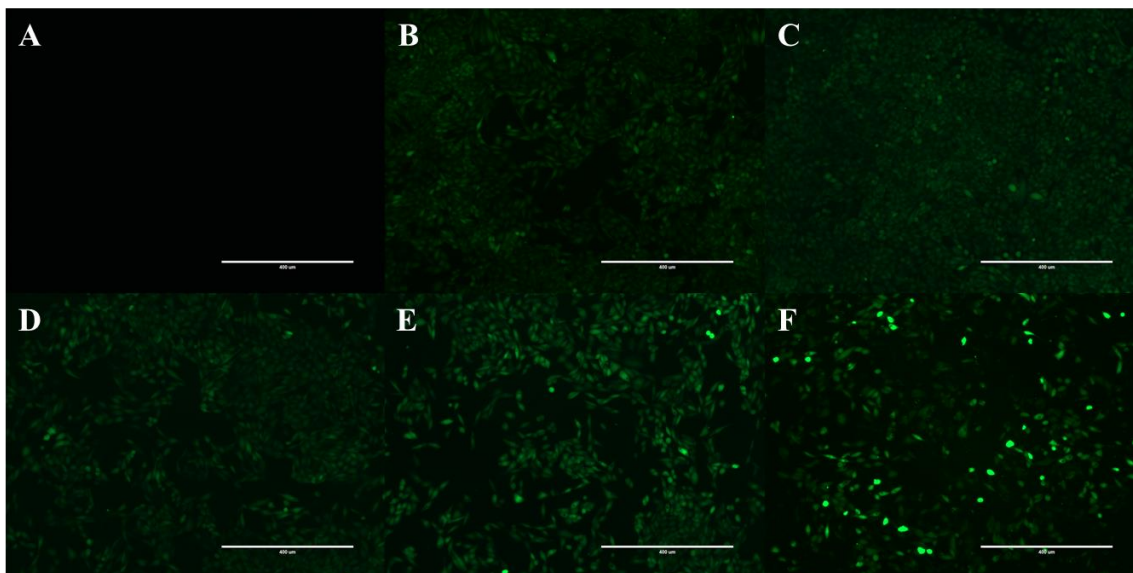


Figure 35. ROS generation in CHO cells with increasing concentration of aminated silica particles: (A) control no DCFDA, (B) control with DCFDA, (C) 0.1, (D) 0.3, (E) 1.0, (F) 3 mg/mL silica.

5.3.5 Macrophage Uptake of Silica Particles

Finally, the efficacy of the different nanoparticle surface coverings for use in the development of a drug delivery vehicle was assessed via incubation with RAW 264.7 macrophage cells. Macrophage cells represent a constituent of the reticuloendothelial system (RES). The RES represents one of the greatest routes of clearance for foreign material entering the body and *in vitro* uptake has been correlated with clearance *in vivo*.¹⁸⁷

Figure 36 displays the median fluorescence intensity (MFI) of the RAW 264.7 cells after four hours of incubation with particles.

At each concentration examined, MFI of PEGylated particles did not differ greatly from the autofluorescence of control cells. The aminated particles showed a dose-dependent response and at each concentration had statistically greater MFI over the PEGylated particles ($p < 0.005$). In general, the highly positive charge of aminated particles far outweighed any differences seen between the PEG coatings. This trend correlates with that observed in the viability assessment, where differences in PEG coating result in minimal effects *in vitro*.

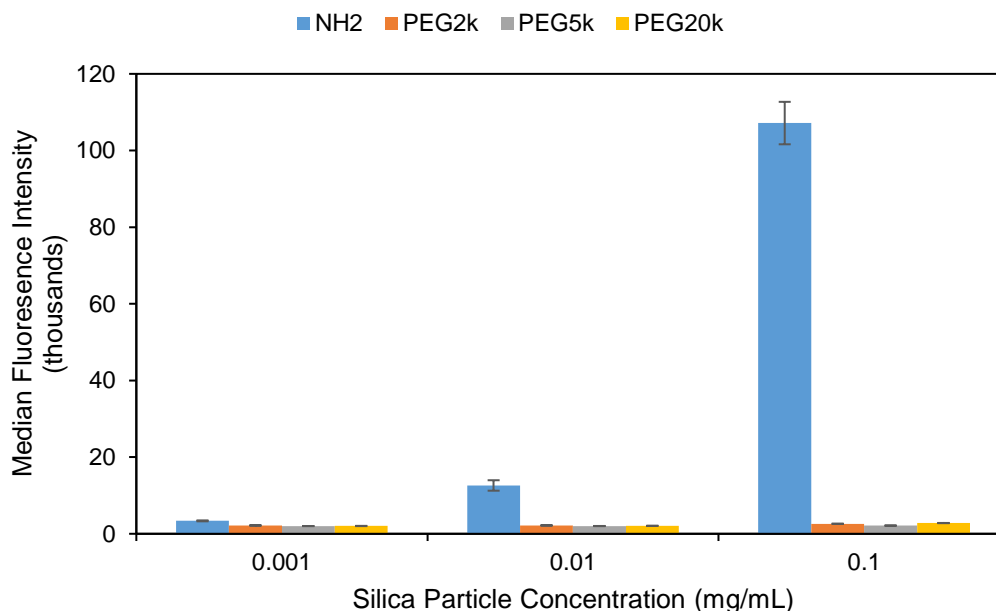


Figure 36. Median fluorescence intensity of 120 nm silica particles with differing surface characteristics.

5.4 Conclusions

The effect of silica nanoparticle size and surface coating on CHO cytotoxicity was assessed. Highly charged surfaces were found to exhibit the greatest effect on MTT staining with minimal differences among PEG Dalton weights determined. Particle uptake was assessed with flow cytometry and the results correlated with MTT staining. Uptake of PEGylated particles was significantly less than aminated particles, with minimal differences among PEG lengths detected. Generation of ROS was determined to be a result of nanoparticle incubation, with increasing concentration resulting in greater ROS generation. Oxidative stress has been linked to cell cytotoxicity in a variety of nanoparticle studies and is like the effect of particle-induced toxicity found here.

Chapter 6: Future Directions

Similar to the goal of the work previously discussed in the document, the following future directions focus around the use of tethered membrane nanoparticles as a drug delivery vehicle. The initial discussion is on the further optimization and investigation of the current model system to gain greater understanding of the nanoparticle supported membranes. Moving forward, there are inherently two major areas in which the composite material developed in this document may be further leveraged. First is via the replacement of the interior core nanoparticle and the second is via the modification of the exterior lipid bilayer.

6.1 Optimization of Tethered Membrane Nanoparticles for Drug Delivery

Much of the focus of this work has been on developing a model system to demonstrate the capability of a nanoparticle-supported bilayer membrane. Provided that this is one of the first demonstrations of a tethered membrane on a nanoparticle, it would serve the scientific community to delve further into the interactions at play. The greater understanding developed in these studies would have a direct impact on the use of nanoparticle-tethered membranes in future applications, as developed in Sections 6.2 and 6.3.

As laid out in Section 2.3.3, there are several factors that govern the formation and interaction of SLB in colloidal systems including pH, ionic strength, temperature and electrostatic charge. In the studies conducted and explored in this document, a single pH

and ionic strength was chosen to reduce the number of factors considered. Additionally, the use of zwitterionic lipids precludes the majority of effects pH might produce in the range utilized for the chosen application, drug delivery. Finally, the use of divalent species such as calcium have been found to affect SLB formation.¹⁰⁹ Although the electrostatic mechanism is not believed to be the driving factor for assembly, inclusion of these types of molecules may prove useful in promoting bilayer formation.

Many studies in literature point out the significance of pH and ionic strength in the assembly of particle supported bilayers.⁹⁸⁻¹⁰⁰ The use of a tethered system as developed herein, presents a unique surface property not previously explored in literature. The PEG brush border is similar to polymer SLB and reduces the effect pH may have on the system. This reduced effect is due to masking of hydroxyl and amine groups on the silica nanoparticle surface – effectively removing the pH (electrostatic) dependence of the vesicle fusion method. However, the inclusion of a phospholipid to the exterior presents a singular characteristic. We have demonstrated that the inclusion of this molecule can be used to drive assembly of a supported bilayer onto the nanoparticle surface. Provided the large amount of hydrophobic characteristic the phospholipid provides, it is reasonable to assume that the driving force for assembly is largely dependent upon hydrophobic interactions. However, altering the tethered phospholipid would allow for an exploration of the effect lipid charge, acyl chain length or even lipid shape may have. Changing the length of the acyl chains would permit an investigation into the relationship between electrostatic and hydrophobic interactions that drive/dictate this assembly. It has been suggested that for every two methylene groups added to the acyl chains, the equilibrium constant changes by a factor of ten in favor of a hydrophobic solvent.^{52,54} Thus, reducing the acyl chain from 18

(used in this work) to 16 or 14 should reduce hydrophobic influence and increase electrostatic effects. It is worth noting, however, that changes in transition temperature of the membrane are accompanied with changes in acyl chain length – an additional factor that would need to be considered.

Ionic strength is known to impact the vesicle fusion process. High ionic strengths ultimately reduce the Debye length and cause aggregation of charge stabilized nanoparticles. Given that the scaffold nanoparticles are inherently unstable in suspension – due to their phospholipid facing exteriors – it is believed that ionic strength would have less of an effect on the overall formation of the particles. However, it is believed that an increase in ionic strength may enhance the overall vesicle fusion process as greater scaffold-liposome interactions would be promoted.

There are many additional factors regarding the tether moiety that can be explored, including length (e.g., PEG₅₀₀₀), composition (e.g., amphiphilic polymers) or even the amount of tethered lipids. It has been suggested that the amount of tethered lipids can have a direct impact on the stability of the membrane,¹⁴⁶ and the current work appears to be operating at the lower bound of tethers needed. Changes in tether length will ultimately change diameter of the particle which will have an impact on the amount of lipid required to form a complete bilayer.

Bilayer composition has shown to be a factor in the production of supported membranes in colloidal systems.¹⁰³ Although much of the work has been focused on evaluating electrostatic interactions, the adoption of a tethered bilayer reduces the dependence on this assembly constraint. A tethering platform allows the inquiry into

bilayer assembly free of these previously essential charge-charge interactions. Relaxation of this constraint permits exploration of lipid formulations with varying degrees of charge, shape, hydrophobic character or cholesterol.

Finally, investigation into the effect of membrane fluidity and inclusion of membrane constituents (e.g., targeting moieties, antigens, proteins, etc.) could lead to the development of a superior cell model or drug delivery vehicle. Membrane fluidity is a hallmark of cellular membranes and incorporation of proteins is necessary to produce a true membrane mimic. Abstraction of the bilayer from the core nanoparticle with a tether also provides the capability of including transmembrane proteins, which are instrumental in transport, signaling and anchoring of the cell.²⁶¹ Membrane fluidity has also been found to be a major factor in the targeting of nanoparticle-supported membranes.¹¹²

These represent a few of the fundamental factors that could be explored. Each would lead to a greater understanding of nanoparticle-tethered membranes. The understanding of these systems is significantly lacking given that there haven't been any experimental studies published. Moreover, the information gained in each study would have a direct impact on the application of these nanomaterials. Application of nanoparticle-supported bilayer technology is nascent and represents the leading-edge of nanoparticle work. Fundamental studies are necessary to develop understanding of these systems for improved application moving forward.

6.2 Applications of Unique Nanoparticle Cores for Drug Delivery

The silica nanoparticle core represents a model particle that can be easily interchanged with other nanoparticle technologies. Its low absorbance and non-existent

fluorescent properties make it an ideal material to use as a building block to which multifunctionality can be applied. Addition of absorptive and fluorescent properties are easily tailored via conjugation of dyes as demonstrated in this work. Many studies have already found silica to be an ideal material for use in drug delivery applications with similar membrane-coated systems, albeit mesoporous in nature.^{112,135,262,263} These particles provide tailorable release kinetics via particle morphology and pore diameter control.²⁶⁴

Application of the tethered membrane as it has been developed herein can easily be applied to inorganic or organic nanoparticles. The NHS/EDC chemistry utilized is commonly exercised in nanoparticle work and can be applied to any particle surface exhibiting primary amines. Should this chemistry not readily translate, many bioconjugation techniques exist that make the application of the tethered bilayer system to other nanoparticle technologies a minimal barrier.

Although mesoporous particles have seen widespread adoption with supported membranes for biomedical applications, the pore size presents a limiting factor. Pore size can affect overall stability of the membrane, as it was determined that the membrane conforms perfectly to the underlying support.¹¹² Davis *et al.*²⁶⁵ found that when pore sizes were less than two times the bilayer thickness fluid bilayers has no issues spanning the surface structures. However, when the pores were larger (much larger than the bilayer thickness), the bilayers invaginated into the pores leading to instability in the bilayer. A similar report by Durfee *et al.*¹⁹ found that MSN with pore diameters of ~18 nm restricted the spreading of the SLB across the particle surface, instead resulting in adsorption and deformation of liposomes to the particle surface. A tethered bilayer would easily mitigate these issues by abstracting the bilayer from the surface of the particle, while also providing

a stable lipid bilayer and even increasing luminal space for drug loading. This inherent advantage over simpler fused systems allows increased control of particle pore sizes. This increased control opens the door to a variety of release strategies and optimization which were previously unattainable.

Other particle technologies have inherent benefits as a result of their component makeup, including iron oxide, PLGA, chitosan or gold. Iron oxide provides an ability to track particle biodistribution with magnetic resonance imaging (MRI) upon administration *in vivo*,²⁶⁶ as well as a biocompatible core. The promise in membrane coated iron oxide is already being investigated with simpler systems,⁸⁵ and liposomes containing magnetic nanoparticles have long been an area of interest.²⁶⁷ It is worth noting that systems utilizing paramagnetic lipids have also been explored.¹³⁰ Gold nanoparticles have seen promise as contrast agents and use in hyperthermia treatments.²⁶⁸ Preliminary studies using membrane coatings have even already begun to be explored.¹²

PLGA nanoparticles provide an FDA approved platform that offers sustained and pH responsive release, incorporation of hydrophobic or hydrophilic drug and are biocompatible and biodegradable.²⁶⁹ However, the polymer suffers from being hydrophobic. Other hydrogel-based systems have already been enveloped in liposomes.²⁷⁰ Chitosan has been found to be non-toxic, biodegradable and mucoadhesive but lacks stability in physiological fluids. Application of a membrane has been demonstrated to stabilize the chitosan particles and shown promise in dictating release.²⁷¹

Many traditionally researched nanoparticle systems have characteristic properties that warrant their use as drug delivery vehicles and some have properties that limit

adoption, such as chitosan's insolubility, that remain to be overcome. Most of these particles stand to benefit from the inclusion of supported membranes via enhancement of their physicochemical characteristics. These enhancements have already seen successes with simpler systems via the manifestation of increased stability, circulation residence times or zwitteration of their surface charges. The use of a tether increases the applicability of supported membranes for many different particle types and reduces the constraints for adoption.

6.3 Increased Specificity of Nanoparticle Carriers with Cell Membrane Coats

Nanoparticle-based drug delivery carriers are lauded for their ability to overcome some of the barriers to therapeutic delivery. One barrier that remains ever-present is the adsorption of serum proteins. This nonspecific adsorption often leads to increased uptake by the reticuloendothelial system (RES) which prevents accumulation in targeted disease tissues.²⁷² The attachment of polyethylene glycol (PEG) has long been used to reduce the effects of nonspecific adsorption, where PEGylated nanoparticles were found to accumulate one-half to one-third the amount of non-PEGylated nanoparticles.²⁷³ This PEG effect has often been called "stealth" behavior.²⁷⁴ Prevention of protein adsorption due to this stealth effect was always known to be incomplete.²⁷⁵ More recently, it has been found that protein adsorption is actually required to enable the stealth effect and prevent nonspecific cellular uptake.²⁷⁶ These results highlight the importance in understanding the protein corona composition that binds to the particle surface, regardless of PEGylation, and opens the door for unique approaches toward dictating protein adsorption *in vivo*. Recent advances in nanoparticle-supported bilayers has led to the incorporation of targeting molecules within the membrane and use of endogenous lipid sources to dictate behavior *in*

vivo. All of these advances have utilized the simplest of SLB systems, fused membranes. Nanoparticle-tethered SLB provide many advantages over these simpler systems.

Nanoparticles enveloped in a lipid bilayer have seen success as drug delivery vehicles.^{19,64,262} The addition of a lipid bilayer to nanoparticles has been linked to longer circulation residence times,¹⁸ increased efficiency in loading and retaining drug,²⁶³ and increased targeting efficacy over traditional liposomes.¹¹² The addition of a membrane reduces the complexity in achieving multifunctionality of these nanocarriers. Incorporation of targeting moieties into the membrane wrap is easier, more effective and opens the door to a wider array of targeting strategies.

The inclusion of a lipid bilayer on nanoparticles provides an avenue for the incorporation of targeting molecules. Additionally, self-assembled monolayers of zwitterionic ligands have proven effective in suppressing corona formation.²⁷⁷⁻²⁷⁹ These two factors highlight significant advantages over traditional nanoparticle systems and reduces the need of attaching polymeric materials (such as PEG) for increased stability. Xu *et al.*¹² capitalized on these two factors and were able to incorporate GM3 within a zwitterionic DPPC bilayer on the surface of gold nanoparticles. This combination yielded enhanced delivery of gold nanoparticles to popliteal lymph nodes in comparison to PEGylated particles, with reduced protein adsorption.

Ashley *et al.*¹¹² utilized a similar zwitterionic system in the targeting of hepatocellular carcinoma. A zwitterionic membrane was employed upon a mesoporous silica particle for the co-delivery of hydrophilic drug. The incorporated targeting peptide achieved an avidity effect due to membrane fluidity, and demonstrated 10,000-fold greater

specificity for hepatocellular carcinoma over hepatocytes, endothelial cells or immune cells.

These two examples demonstrate the capability of incorporating a targeting strategy within a nanoparticle-supported lipid bilayer for enhanced cellular targeting over traditional nanoparticle systems. The next stage of targeting and camouflage is via the incorporation of endogenous cellular membranes. Provided the enhanced bilayer fluidity, stability and support, tethered membrane nanoparticles provide the most logical nanoparticle substrate for these cell membrane based composites. Tethered systems also don't require the use of electrostatic interactions to form the bilayer, as was demonstrated in Chapter 3. This ultimately allows the use of more complex membranes, where charge-charge interaction may be non-ideal. This work has already demonstrated the use of two separate liposomal formulations in the production of tethered membrane nanoparticles. A tertiary formulation was also explored with DPPC as the major lipid component. DPPC is still a fully saturated lipid but contains two less CH₂ groups in the aliphatic chains which reduce van der Waals associations and hydrophobic interactions. This formulation consisted of a 77.5:20:2.5 molar ratio of DPPC/cholesterol/DSPE-PEG and was the same utilized by Meng *et al.*⁶⁴ **Figure 37** shows TEM micrographs of the three formulations explored in this work. These results demonstrate a capability in extending the currently developed model system to include additional lipid formulations.

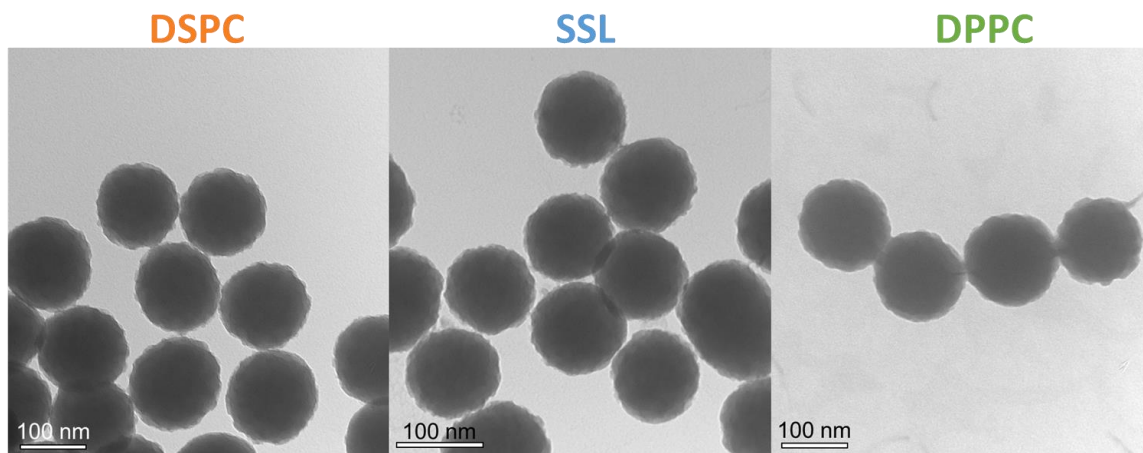


Figure 37. Transmission electron microscopy images tethered membrane nanoparticle produced with three separate liposomal formulations DSPC (left), SSL (middle) and DPPC (right).

Erythrocyte-coated nanoparticles have been explored as a way to enhance the circulation half-life of PLGA nanoparticles. Hu *et al.*¹⁴² found that there was significant retention of the particles in the blood after 72 hours in comparison to previous reports of RBC-derived liposomes. A combination of these two studies could realistically produce an erythrocyte mimic. Another study explored applying platelet membranes onto the surface of PLGA nanoparticles and found increased stability, retention of membrane protein content and right-side-out membrane orientation in translocated membranes.¹⁴³

These studies validate the feasibility in harnessing biomembrane interfaces for the development of enhanced drug delivery vehicles. Incorporation of the tethered nanoparticle system developed herein serves as the next step in developing these schemes. The tethered structures provide the greatest ability in recapitulating the cellular membrane environment, therefore, it serves that these particles may prove most effective in supporting endogenous membranes. These PLGA nanoparticles were loaded with vancomycin (antibiotic) and showed greater efficacy in treating *Staphylococcus aureus in vivo*. This greater efficacy

was a result of the preferential binding of the bacteria to the platelet coated nanoparticles and was found to be membrane specific over red blood cell coated nanoparticles.¹⁴³

In addition to anchoring the lipid bilayer into the surface of the nanoparticle, tethering provides an ability to abstract the lipid bilayer from the surface of the particles. This separation prevents denaturation of membrane proteins and enhances bilayer fluidity, as was discussed in Section 2.34. For these reasons, tethered-SLB provide the greatest mammalian membrane analog. The nanoparticle core dictates the shape of the cell and the PEG molecules provide support in a similar manner to the cytoskeleton. Thus, the incorporation of these cellular membranes within a tethered system would be ideal over fusion to the nanoparticle surface. In the simpler systems discussed, increased fluidity of the membrane also provides the potential for an avidity effect with incorporated targeting ligands and imparts all of the biomimetic/anti-biofouling properties of cellular membrane. This increased fluidity is a result of the lubricating properties the PEG layer provides over the bare nanoparticle core.

These examples demonstrate the synergistic combination of materials and biophysical properties towards the development of a drug delivery vehicle. The incorporation of a tethered system would provide many advantages over the currently used systems. The comparison of endogenous membranes fused to nanoparticle surfaces with tethered bilayers would lead to a greater understanding of cellular membranes, supported lipid bilayers and nanoparticle based drug delivery.

Given that tethered-SLB provide the greatest mammalian membrane analog, the analysis of these nanoparticles with other membranes may provide a more realistic

understanding of how cells interact – especially cells that tend to travel through the body such as red blood cells. Quartz crystal microbalance with dissipation monitoring (QCM-D) has been used to evaluate nanoparticle interactions with lipid bilayers.²⁸⁰

Chapter 7: Summary and Significance

In this work we have demonstrated the controlled self-assembly of a SLB on a silica nanoparticle scaffold of uniform size and shape and observed high colloidal stability under physiologic and storage conditions. A modified vesicle fusion technique was employed towards the creation of a unilamellar lipid bilayer encompassing the particles. A tethered-nanoparticle supported membrane has inherent advantages to polymer and water supported systems previously explored in literature. The tethered system is more complex than these constructs, but the advantages of the system may yield greater success in biomedical applications.

Within the field of drug delivery, inorganic nanoparticles are lauded for their monodisperse sizes, large specific surface area, ability to load drug in their pores and conjugate biomolecules to their surfaces.²⁸¹ This has led to the development of several nanoparticle-based SLB for drug delivery.^{97,263} These membrane laden materials exhibit clear advantages over traditional nanoparticle systems, including increased stability in physiologic conditions and circulation half-lives. Tethered membranes represent the next stage of SLB, with many advantages over these already advanced systems.

In Chapter 3, a study aimed at producing tethered membrane nanoparticles and eliciting the advantages of these systems was explored. A phospholipid was anchored to the surface of the silica particles via a PEG linker. This construct served as a scaffold to which a lipid bilayer was formed. The nanoparticle scaffold utilized hydrophobic

interactions and van der Waals attraction forces between exterior facing DSPE molecules and extraneous liposomes to drive assembly. A modified vesicle fusion method yielded a single lipid bilayer encasing the nanoparticles. Adsorption isotherm data indicated the presence of the exterior facing DSPE molecule drove significantly greater association of lipid in comparison to PEGylated silica. These results were similar to the electrostatically driven association between positively charged amine coated particles and the slightly negative lipid formulation.

An optimal lipid-to-scaffold particle ratio was developed after evaluating changes to hydrodynamic diameter and zeta potential of the membrane laden nanoparticles. Method development of the TMN was optimized via sonication time, temperature and total energy input. The leakiness of the encompassing bilayer was assessed via encapsulation and release of a fluorophore. Release rates were diminished at higher lipid-to-particle ratios, coinciding with more complete bilayer formation. This synthesis study represents the first production and characterization of a nanoparticle-tethered lipid bilayer. Commercially available materials and simple production techniques were employed to enable rapid adoption of the tethering technology.

In Chapter 4, we applied the TMN in the treatment of prostate cancer. A sterically stabilized lipid formulation that included an exterior brush border of PEG was formed around the nanoparticles. Application of this PEG layer was found to inhibit macrophage uptake. These results in combination with previous work from our lab suggest an ability to predict nanocarrier clearance *in vivo* via the selection of exterior facing bilayer properties. TMN were loaded with doxorubicin utilizing a remote loading strategy with high efficiency and MTT staining (PC-3) results indicated a statistically similar performance to liposomal

doxorubicin. The inherent limitations of a solid, silica nanoparticle core did not prevent its use as a drug delivery vehicle. Incorporation of the tethered supports onto mesoporous particles, or other nanoparticle technology, would immediately increase the functionality of the model system explored in this work.

As more complex nanomaterials and nanomaterial-based components are being explored for drug delivery vehicles, toxicity of these components remains an issue. Proper evaluation of nanomaterial toxicity remains deficient in literature, but this topic is quickly gaining attention. In Chapter 5, the toxicity of the underlying component materials was examined with an *in vitro* cell model. Chinese hamster ovary (CHO) cells were incubated with silica nanoparticles of two sizes with different surface characteristics. It was found that a highly positively charged surface led to greater nanoparticle association and uptake with the CHO cells which ultimately increased cytotoxicity. MTT staining did not differ significantly with varying PEG Dalton weight. The mechanism of toxicity was linked to production of reactive oxygen species (ROS) in the presence of the particles, as is typical of nanoparticles. Viability and ROS generation were found to be concentration dependent. In general, the bare and PEGylated silica nanoparticles were not inherently toxic. This study lays the groundwork for future evaluation of composite systems that incorporate these components.

The inherent advantages of tethered membrane nanoparticle systems were theorized in Chapter 2 and developed in Chapters 3 and 4. Based on these findings, future directions of these systems were proposed in Chapter 6. As researchers move towards decorating nanoparticle surfaces with more complex membranes and biological components, the tethered support provides enhanced stability and directed assembly over

the other previously explored colloidal supports. The elimination of a reliance on electrostatic interactions to produce nanoparticle supports extends the array of membranes that can be incorporated on these nanoparticles. These membranes include endogenous-derived lipid sources and previous publications have already demonstrated use of erythrocytes, immune cells and/or cancer cells. However, these early studies have resulted in fused membranes on nanoparticle surfaces, lacking proper membrane fluidity. Previously explored polymer supports offer separation of the lipid bilayer from the nanoparticle surface but are deficient at retaining the bilayer.¹¹⁴ This sets the stage for the application of the tethered system. The inclusion of a tether provides the same separation of the lipid bilayer/membrane from the surface of the nanoparticle as observed in polymer supported systems but anchors the bilayer into the surface, increasing stability and retention. The tether also imparts greater fluidity to the anchored membrane, which has already demonstrated advantages in targeting¹¹², and creates a sub-membrane space that can be used to load drug.

The development of tethered membrane nanoparticles has eluded scientific literature, however, the advantages of such systems have been discussed since the inception of supported lipid bilayers on planar surfaces. Some of these advantages were developed and explored in this work. These include the ability to drive assembly of a lipid bilayer on nanoparticle surfaces without the use of electrostatic interactions (zwitterionic lipids), creation of a sub-membrane space for drug loading and the ability to maintain the supported bilayer under harsh conditions. These advantages have direct applications in drug delivery and several avenues of incorporation have been proposed.

The true accomplishment of this work is the development of a platform that has applications in a myriad of scientific fields. Applications have been already been developed in drug delivery, sensors and separations using similar, less complex systems. The core advantages simply need to be evaluated for each application and constituent components selected. This work presents the founding construct from which additional complexities can be tailored. Within the field of drug delivery, this might entail modifying the materials for a specific drug, disease or combination.

It is important to consider design complexity and cost of each component when designing a nanocarrier for the clinic. Nanoparticle-supported lipid bilayers hold several additional advantages over traditional nanoparticle technologies. The bilayer enables a high drug loading and entrapment as well as co-delivery of hydrophilic and hydrophobic drugs. The bilayer also enables the addition of imaging agents and targeting ligands while contributing to the safety of the nanoparticle platform. Finally, the membrane provides a readily available pathway towards achieving greater functionality over the nanoparticle core.

The use of a tether compounds these advantages in a number of ways. A tether provides increased stability and fluidity of the membrane and permits incorporation of transmembrane proteins – useful in recapitulating membrane mimics. Abstracting the bilayer from the particle surface allows a wider range of membrane compositions and relaxes the requirement of electrostatic interactions to drive assembly. Finally, the tether provides yet another component for optimization of drug release profiles. These key factors enable many enhancements to the most recent, advanced reports of nanoparticle-based, targeted drug delivery vehicles. It is our current belief that a combinatorial approach of a

tethered paradigm with endogenous-derived membranes may enable nanoparticle-based drug delivery vehicles' transition into the next stage of targeting and therapeutic transport, previously unattainable.

References

- (1) Rao, C.; Müller, A.; Cheetham, A. *The Chemistry of Nanomaterials: Synthesis, Properties and Applications*; 2006.
- (2) Ju-Nam, Y.; Lead, J. R. Manufactured Nanoparticles: An Overview of Their Chemistry, Interactions and Potential Environmental Implications. *Sci. Total Environ.* **2008**, *400*, 396–414.
- (3) Silva, G. A. Introduction to Nanotechnology and Its Applications to Medicine. *Surg. Neurol.* **2004**, *61*, 216–220.
- (4) Zang, L. *Energy Efficiency and Renewable Energy Through Nanotechnology*; Zang, L., Ed.; Green Energy and Technology; Springer London: London, 2011.
- (5) Kung, H. H.; Kung, M. C. Nanotechnology: Applications and Potentials for Heterogeneous Catalysis. *Catal. Today* **2004**, *97*, 219–224.
- (6) Allen, T. M.; Cullis, P. R. Liposomal Drug Delivery Systems: From Concept to Clinical Applications. *Adv. Drug Deliv. Rev.* **2013**, *65*, 36–48.
- (7) Yih, T. C.; Al-Fandi, M. Engineered Nanoparticles as Precise Drug Delivery Systems. *J. Cell. Biochem.* **2006**, *97*, 1184–1190.
- (8) De Jong, W. H.; Borm, P. J. Drug Delivery and Nanoparticles: Applications and Hazards. *Int. J. Nanomedicine* **2008**, *3*, 133–149.
- (9) Malam, Y.; Loizidou, M.; Seifalian, A. M. Liposomes and Nanoparticles: Nanosized Vehicles for Drug Delivery in Cancer. *Trends Pharmacol. Sci.* **2009**, *30*, 592–599.
- (10) Siegel, R. W.; Hu, E.; Cox, D. M.; Goronkin, H.; Jelinski, L.; Koch, C. C.; Mendel, J.; Roco, M. C.; Shaw, D. T. *Nanostructure Science and Technology*; Springer Netherlands: Dordrecht, 1999.
- (11) Dehaini, D.; Fang, R. H.; Zhang, L. Biomimetic Strategies for Targeted Nanoparticle Delivery. *Bioeng. Transl. Med.* **2016**, *1*, 30–46.
- (12) Xu, F.; Reiser, M.; Yu, X.; Gummuluru, S.; Wetzler, L.; Reinhard, B. M. Lipid-Mediated Targeting with Membrane-Wrapped Nanoparticles in the Presence of Corona Formation. *ACS Nano* **2016**, *10*, 1189–1200.
- (13) Schlenoff, J. B. Zwitteration: Coating Surfaces with Zwitterionic Functionality to

- Reduce Nonspecific Adsorption. *Langmuir* **2014**, 9625–9636.
- (14) Bretscher, M. S. Asymmetrical Lipid Bilayer Structure for Biological Membranes. *Nat. New Biol.* **1972**, 236, 11–12.
 - (15) Marquardt, D.; Geier, B.; Pabst, G. Asymmetric Lipid Membranes: Towards More Realistic Model Systems. *Membranes (Basel)*. **2015**, 5, 180–196.
 - (16) Segawa, K.; Nagata, S.; Fadok, V. A.; al., et; Gardai, S. J.; al., et; Leventis, P. A.; Grinstein, S.; Tanaka, Y.; Schroit, A. J.; *et al.* An Apoptotic “Eat Me” Signal: Phosphatidylserine Exposure. *Trends Cell Biol.* **2015**, 25, 639–650.
 - (17) Wang, L.-S.; Wu, L.-C.; Lu, S.-Y.; Chang, L.-L.; Teng, I.-T.; Yang, C.-M.; Ho, J. A. Biofunctionalized Phospholipid-Capped Mesoporous Silica Nanoshuttles for Targeted Drug Delivery: Improved Water Susceptibility and Decreased Nonspecific Protein Binding. *ACS Nano* **2010**, 4, 4371–4379.
 - (18) van Schooneveld, M. M.; Vucic, E.; Koole, R.; Zhou, Y.; Stocks, J.; Cormode, D. P.; Tang, C. Y.; Gordon, R. E.; Nicolay, K.; Meijerink, A.; *et al.* Improved Biocompatibility and Pharmacokinetics of Silica Nanoparticles by Means of a Lipid Coating: A Multimodality Investigation. *Nano Lett.* **2008**, 8, 2517–2525.
 - (19) Durfee, P. N.; Lin, Y.-S.; Dunphy, D. R.; Muñiz, A. J.; Butler, K. S.; Humphrey, K. R.; Lokke, A. J.; Agola, J. O.; Chou, S. S.; Chen, I.-M.; *et al.* Mesoporous Silica Nanoparticle-Supported Lipid Bilayers (Protocells) for Active Targeting and Delivery to Individual Leukemia Cells. *ACS Nano* **2016**, 10, 8325–8345.
 - (20) Tang, L.; Cheng, J. Nonporous Silica Nanoparticles for Nanomedicine Application. *Nano Today* **2013**, 8, 290–312.
 - (21) Cho, K.; Chang, H.; Kil, D. S.; Park, J.; Jang, H. D.; Sohn, H. Y. Mechanisms of the Formation of Silica Particles from Precursors with Different Volatilities by Flame Spray Pyrolysis. *Aerosol Sci. Technol.* **2009**, 43, 911–920.
 - (22) Rahman, I. A.; Padavettan, V.; Rahman, I. A.; Padavettan, V. Synthesis of Silica Nanoparticles by Sol-Gel: Size-Dependent Properties, Surface Modification, and Applications in Silica-Polymer Nanocomposites—A Review. *J. Nanomater.* **2012**, 2012, 1–15.
 - (23) G.H. Bogush, M. A. T. and C. F. Z. ukoski I. Preparation of Monodisperse Silica Particles: Control of Size and Mass Fraction. *J. Non. Cryst. Solids* **1988**, 104, 95–106.
 - (24) Stober, W. Controlled Growth of Monodisperse Silica Spheres in the Micron Size Range 1. *J. Colloid Interface Sci.* **1968**, 26, 62–69.
 - (25) Scherer, G. W.; Brinker, C. J. Sol-Gel Science: The Physics and Chemistry of Sol-Gel Processing. *Academic: New York*, 1990.
 - (26) Barbé, C.; Bartlett, J.; Kong, L.; Finnie, K.; Lin, H. Q.; Larkin, M.; Calleja, S.;

- Bush, A.; Calleja, G. Silica Particles: A Novel Drug-Delivery System. *Adv. Mater.* **2004**, *16*, 1959–1966.
- (27) Vivero-Escoto, J. L.; Slowing, I. I.; Trewyn, B. G.; Lin, V. S.-Y.; Slowing II. Mesoporous Silica Nanoparticles for Intracellular Controlled Drug Delivery. *Small* **2010**, *6*, 1952–1967.
- (28) Nooney, R. I.; Thirunavukkarasu, D.; Chen, Y.; Josephs, R.; Ostafin, A. E. Synthesis of Nanoscale Mesoporous Silica Spheres with Controlled Particle Size. **2002**, 4721–4728.
- (29) Mamaeva, V.; Sahlgren, C.; Lindén, M. Mesoporous Silica Nanoparticles in Medicine-Recent Advances. *Adv. Drug Deliv. Rev.* **2013**, *65*, 689–702.
- (30) Lamer, V. K.; Dinagar, R. H. Theory, Production and Mechanism of Formation of Monodispersed Hydrosols. *Edwards Bros. J. J. Frenkel* **1949**.
- (31) Carcouët, C. C. M. C.; Van De Put, M. W. P.; Mezari, B.; Magusin, P. C. M. M.; Laven, J.; Bomans, P. H. H.; Friedrich, H.; Esteves, a. C. C.; Sommerdijk, N. a J. M.; Van Benthem, R. a T. M.; *et al.* Nucleation and Growth of Monodisperse Silica Nanoparticles. *Nano Lett.* **2014**, *14*, 1433–1438.
- (32) Li, S.; Wan, Q.; Qin, Z.; Fu, Y.; Gu, Y. Understanding Stöber Silica's Pore Characteristics Measured by Gas Adsorption. *Langmuir* **2015**, *31*, 824–832.
- (33) Soto-cantu, E.; Cueto, R.; Koch, J.; Russo, P. S. Synthesis and Rapid Characterization of Amine-Functionalized Silica. *Langmuir* **2012**, *28*, 5562–5569.
- (34) Peng, F.; Liu, Y.; Li, X.; Sun, L.; Zhao, D.; Wang, Q.; Ma, G.; Su, Z. PEGylation of G-CSF in Organic Solvent Markedly Increase the Efficacy and Reactivity through Protein Unfolding, Hydrolysis Inhibition and Solvent Effect. *J. Biotechnol.* **2014**, *170*, 42–49.
- (35) Olde Damink, L. H. H.; Dijkstra, P. J.; Van Luyn, M. J. a; Van Wachem, P. B.; Nieuwenhuis, P.; Feijen, J. Cross-Linking of Dermal Sheep Collagen Using a Water-Soluble Carbodiimide. *Biomaterials* **1996**, *17*, 765–773.
- (36) Sehgal, D.; Vijay, I. K. A Method for the High Efficiency of Water-Soluble Carbodiimide-Mediated Amidation. *Analytical biochemistry*, 1994, *218*, 87–91.
- (37) Staros, J. V.; Wright, R. W.; Swingle, D. M. Enhancement by N-Hydroxysulfosuccinimide of Water-Soluble Carbodiimide-Mediated Coupling Reactions. *Anal. Biochem.* **1986**, *156*, 220–222.
- (38) Bangham, A. D.; Horne, R. W. Negative Staining of Phospholipids and Their Structural Modification by Surface-Active Agents as Observed in the Electron Microscope. *J. Mol. Biol.* **1964**, *8*, 660–IN10.
- (39) DOXIL Approved by FDA. *AIDS Patient Care* **1995**, *9*, 306.

- (40) Chang, H.-I.; Yeh, M.-K. Clinical Development of Liposome-Based Drugs: Formulation, Characterization, and Therapeutic Efficacy. *Int. J. Nanomedicine* **2012**, *7*, 49–60.
- (41) Lasic, D. D. *Liposomes: From Physics to Applications*; Elsevier Science Ltd., 1993.
- (42) Sales-Campos, H.; Souza, P. R. de; Peghini, B. C.; da Silva, J. S.; Cardoso, C. R. An Overview of the Modulatory Effects of Oleic Acid in Health and Disease. *Mini Rev. Med. Chem.* **2013**, *13*, 201–210.
- (43) Paltauf, F.; Hermetter, A. Phospholipids — Natural, Semisynthetic, Synthetic. In *Phospholipids*; Springer US: Boston, MA, 1990; pp. 1–12.
- (44) Cevc, G. *Phospholipids Handbook*; Cevc, G., Ed.; CRC Press: New York, 1993.
- (45) Akbarzadeh, A.; Rezaei-Sadabady, R.; Davaran, S.; Joo, S. W.; Zarghami, N.; Hanifehpour, Y.; Samiei, M.; Kouhi, M.; Nejati-Koshki, K. Liposome: Classification, Preparation, and Applications. *Nanoscale Res. Lett.* **2013**, *8*, 102.
- (46) Li, J.; Wang, X.; Zhang, T.; Wang, C.; Huang, Z.; Luo, X.; Deng, Y. A Review on Phospholipids and Their Main Applications in Drug Delivery Systems. *Asian Journal of Pharmaceutical Sciences*, 2014, *10*, 81–98.
- (47) van Swaay, D.; deMello, A. Microfluidic Methods for Forming Liposomes. *Lab Chip* **2013**, *13*, 752.
- (48) Ulrich, A. S. Biophysical Aspects of Using Liposomes as Delivery Vehicles Liposome Composition and Size. *Biosci. Rep.* **2002**, *22*.
- (49) Dé, F.; De Meyer, R.; Smit, B.; Klein, M. L. Effect of Cholesterol on the Structure of a Phospholipid Bilayer.
- (50) Brown, D. A.; London, E. Functions of Lipid Rafts in Biological Membranes. *Annu. Rev. Cell Dev. Biol.* **1998**, *14*, 111–136.
- (51) Eze, M. O. Phase Transitions in Phospholipid Bilayers: Lateral Phase Separations Play Vital Roles in Biomembranes. *Biochem. Educ.* **1991**, *19*, 204–208.
- (52) Gennis Robert B. *Biomembranes: Molecular Structure and Function*; Cantor, C. R., Ed.; 1989.
- (53) Chandler, D. Interfaces and the Driving Force of Hydrophobic Assembly. *Nature*, 2005, *437*, 640–647.
- (54) Marsh, D. Equation of State for Phospholipid Self-Assembly. *Biophys. J.* **2016**, *110*, 188–196.
- (55) Marsh, D. Thermodynamics of Phospholipid Self-Assembly. *Biophys. J.* **2012**, *102*, 1079–1087.

- (56) Wicken, A. J.; Evans, J. D.; Knox, K. W. Critical Micelle Concentrations of Lipoteichoic Acids. *J. Bacteriol.* **1986**, *166*, 72–77.
- (57) Israelachvili, J. N. *Intermolecular and Surface Forces*; Academic Press, 2011.
- (58) Shen, Y.; Saboe, P. O.; Sines, I. T.; Erbakan, M.; Kumar, M. Biomimetic Membranes: A Review. *J. Memb. Sci.* **2014**, *454*, 359–381.
- (59) Tamm, L. K.; McConnell, H. M. Supported Phospholipid Bilayers. *Biophys. J.* **1985**, *47*, 105–113.
- (60) Sackmann, E. Supported Membranes: Scientific and Practical Applications. *Science (80-.)*. **1996**, *271*, 43–48.
- (61) Tanaka, M. Polymer-Supported Membranes: Physical Models of Cell Surfaces. **2006**, *31*, 513–520.
- (62) Eeman, M.; Deleu, M. From Biological Membranes to Biomimetic Model Membranes. *Biotechnol. Agron. Soc. Environ.* **2010**, *14*, 719–736.
- (63) Bally, M.; Bailey, K.; Sugihara, K.; Grieshaber, D.; Vörös, J.; Städler, B. Liposome and Lipid Bilayer Arrays Towards Biosensing Applications. *Small* **2010**, *6*, 2481–2497.
- (64) Meng, H.; Wang, M.; Liu, H.; Liu, X.; Situ, A.; Wu, B.; Ji, Z.; Chang, C. H.; Nel, A. E. Use of a Lipid-Coated Mesoporous Silica Nanoparticle Platform for Synergistic Gemcitabine and Paclitaxel Delivery to Human Pancreatic Cancer in Mice. *ACS Nano* **2015**, *9*, 3540–3557.
- (65) Wenzl, P.; Fringeli, M.; Goette, J.; Fringeli, U. P. Supported Phospholipid Bilayers Prepared by the LB/Vesicle Attenuated Total Reflection Spectroscopic Study on Structure and Stability Vesicle Method " : A Fourier Transform Infrared. *Langmuir* **1994**, *10*, 4253–4264.
- (66) Thomson, N. L.; Pearce, K. H.; Hsieh, H. V.; Thompson; Pearce; Hsieh, H. V. Total Internal Reflection Fluorescence Microscopy: Application to Substrate-Supported Planar Membranes. *Eur. Biophys. J.* **1993**, *22*, 367–378.
- (67) Tamm, L. K.; Tatulian, S. A. Infrared Spectroscopy of Proteins and Peptides in Lipid Bilayers. *Quarterly Reviews of Biophysics*, 1997, *30*, 365–429.
- (68) Wagner, M. L.; Tamm, L. K. Tethered Polymer-Supported Planar Lipid Bilayers for Reconstitution of Integral Membrane Proteins: Silane-Polyethyleneglycol-Lipid as a Cushion and Covalent Linker. *Biophys. J.* **2000**, *79*, 1400–1414.
- (69) Johnson, S. J.; Bayerl, T. M.; McDermott, D. C.; Adam, G. W.; Rennie, A. R.; Thomas, R. K.; Sackmann, E. Structure of an Adsorbed Dimyristoylphosphatidylcholine Bilayer Measured with Specular Reflection of Neutrons. *Biophys. J.* **1991**, *59*, 289–294.

- (70) Tamm, L. K. Lateral Diffusion and Fluorescence Microscope Studies on a Monoclonal Antibody Specifically Bound to Supported Phospholipid Bilayers. *Biochemistry* **1988**, *27*, 1450–1457.
- (71) Thompson, N. L.; Poglitsch, C. L.; Timbs, M. M.; Pisarchick, M. L. Dynamics of Antibodies on Planar Model Membranes. *Acc. Chem. Res.* **1993**, *26*, 567–573.
- (72) Kuhner, M.; Tampe, R.; Sackmann, E. Lipid Mono- and Bilayer Supported on Polymer Films: Composite Polymer-Lipid Films on Solid Substrates. *Biophys. J.* **1994**, *67*, 217–226.
- (73) Elender, G.; Kühner, M.; Sackmann, E. Functionalisation of Si/SiO₂ and Glass Surfaces with Ultrathin Dextran Films and Deposition of Lipid Bilayers. *Biosens. Bioelectron.* **1996**, *11*, 565–577.
- (74) Schmitt, J.; Danner, B.; Bayerl, T. M. Polymer Cushions in Supported Phospholipid Bilayers Reduce Significantly the Frictional Drag between Bilayer and Solid Surface. *Langmuir* **2001**, *17*, 244–246.
- (75) Goennenwein, S.; Tanaka, M.; Hu, B.; Moroder, L.; Sackmann, E. Functional Incorporation of Integrins into Solid Supported Membranes on Ultrathin Films of Cellulose: Impact on Adhesion. *Biophys. J.* **2003**, *85*, 646–655.
- (76) Beyer, D.; Elender, G.; Knoll, W.; Kühner, M.; Maus, S.; Ringsdorf, H.; Sackmann, E. Influence of Anchor Lipids on the Homogeneity and Mobility of Lipid Bilayers on Thin Polymer Films. *Angew. Chemie Int. Ed. English* **1996**, *35*, 1682–1685.
- (77) Wagner, M. L.; Tamm, L. K. Tethered Polymer-Supported Planar Lipid Bilayers for Reconstitution of Integral Membrane Proteins: Silane-Polyethyleneglycol-Lipid as a Cushion and Covalent Linker. *Biophys. J.* **2000**, *79*, 1400–1414.
- (78) Tanaka, M.; Sackmann, E. Polymer-Supported Membranes as Models of the Cell Surface. *Nature* **2005**, *437*, 656–663.
- (79) Tanaka, M.; Rehfeldt, F.; Schneider, M. F.; Mathe, G.; Albersdörfer, A.; Neumaier, K. R.; Purrucker, O.; Sackmann, E. Wetting and Dewetting of Extracellular Matrix and Glycocalyx Models. *J. Phys. Condens. Matter* **2005**, *17*, 649–663.
- (80) Nissen, J.; Gritsch, S.; Wiegand, G.; Rädler, J. O. Wetting of Phospholipid Membranes on Hydrophilic Surfaces – Concepts towards Self-Healing Membranes. *Eur. Phys. J. B* **1999**, *10*, 335–344.
- (81) Sackmann, E.; Tanaka, M. Supported Membranes on Soft Polymer Cushions: Fabrication, Characterization and Applications. *Trends Biotechnol.* **2000**, *18*, 58–64.
- (82) Knoll, W.; Frank, C. W.; Heibel, C.; Naumann, R.; Offenhäusser, a; Rühle, J.; Schmidt, E. K.; Shen, W. W.; Sinner, a. Functional Tethered Lipid Bilayers. *J.*

Biotechnol. **2000**, *74*, 137–158.

- (83) Mecke, A.; Dittrich, C.; Meier, W.; Discher, D. E.; Eisenberg, A.; Kita-Tokarczyk, K.; Grumelard, J.; Haefele, T.; Meier, W.; Hamley, I. W.; *et al.* Biomimetic Membranes Designed from Amphiphilic Block Copolymers. *Soft Matter* **2006**, *2*, 751.
- (84) Castellana, E. T.; Cremer, P. S. Solid Supported Lipid Bilayers: From Biophysical Studies to Sensor Design. *Surf. Sci. Rep.* **2006**, *61*, 429–444.
- (85) Mattingly, S. J.; O’Toole, M. G.; James, K. T.; Clark, G. J.; Nantz, M. H. Magnetic Nanoparticle-Supported Lipid Bilayers for Drug Delivery. *Langmuir* **2015**, *31*, 3326–3332.
- (86) Sugihara, K.; Jang, B.; Schneider, M.; Vörös, J.; Zambelli, T. A Universal Method for Planar Lipid Bilayer Formation by Freeze and Thaw. *Soft Matter* **2012**, *8*, 5525.
- (87) Tabaei, S. R.; Choi, J.-H.; Haw Zan, G.; Zhdanov, V. P.; Cho, N.-J. Solvent-Assisted Lipid Bilayer Formation on Silicon Dioxide and Gold. *Langmuir* **2014**, *30*, 10363–10373.
- (88) Cho, N.-J.; Cho, S.-J.; Cheong, K. H.; Glenn, J. S.; Frank, C. W. Employing an Amphipathic Viral Peptide to Create a Lipid Bilayer on Au and TiO₂. *J. Am. Chem. Soc.* **2007**, *129*, 10050–10051.
- (89) Vacklin, H. P.; Tiberg, F.; Thomas, R. K. Formation of Supported Phospholipid Bilayers via Co-Adsorption with β -D-Dodecyl Maltoside. *Biochim. Biophys. Acta - Biomembr.* **2005**, *1668*, 17–24.
- (90) And, A. A. B.; Mcconnell, H. M. Allogeneic Stimulation of Cytotoxic T Cells by Supported Planar Membranes (Class I Major Histocompatibility Antigen/membrane Reconstitution/antigen processing/LFA-1 Cell Surface Protein/lateral Diffusion). *Immunology* **1984**, *81*, 6159–6163.
- (91) Kalb, E.; Frey, S.; Tamm, L. K. Formation of Supported Planar Bilayers by Fusion of Vesicles to Supported Phospholipid Monolayers. *Biochim. Biophys. Acta* **1992**, *1103*, 307–316.
- (92) Hamai, C.; Cremer, P. S.; Musser, S. M. Single Giant Vesicle Rupture Events Reveal Multiple Mechanisms of Glass-Supported Bilayer Formation. *Biophys. J.* **2007**, *92*, 1988–1999.
- (93) Schönherr, H.; Johnson, J. M.; Lenz, P.; Frank, C. W.; Boxer, S. G. Vesicle Adsorption and Lipid Bilayer Formation on Glass Studied by Atomic Force Microscopy. *Langmuir* **2004**, *20*, 11600–11606.
- (94) Weirich, K. L.; Israelachvili, J. N.; Fygenson, D. K. Bilayer Edges Catalyze Supported Lipid Bilayer Formation. *Biophys. J.* **2010**, *98*, 85–92.

- (95) Richter, R. P.; Bérat, R.; Brisson, A. R. Formation of Solid-Supported Lipid Bilayers: An Integrated View.
- (96) Dynamics of Supported Lipid Bilayer Deposition from Vesicle Suspensions. *J. Colloid Interface Sci.* **2010**, *348*, 608–614.
- (97) Carmona-Ribeiro, A. M.; Carmona-, A. M. Biomimetic Nanoparticles: Preparation, Characterization and Biomedical Applications. *Int. J. Nanomedicine* **2010**, *5*, 249–259.
- (98) Bucak, S.; Wang, C.; Laibinis, P. E.; Hatton, T. A. Dynamics of Supported Lipid Bilayer Deposition from Vesicle Suspensions. *J. Colloid Interface Sci.* **2010**, *348*, 608–614.
- (99) Anne-Lise Troutier; Thierry Delair; Christian Pichot, and; Ladavière*, C.; Troutier, A.-L.; Delair, T.; Pichot, C.; Ladavière, C. Physicochemical and Interfacial Investigation of Lipid/Polymer Particle Assemblies. *Langmuir* **2005**, *21*, 1305–1313.
- (100) Thevenot, J.; Troutier, A.-L.; Putaux, J.-L.; Delair, T.; Ladavière, C. Effect of the Polymer Nature on the Structural Organization of Lipid/Polymer Particle Assemblies. *J. Phys. Chem. B* **2008**, *112*, 13812–13822.
- (101) Rapuano; Carmona-Ribeiro. Physical Adsorption of Bilayer Membranes on Silica. *J. Colloid Interface Sci.* **1997**, *193*, 104–111.
- (102) Rapuano, R.; Carmona-Ribeiro, A. M. Supported Bilayers On Silica. *J. Colloid Interface Sci.* **2000**, *226*, 299–307.
- (103) Carmona-Ribeiro, A. M.; Midmore, B. R. Synthetic Bilayer Adsorption onto Polystyrene Microspheres. *Langmuir* **1992**, *8*, 801–806.
- (104) Duro, N.; Gjika, M.; Siddiqui, A.; Scott, H. L.; Varma, S. POPC Bilayers Supported on Nanoporous Substrates: Specific Effects of Silica-Type Surface Hydroxylation and Charge Density. *Langmuir* **2016**, *32*, 6766–6774.
- (105) Moura, S. P.; Carmona-Ribeiro, A. M. Biomimetic Particles: Optimization of Phospholipid Bilayer Coverage on Silica and Colloid Stabilization. *Langmuir* **2005**, *21*, 10160–10164.
- (106) Moura, S. P.; Carmona-Ribeiro, A. M. Adsorption Behavior of DODAB/DPPC Vesicles on Silica. *J. Colloid Interface Sci.* **2007**, *313*, 519–526.
- (107) Richter, R.; Mukhopadhyay, A.; Brisson, A. Pathways of Lipid Vesicle Deposition on Solid Surfaces: A Combined QCM-D and AFM Study. *Biophys. J.* **2003**, *85*, 3035–3047.
- (108) Michel, R.; Gradzielski, M. Experimental Aspects of Colloidal Interactions in Mixed Systems of Liposome and Inorganic Nanoparticle and Their Applications. *Int. J. Mol. Sci.* **2012**, *13*, 11610–11642.

- (109) Richter, R. P.; Brisson, A. R. Following the Formation of Supported Lipid Bilayers on Mica: A Study Combining AFM, QCM-D, and Ellipsometry. *Biophys. J.* **2005**, *88*, 3422–3433.
- (110) Käsbauer, M.; Junglas, M.; Bayerl, T. M. Effect of Cationic Lipids in the Formation of Asymmetries in Supported Bilayers. *Biophys. J.* **1999**, *76*, 2600–2605.
- (111) Liu, J.; Stace-Naughton, A.; Jiang, X.; Brinker, C. J. Porous Nanoparticle Supported Lipid Bilayers (Protocells) as Delivery Vehicles. *J. Am. Chem. Soc.* **2009**, *131*, 1354–1355.
- (112) Ashley, C. E.; Carnes, E. C.; Phillips, G. K.; Padilla, D.; Durfee, P. N.; Brown, P. A.; Hanna, T. N.; Liu, J.; Phillips, B.; Carter, M. B.; *et al.* The Targeted Delivery of Multicomponent Cargos to Cancer Cells by Nanoporous Particle-Supported Lipid Bilayers. *Nat. Mater.* **2011**, *10*, 389–397.
- (113) Fenart, L.; Casanova, A.; Dehouck, B.; Duhem, C.; Slupek, S.; Cecchelli, R.; Betbeder, D. Evaluation of Effect of Charge and Lipid Coating on Ability of 60-Nm Nanoparticles to Cross an in Vitro Model of the Blood-Brain Barrier. *J. Pharmacol. Exp. Ther.* **1999**, *291*, 1017–1022.
- (114) Ross, E. E.; Mok, S. W.; Bugni, S. R. Assembly of Lipid Bilayers on Silica and Modified Silica Colloids by Reconstitution of Dried Lipid Films. *Langmuir* **2011**, *27*, 8634–8644.
- (115) Nabika, H.; Fukasawa, A.; Murakoshi, K. Tuning the Dynamics and Molecular Distribution of the Self-Spreading Lipid Bilayer. *Phys. Chem. Chem. Phys.* **2008**, *10*, 2243.
- (116) Jackman, J. A.; Tabaei, S. R.; Zhao, Z.; Yorulmaz, S.; Cho, N. J. Self-Assembly Formation of Lipid Bilayer Coatings on Bare Aluminum Oxide: Overcoming the Force of Interfacial Water. *ACS Appl. Mater. Interfaces* **2015**, *7*, 959–968.
- (117) Tadmor, R. The London-van Der Waals Interaction Energy between Objects of Various Geometries. *J. Phys. Condens. Matter* **2001**, *13*, L195–L202.
- (118) Israelachvili, J. N. The Calculation of van Der Waals Dispersion Forces between Macroscopic Bodies. *Proc. R. Soc. London. Ser. A, Math. Phys. Sci. Proc. R. Soc. London. Ser. A* **1972**, *331204233132*, 39–55.
- (119) Markovich, T.; Andelman, D.; Podgornik, R. Charged Membranes: Poisson-Boltzmann Theory, DLVO Paradigm and beyond. **2016**.
- (120) Hogg, R.; Healy, T. W.; Fuerstenau, D. W. Mutual Coagulation of Colloidal Dispersions. *Trans. Faraday Soc.* **1966**, *62*, 1638.
- (121) Jackman, J. A.; Zan, G. H.; Zhao, Z.; Cho, N. J. Contribution of the Hydration Force to Vesicle Adhesion on Titanium Oxide. *Langmuir* **2014**, *30*, 5368–5372.

- (122) Tero, R.; Ujihara, T.; Urisu, T. Lipid Bilayer Membrane with Atomic Step Structure: Supported Bilayer on a Step-and-Terrace TiO₂ (100) Surface. *Langmuir* **2008**, *24*, 11567–11576.
- (123) Oleson, T. A.; Sahai, N. Interaction Energies between Oxide Surfaces and Multiple Phosphatidylcholine Bilayers from Extended-DLVO Theory. *J. Colloid Interface Sci.* **2010**, *352*, 316–326.
- (124) Israelachvili, J. N.; Wennerstrom, H. Hydration or Steric Forces between Amphiphilic Surfaces? *Langmuir* **1990**, *6*, 873–876.
- (125) Ahmed, S.; Savarala, S.; Chen, Y.; Bothun, G.; Wunder, S. L. Formation of Lipid Sheaths around Nanoparticle-Supported Lipid Bilayers. *Small* **2012**, *8*, 1740–1751.
- (126) Seifert, U.; Lipowsky, R. Adhesion of Vesicles. *Phys. Rev. A* **1990**, *42*, 4768–4771.
- (127) Richter, R. P.; Bérat, R.; Brisson, A. R. Formation of Solid-Supported Lipid Bilayers: An Integrated View. *Langmuir* **2006**, *22*, 3497–3505.
- (128) Sharma, P.; Ganta, S.; Denny, W. A.; Garg, S. Formulation and Pharmacokinetics of Lipid Nanoparticles of a Chemically Sensitive Nitrogen Mustard Derivative: Chlorambucil. *Int. J. Pharm.* **2009**, *367*, 187–194.
- (129) Burger, K. N. J.; Staffhorst, R. W. H. M.; De Vijlder, H. C.; Velinova, M. J.; Bomans, P. H.; Frederik, P. M.; De Kruijff, B. Nanocapsules: Lipid-Coated Aggregates of Cisplatin with High Cytotoxicity. *Nat. Med.* **2002**, *8*, 81–84.
- (130) Koole, R.; van Schooneveld, M. M.; Hilhorst, J.; Castermans, K.; Cormode, D. P.; Strijkers, G. J.; de Mello Donegá, C.; Vanmaekelbergh, D.; Griffioen, A. W.; Nicolay, K.; *et al.* Paramagnetic Lipid-Coated Silica Nanoparticles with a Fluorescent Quantum Dot Core: A New Contrast Agent Platform for Multimodality Imaging. *Bioconjug. Chem.* **2008**, *19*, 2471–2479.
- (131) Liu, J.; Jiang, X.; Ashley, C.; Brinker, C. J. Electrostatically Mediated Liposome Fusion and Lipid Exchange with a Nanoparticle-Supported Bilayer for Control of Surface Charge, Drug Containment, and Delivery. *J. Am. Chem. Soc.* **2009**, *131*, 7567–7569.
- (132) Yang, Y.; Song, W.; Wang, A.; Zhu, P.; Fei, J.; Li, J. Lipid Coated Mesoporous Silica Nanoparticles as Photosensitive Drug Carriers. *Phys. Chem. Chem. Phys.* **2010**, *12*, 4418.
- (133) Cauda, V.; Engelke, H.; Sauer, A.; Arcizet, D.; Rädler, J.; Bein, T. Colchicine-Loaded Lipid Bilayer-Coated 50 Nm Mesoporous Nanoparticles Efficiently Induce Microtubule Depolymerization upon Cell Uptake. *Nano Lett.* **2010**, *10*, 2484–2492.
- (134) Ashley, C. E.; Carnes, E. C.; Epler, K. E.; Padilla, D. P.; Phillips, G. K.; Castillo, R. E.; Wilkinson, D. C.; Wilkinson, B. S.; Burgard, C. A.; Kalinich, R. M.; *et al.*

Delivery of Small Interfering RNA by Peptide-Targeted Mesoporous Silica Nanoparticle-Supported Lipid Bilayers. *ACS Nano* **2012**, *6*, 2174–2188.

- (135) Dengler, E. C.; Liu, J.; Kerwin, A.; Torres, S.; Olcott, C. M.; Bowman, B. N.; Armijo, L.; Gentry, K.; Wilkerson, J.; Wallace, J.; *et al.* Mesoporous Silica-Supported Lipid Bilayers (Protocells) for DNA Cargo Delivery to the Spinal Cord. *J. Control. Release* **2013**, *168*, 209–224.
- (136) Gonzalez Porras, M. A.; Durfee, P.; Giambini, S.; Sieck, G. C.; Brinker, C. J.; Mantilla, C. B. Uptake and Intracellular Fate of Cholera Toxin Subunit B-Modified Mesoporous Silica Nanoparticle-Supported Lipid Bilayers (Aka Protocells) in Motoneurons. *Nanomedicine Nanotechnology, Biol. Med.* **2018**, *14*, 661–672.
- (137) Rocío Villegas, M.; Baeza, A.; Nouredine, A.; Durfee, P. N.; Butler, K. S.; Ongudi Agola, J.; Jeffrey Brinker, C.; Vallet-Regí, M. Multifunctional Protocells for Enhanced Penetration in 3D Extracellular Tumoral Matrices.
- (138) Datz, S.; Engelke, H.; Schirnding, C. v.; Nguyen, L.; Bein, T. Lipid Bilayer-Coated Curcumin-Based Mesoporous Organosilica Nanoparticles for Cellular Delivery. *Microporous Mesoporous Mater.* **2016**, *225*, 371–377.
- (139) Zhang, X.; Li, F.; Guo, S.; Chen, X.; Wang, X.; Li, J.; Gan, Y. Biofunctionalized Polymer-Lipid Supported Mesoporous Silica Nanoparticles for Release of Chemotherapeutics in Multidrug Resistant Cancer Cells. *Biomaterials* **2014**, *35*, 3650–3665.
- (140) Han, N.; Wang, Y.; Bai, J.; Liu, J.; Wang, Y.; Gao, Y.; Jiang, T.; Kang, W.; Wang, S. Facile Synthesis of the Lipid Bilayer Coated Mesoporous Silica Nanocomposites and Their Application in Drug Delivery. *Microporous Mesoporous Mater.* **2016**, *219*, 209–218.
- (141) Tu, J.; Bussmann, J.; Du, G.; Gao, Y.; Bouwstra, J. A.; Kros, A. Lipid Bilayer-Coated Mesoporous Silica Nanoparticles Carrying Bovine Hemoglobin towards an Erythrocyte Mimic. *Int. J. Pharm.* **2018**.
- (142) Hu, C.-M. J.; Zhang, L.; Aryal, S.; Cheung, C.; Fang, R. H.; Zhang, L. Erythrocyte Membrane-Camouflaged Polymeric Nanoparticles as a Biomimetic Delivery Platform. *Proc. Natl. Acad. Sci.* **2011**, *108*, 10980–10985.
- (143) Hu, C. M. J.; Fang, R. H.; Wang, K. C.; Luk, B. T.; Thamphiwatana, S.; Dehaini, D.; Nguyen, P.; Angsantikul, P.; Wen, C. H.; Kroll, A. V.; *et al.* Nanoparticle Biointerfacing by Platelet Membrane Cloaking. *Nature* **2015**, *526*, 118–121.
- (144) Raemdonck, K.; Braeckmans, K.; Demeester, J.; De Smedt, S. C. Merging the Best of Both Worlds: Hybrid Lipid- Enveloped Matrix Nanocomposites in Drug Delivery. *Chem. Soc. Rev. Chem. Soc. Rev* **2014**, *444*, 444–472.
- (145) Wang, L.-S.; Wu, L.-C.; Lu, S.-Y.; Chang, L.-L.; Teng, I.-T.; Yang, C.-M.; Annie

- Ho, J. Biofunctionalized Phospholipid-Capped Mesoporous Silica Nanoshuttles for Targeted Drug Delivery: Improved Water Suspending and Decreased Nonspecific Protein Binding.
- (146) Hu, M.; Stanzione, F.; Sum, A. K.; Faller, R.; Deserno, M. Design Principles for Nanoparticles Enveloped by a Polymer-Tethered Lipid Membrane. *ACS Nano* **2015**, *9*, 9942–9954.
- (147) Fried, E. S.; Luchan, J.; Gilchrist, M. L. Biodegradable, Tethered Lipid Bilayer–Microsphere Systems with Membrane-Integrated α -Helical Peptide Anchors. *Langmuir* **2016**, *32*, 3470–3475.
- (148) Naumann, R.; Nowak, C. Lipid Membrane Enveloped Particles with Membrane Proteins. EP 2 746 772 A1, 2014.
- (149) Gabizon, A.; Papahadjopoulos, D. Liposome Formulations with Prolonged Circulation Time in Blood and Enhanced Uptake by Tumors. *Proc. Natl. Acad. Sci. U. S. A.* **1988**, *85*, 6949–6953.
- (150) Kirby, C.; Clarke, J.; Gregoriadis, G. Cholesterol Content of Small Unilamellar Liposomes Controls Phospholipid Loss to High Density Lipoproteins in the Presence of Serum. *FEBS Lett.* **1980**, *111*, 324–328.
- (151) Mayer, L. D.; Bally, M. B.; Cullis, P. R. Strategies for Optimizing Liposomal Doxorubicin. *J. Liposome Res.* **1990**, 46348021.
- (152) Bunker, A.; Magarkar, A.; Viitala, T. Rational Design of Liposomal Drug Delivery Systems, a Review: Combined Experimental and Computational Study of Lipid Membranes, Liposomes and Their PEGylation. *Biochim. Biophys. Acta - Biomembr.* **2016**.
- (153) Lin, Y.-S.; Haynes, C. L. Impacts of Mesoporous Silica Nanoparticle Size, Pore Ordering, and Pore Integrity on Hemolytic Activity. *J. Am. Chem. Soc.* **2010**, *132*, 4834–4842.
- (154) Lodha, A.; Lodha, M.; Patel, A.; Chaudhuri, J.; Dalal, J.; Edwards, M.; Douroumis, D. Synthesis of Mesoporous Silica Nanoparticles and Drug Loading of Poorly Water Soluble Drug Cyclosporin A. *J. Pharm. Bioallied Sci.* **2012**, *4*, S92-4.
- (155) Doadrio, J. C.; Sousa, E. M. B.; Izquierdo-Barba, I.; Doadrio, A. L.; Perez-Pariante, J.; Vallet-Regí, M. Functionalization of Mesoporous Materials with Long Alkyl Chains as a Strategy for Controlling Drug Delivery Pattern. *J. Mater. Chem.* **2006**, *16*, 462–466.
- (156) Trewyn, B. G.; Giri, S.; Slowing, I. I.; Lin, V. S.-Y. Mesoporous Silica Nanoparticle Based Controlled Release, Drug Delivery, and Biosensor Systems. *Chem. Commun.* **2007**, 3236.
- (157) Yang, K.-N.; Zhang, C.-Q.; Wang, W.; Wang, P. C.; Zhou, J.-P.; Liang, X.-J. pH-

- Responsive Mesoporous Silica Nanoparticles Employed in Controlled Drug Delivery Systems for Cancer Treatment. *Cancer Biol. Med.* **2014**, *11*, 34–43.
- (158) Slowing, I. I.; Vivero-Escoto, J. L.; Wu, C.-W.; Lin, V. S.-Y. Mesoporous Silica Nanoparticles as Controlled Release Drug Delivery and Gene Transfection Carriers. *Adv. Drug Deliv. Rev.* **2008**, *60*, 1278–1288.
- (159) Praetorius, M.; Brunner, C.; Lehnert, B.; Klingmann, C.; Schmidt, H.; Staecker, H.; Schick, B. Transsynaptic Delivery of Nanoparticles to the Central Auditory Nervous System. *Acta Otolaryngol.* **2007**, *127*, 486–490.
- (160) Gerion, D.; Herberg, J.; Bok, R.; Gjersing, E.; Ramon, E.; Maxwell, R.; Kurhanewicz, J.; Budinger, T. F.; Gray, J. W.; Shuman, M. A.; *et al.* Paramagnetic Silica-Coated Nanocrystals as an Advanced MRI Contrast Agent. *J. Phys. Chem. C* **2007**, *111*, 12542–12551.
- (161) Taylor, K. M. L.; Kim, J. S.; Rieter, W. J.; An, H.; Lin, W.; Lin, W. Mesoporous Silica Nanospheres as Highly Efficient MRI Contrast Agents. *J. Am. Chem. Soc.* **2008**, *130*, 2154–2155.
- (162) Meng, H.; Yang, S.; Li, Z.; Xia, T.; Chen, J.; Ji, Z.; Zhang, H.; Wang, X.; Lin, S.; Huang, C.; *et al.* Aspect Ratio Determines the Quantity of Mesoporous Silica Nanoparticle Uptake by a Small GTPase-Dependent Macropinocytosis Mechanism. **2011**, *5*, 4434–4447.
- (163) Mayer, L. D.; Bally, M. B.; Cullis, P. R. Strategies for Optimizing Liposomal Doxorubicin. *J. Liposome Res.* **1990**, 46348021.
- (164) Targeted Silica Nanoparticles for Real-Time Image-Guided Intraoperative Mapping of Nodal Metastases
<https://clinicaltrials.gov/ct2/show/NCT02106598?term=silica+nanoparticles&rank=1> (accessed Mar 1, 2018).
- (165) He, Q.; Zhang, Z.; Gao, F.; Li, Y.; Shi, J. In Vivo Biodistribution and Urinary Excretion of Mesoporous Silica Nanoparticles: Effects of Particle Size and PEGylation. *Small* **2011**, *7*, 271–280.
- (166) Lind, T. K.; Cárdenas, M. Understanding the Formation of Supported Lipid Bilayers via Vesicle fusion—A Case That Exemplifies the Need for the Complementary Method Approach (Review) Understanding the Formation of Supported Lipid Bilayers via Vesicle Fusion— A Case That Exemplifies the Need for the Complementary Method Approach (Review). *Cit. Biointerphases* **2016**, *11*.
- (167) Tristram-Nagle, S.; Nagle, J. F. Lipid Bilayers: Thermodynamics, Structure, Fluctuations, and Interactions. *Chem. Phys. Lipids* **2004**, *127*, 3–14.
- (168) Riske, K. A.; Barroso, R. P.; Vequi-Suplicy, C. C.; Germano, R.; Henriques, V. B.; Lamy, M. T. Lipid Bilayer Pre-Transition as the Beginning of the Melting Process. *Biochim. Biophys. Acta - Biomembr.* **2009**, *1788*, 954–963.

- (169) Naumann, C.; Brumm, T.; Bayerl, T. M. Phase Transition Behavior of Single Phosphatidylcholine Bilayers on a Solid Spherical Support Studied by DSC, NMR and FT-IR. *Biophys. J.* **1992**, *63*, 1314–1319.
- (170) Wang, B.; Zhang, L.; Bae, S. C.; Granick, S. Nanoparticle-Induced Surface Reconstruction of Phospholipid Membranes. *Proc. Natl. Acad. Sci.* **2008**, *105*, 18171–18175.
- (171) Lehman, S. E.; Mudunkotuwa, I. A.; Grassian, V. H.; Larsen, S. C. Nano–Bio Interactions of Porous and Nonporous Silica Nanoparticles of Varied Surface Chemistry: A Structural, Kinetic, and Thermodynamic Study of Protein Adsorption from RPMI Culture Medium.
- (172) Kubiak-Ossowska, K.; Tokarczyk, K.; Jachimska, B.; Mulheran, P. A.; Haber, J. Bovine Serum Albumin Adsorption at a Silica Surface Explored by Simulation and Experiment.
- (173) Huang, R.; Lau, B. L. T. Biomolecule-Nanoparticle Interactions: Elucidation of the Thermodynamics by Isothermal Titration Calorimetry. *Biochim. Biophys. Acta - Gen. Subj.* **2016**, *1860*, 945–956.
- (174) Loosli, F.; Vitorazi, L.; Berret, J.-F.; Stoll, S. Isothermal Titration Calorimetry as a Powerful Tool to Quantify and Better Understand Agglomeration Mechanisms during Interaction Processes between TiO₂ Nanoparticles and Humic Acids. *Environ. Sci. Nano* **2015**, *2*, 541–550.
- (175) Seeger, H. M.; Marino, G.; Alessandrini, A.; Facci, P. Effect of Physical Parameters on the Main Phase Transition of Supported Lipid Bilayers. *Biophys. J.* **2009**, *97*, 1067–1076.
- (176) Savarala, S.; Ahmed, S.; Ilies, M. A.; Wunder, S. L. Formation and Colloidal Stability of DMPC Supported Lipid Bilayers on SiO₂ Nanobeads. *Langmuir* **2010**, *26*, 12081–12088.
- (177) Allen, T. M. Drug Delivery Systems: Entering the Mainstream. *Science (80-.)*. **2004**, *303*, 1818–1822.
- (178) Peer, D.; Karp, J. M.; Hong, S.; Farokhzad, O. C.; Margalit, R.; Langer, R. Nanocarriers as an Emerging Platform for Cancer Therapy. *Nat. Nanotechnol.* **2007**, *2*, 751–760.
- (179) Ojea-Jiménez, I.; Comenge, J.; García-Fernández, L.; Megson, Z. A.; Casals, E.; Puentes, V. F. Engineered Inorganic Nanoparticles for Drug Delivery Applications. *Curr. Drug Metab.* **2013**, *14*, 518–530.
- (180) De Cuyper, M.; Joniau, M. Magnetoliposomes. *Eur. Biophys. J.* **1988**, *15*, 311–319.
- (181) Carmona-Ribeiro, A.; Herrington, T. M. Phospholipid Adsorption onto Polystyrene Microspheres. *J. Colloid Interface Sci.* **1993**, *156*, 19–23.

- (182) Gilbert, G. E.; Drinkwater, D.; Barter, S.; Clouse, S. B. Specificity of Phosphatidylserine-Containing Membrane Binding Sites for Factor VIII. Studies with Model Membranes Supported by Glass Microspheres (Lipospheres). *J. Biol. Chem.* **1992**, *267*, 15861–15868.
- (183) Troutier, A. L.; Ladavière, C. An Overview of Lipid Membrane Supported by Colloidal Particles. *Advances in Colloid and Interface Science*, 2007, *133*, 1–21.
- (184) Castillo, R. R.; Colilla, M.; Vallet-Regí, M. Advances in Mesoporous Silica-Based Nanocarriers for Co-Delivery and Combination Therapy against Cancer. *Expert Opin. Drug Deliv.* **2016**, *5247*, 17425247.2016.1211637.
- (185) Liu, J.; Stace-Naughton, A.; Jiang, X.; Brinker, C. J. Porous Nanoparticle Supported Lipid Bilayers (Protocells) as Delivery Vehicles. *J. Am. Chem. Soc.* **2009**, *131*, 1354–1355.
- (186) Mackowiak, S. A.; Schmidt, A.; Weiss, V.; Argyo, C.; von Schirnding, C.; Bein, T.; Bräuchle, C. Targeted Drug Delivery in Cancer Cells with Red-Light Photoactivated Mesoporous Silica Nanoparticles. *Nano Lett.* **2013**, *13*, 2576–2583.
- (187) Cole, A. J.; David, A. E.; Wang, J.; Galbán, C. J.; Hill, H. L.; Yang, V. C. Polyethylene Glycol Modified, Cross-Linked Starch-Coated Iron Oxide Nanoparticles for Enhanced Magnetic Tumor Targeting. *Biomaterials* **2011**, *32*, 2183–2193.
- (188) Bartlett, G. R. Phosphorus Assay in Column Chromatography. *J. Biol. Chem.* **1959**, *234*, 466–468.
- (189) Schneider, C. A.; Rasband, W. S.; Eliceiri, K. W. NIH Image to ImageJ: 25 Years of Image Analysis. *Nat. Methods* **2012**, *9*.
- (190) Chen, Y.; Zhang, Y. Fluorescent Quantification of Amino Groups on Silica Nanoparticle Surfaces. *Anal. Bioanal. Chem.* **2011**, *399*, 2503–2509.
- (191) Coradin, T.; Eglin, D.; Livage, J. The Silicomolybdic Acid Spectrophotometric Method and Its Application to Silicate/biopolymer Interaction Studies. *Spectroscopy* **2004**, *18*, 567–576.
- (192) Mock, J. N.; Costyn, L. J.; Wilding, S. L.; Arnoldz, R. D.; Cummings, B. S. Evidence for Distinct Mechanisms of Uptake and Antitumor Activity of Secretory Phospholipase A 2 Responsive Liposome in Prostate Cancer. *Integr. Biol. Integr. Biol* **2013**, *5*, 172–182.
- (193) Asghari Adib, A.; Nazemidashtarjandi, S.; Kelly, A.; Kruse, A.; Cimatu, K.; David, A. E.; Farnoud, A. M. Engineered Silica Nanoparticles Interact Differently with Lipid Monolayers Compared to Lipid Bilayers. *Environ. Sci. Nano* **2018**, *5*, 289–303.
- (194) Sila, M.; Au, S.; Weiner, N. Effects of Triton X-100 Concentration and Incubation Temperature on Carboxyfluorescein Release from Multilamellar Liposomes.

Biochim. Biophys. Acta **1986**, 859, 165–170.

- (195) Rahme, K.; Chen, L.; Hobbs, R. G.; Morris, M. A.; O 'driscoll, C.; Holmes, J. D.; Chen, L.; Morris, M. A.; O 'driscoll, C.; Holmes, J. D. PEGylated Gold Nanoparticles: Polymer Quantification as a Function of PEG Lengths and Nanoparticle Dimensions. *RSC Adv.* **2013**, 6085–6094.
- (196) Uz, M.; Bulmus, V.; Altinkaya, S. A.; Alsoy Altinkaya, S. Effect of PEG Grafting Density and Hydrodynamic Volume on Gold Nanoparticle–Cell Interactions: An Investigation on Cell Cycle, Apoptosis, and DNA Damage. *Langmuir* **2016**, 32, 5997–6009.
- (197) Damodaran, V. B.; Fee, C. J.; Ruckh, T.; Popat, K. C. Conformational Studies of Covalently Grafted Poly(ethylene Glycol) on Modified Solid Matrices Using X-Ray Photoelectron Spectroscopy. *Langmuir* **2010**, 26, 7299–7306.
- (198) Adumeau, L.; Genevois, C.; Roudier, L.; Schatz, C.; Couillaud, F.; Mornet, S.; Saboungi, M.-L.; Bader, S. D. Impact of Surface Grafting Density of PEG Macromolecules on Dually Fluorescent Silica Nanoparticles Used for the in Vivo Imaging of Subcutaneous Tumors. *Biochim. Biophys. Acta - Gen. Subj.* **2017**, 1861, 1587–1596.
- (199) Coates, J. Interpretation of Infrared Spectra, A Practical Approach. In *Encyclopedia of Analytical Chemistry*; 2006; pp. 10815–10837.
- (200) Xu, H.; Yan, F.; Monson, E. E.; Kopelman, R. Room-Temperature Preparation and Characterization of Poly (Ethylene Glycol)-Coated Silica Nanoparticles for Biomedical Applications. *J. Biomed. Mater. Res.* **2003**, 66A, 870–879.
- (201) Wu, F.-G.; Luo, J.-J.; Yu, Z.-W. Infrared Spectroscopy Reveals the Nonsynchronicity Phenomenon in the Glassy to Fluid Micellar Transition of DSPE-PEG2000 Aqueous Dispersions. *Langmuir* **2010**, 26, 12777–12784.
- (202) Condorelli, G. G.; Tudisco, C.; Motta, A.; Di Mauro, A.; Lupo, F.; Gulino, A.; Fragalà, I. L. Multistep Anchoring Route of Luminescent (5-Amino-1,10-phenanthroline)tris(dibenzoylmethane)europium(III) on Si(100). *Eur. J. Inorg. Chem.* **2010**, 2010, 4121–4129.
- (203) Kučerka, N.; Nieh, M. P.; Katsaras, J. Fluid Phase Lipid Areas and Bilayer Thicknesses of Commonly Used Phosphatidylcholines as a Function of Temperature. *Biochim. Biophys. Acta - Biomembr.* **2011**, 1808, 2761–2771.
- (204) Lewis, B. A.; Engelman, D. M. Lipid Bilayer Thickness Varies Linearly with Acyl Chain Length in Fluid Phosphatidylcholine Vesicles. *J. Mol. Biol.* **1983**, 166, 211–217.
- (205) Magarkar, A.; Dhawan, V.; Kallinteri, P.; Viitala, T.; Elmowafy, M.; Róg, T.; Bunker, A. Cholesterol Level Affects Surface Charge of Lipid Membranes in Saline Solution. *Sci. Rep.* **4**, 5005.

- (206) Carmona-Ribeiro, A.; Herrington, T. M. Phospholipid Adsorption onto Polystyrene Microspheres. *J. Colloid Interface Sci.* **1993**, *156*, 19–23.
- (207) Shen, W. W.; Boxer, S. G.; Knoll, W.; Frank, C. W. Polymer-Supported Lipid Bilayers on Benzophenone-Modified Substrates. *Biomacromolecules* **2001**, *2*, 70–79.
- (208) Savarala, S.; Monson, F.; Ilies, M. A.; Wunder, S. L. Supported Lipid Bilayer NanoSystems: Stabilization by Undulatory-Protrusion Forces and Destabilization by Lipid Bridging. *Langmuir* **2011**, *27*, 5850–5861.
- (209) Mornet, S.; Lambert, O.; Duguet, E.; Brisson, A. The Formation of Supported Lipid Bilayers on Silica Nanoparticles Revealed by Cryoelectron Microscopy. *Nano Lett.* **2005**, *5*, 281–285.
- (210) Jing, Y.; Trefna, H.; Persson, M.; Kasemo, B.; Svedhem, S. Formation of Supported Lipid Bilayers on Silica: Relation to Lipid Phase Transition Temperature and Liposome Size. *Soft Matter* **2014**, *10*, 187–195.
- (211) Bhattacharjee, S. DLS and Zeta Potential – What They Are and What They Are Not? *J. Control. Release* **2016**, *235*, 337–351.
- (212) Szoka, F.; Papahadjopoulos, D. Comparative Properties and Methods of Preparation of Lipid Vesicles (Liposomes). *Annu. Rev. Biophys. Bioeng.* **1980**, *9*, 467–508.
- (213) Zhu, G.; Mock, J. N.; Aljuffali, I.; Cummings, B. S.; Arnold, R. D. Secretary Phospholipase A2 Responsive Liposomes. *J. Pharm. Sci.* **2011**, *100*, 3146–3159.
- (214) Ritger, P. L.; Peppas, N. A. A Simple Equation for Description of Solute Release II. Fickian and Anomalous Release from Swellable Devices. *J. Control. Release* **1987**, *5*, 37–42.
- (215) Peppas, N. A. Higuchi Equation: Derivation, Applications, Use and Misuse. *Int. J. Pharm.* **2011**, *418*, 6–12.
- (216) Higuchi, T. Rate of Release of Medicaments from Ointment Bases Containing Drugs in Suspension. *J. Pharm. Sci.* **1961**, *50*, 874–875.
- (217) Kelly, J. M.; Gross, A. L.; Martin, D. R.; Byrne, M. E. Polyethylene Glycol-B-Poly(lactic Acid) Polymersomes as Vehicles for Enzyme Replacement Therapy. *Nanomedicine* **2017**, *12*, 2591–2606.
- (218) Siegel, R. L.; Miller, K. D.; Jemal, A. Cancer Statistics, 2018. *CA. Cancer J. Clin.* **2018**, *68*, 7–30.
- (219) Ruppender, N. S.; Morrissey, C.; Lange, P. H.; Vessella, R. L. Dormancy in Solid Tumors: Implications for Prostate Cancer. *Cancer Metastasis Rev.* **2013**, *32*, 501–509.

- (220) Nakamura, Y.; Mochida, A.; Choyke, P. L.; Kobayashi, H. Nanodrug Delivery: Is the Enhanced Permeability and Retention Effect Sufficient for Curing Cancer? *Bioconjugate Chemistry*, 2016, 27, 2225–2238.
- (221) Sfanos, K. S.; Yegnasubramanian, S.; Nelson, W. G.; De Marzo, A. M. The Inflammatory Microenvironment and Microbiome in Prostate Cancer Development. *Nat. Rev. Urol.* **2017**, 15, 11–24.
- (222) Sanna, V.; Sechi, M. Nanoparticle Therapeutics for Prostate Cancer Treatment. *Maturitas* **2012**, 73, 27–32.
- (223) Sanna, V.; Singh, C. K.; Jashari, R.; Adhami, V. M.; Chamcheu, J. C.; Rady, I.; Sechi, M.; Mukhtar, H.; Siddiqui, I. A. Targeted Nanoparticles Encapsulating (–)-Epigallocatechin-3-Gallate for Prostate Cancer Prevention and Therapy. *Sci. Rep.* **2017**, 7, 41573.
- (224) Du, G.-J.; Zhang, Z.; Wen, X.-D.; Yu, C.; Calway, T.; Yuan, C.-S.; Wang, C.-Z. Epigallocatechin Gallate (EGCG) Is the Most Effective Cancer Chemopreventive Polyphenol in Green Tea. *Nutrients* **2012**, 4, 1679–1691.
- (225) Kamps, J. A.; Morselt, H. W.; Swart, P. J.; Meijer, D. K.; Scherphof, G. L. Massive Targeting of Liposomes, Surface-Modified with Anionized Albumins, to Hepatic Endothelial Cells. *Proc. Natl. Acad. Sci. U. S. A.* **1997**, 94, 11681–11685.
- (226) Arnold, R. D. Effect of Repetitive Administration of Doxorubicin-Containing Liposomes on Plasma Pharmacokinetics and Drug Biodistribution in a Rat Brain Tumor Model. *Clin. Cancer Res.* **2005**, 11, 8856–8865.
- (227) Haran, G.; Cohen, R.; Bar, L. K.; Barenholz, Y. Transmembrane Ammonium Sulfate Gradients in Liposomes Produce Efficient and Stable Entrapment of Amphipathic Weak Bases. *BBA - Biomembr.* **1993**, 1151, 201–215.
- (228) Mock, J. N.; Costyn, L. J.; Wilding, S. L.; Arnold, R. D.; Cummings, B. S. Evidence for Distinct Mechanisms of Uptake and Antitumor Activity of Secretory Phospholipase A2 Responsive Liposome in Prostate Cancer. *Integr. Biol.* **2013**, 5, 172–182.
- (229) Twentyman, P. R.; Luscombe, M. A Study of Some Variables in a Tetrazolium Dye (MTT) Based Assay for Cell Growth and Chemosensitivity. *Br. J. Cancer* **1987**, 56, 279–285.
- (230) Monopoli, M. P.; Åberg, C.; Salvati, A.; Dawson, K. A. Biomolecular Coronas Provide the Biological Identity of Nanosized Materials. *Nat. Nanotechnol.* **2012**, 7, 779–786.
- (231) Tenzer, S.; Docter, D.; Kuharev, J.; Musyanovych, A.; Fetz, V.; Hecht, R.; Schlenk, F.; Fischer, D.; Kiouptsi, K.; Reinhardt, C.; *et al.* Rapid Formation of Plasma Protein Corona Critically Affects Nanoparticle Pathophysiology. *Nat. Nanotechnol.* **2013**, 8, 772–781.

- (232) Wang, H.; Lin, Y.; Nienhaus, K.; Nienhaus, G. U. The Protein Corona on Nanoparticles as Viewed from a Nanoparticle-Sizing Perspective. *Wiley Interdiscip. Rev. Nanomedicine Nanobiotechnology* **2017**, e1500.
- (233) Docter, D.; Westmeier, D.; Markiewicz, M.; Stolte, S.; Knauer, S. K.; Stauber, R. H. The Nanoparticle Biomolecule Corona: Lessons Learned – Challenge Accepted? *Chem. Soc. Rev. Chem. Soc. Rev* **2015**, 6094, 6094–6121.
- (234) Nguyen, V. H.; Lee, B.-J. Protein Corona: A New Approach for Nanomedicine Design. *Int. J. Nanomedicine* **2017**, 12, 3137–3151.
- (235) Saha, K.; Rahimi, M.; Yazdani, M.; Kim, S. T.; Moyano, D. F.; Hou, S.; Das, R.; Mout, R.; Rezaee, F.; Mahmoudi, M.; *et al.* Regulation of Macrophage Recognition through the Interplay of Nanoparticle Surface Functionality and Protein Corona. *ACS Nano* **2016**, 10, 4421–4430.
- (236) Stelzle, M.; Weissmueller, G.; Sackmann, E. On the Application of Supported Bilayers as Receptive Layers for Biosensors with Electrical Detection. *J. Phys. Chem.* **1993**, 97, 2974–2981.
- (237) Wittmaack, K. Novel Dose Metric for Apparent Cytotoxicity Effects Generated by in Vitro Cell Exposure to Silica Nanoparticles Introduction 1 Data Basis 2 Results and Discussion 3 Assessment of NP Delivery to Cells 3 Variability of the Cell Response Data 4 Comparison of Cytotoxicity Assays 5 Correlation between the Level of Cytotoxicity and the Areal Density of NP Mass Delivered to the Cells 6 Conclusions and Perspectives 8. *Chem. Res. Toxicol* **2011**, 24, 150–158.
- (238) Teeguarden, J. G.; Hinderliter, P. M.; Orr, G.; Thrall, B. D.; Pounds, J. G. Particokinetics In Vitro: Dosimetry Considerations for In Vitro Nanoparticle Toxicity Assessments. *Toxicol. Sci.* **2006**, 95, 300–312.
- (239) Kroon, J.; Metselaar, J. M.; Storm, G.; Van Der Pluijm, G. Liposomal Nanomedicines in the Treatment of Prostate Cancer Introduction on Prostate Cancer and Liposomal Drug Delivery. *Cancer Treat. Rev.* **2014**, 40, 578–584.
- (240) Fritze, A.; Hens, F.; Kimpfler, A.; Schubert, R.; Peschka-Süss, R. Remote Loading of Doxorubicin into Liposomes Driven by a Transmembrane Phosphate Gradient. *Biochim. Biophys. Acta* **2006**, 1758, 1633–1640.
- (241) Karatasos, K. Self-Association and Complexation of the Anti-Cancer Drug Doxorubicin with PEGylated Hyperbranched Polyesters in an Aqueous Environment. *J. Phys. Chem. B* **2013**, 117, 2564–2575.
- (242) Mock, J. N.; Costyn, L. J.; Wilding, S. L.; Arnoldz, R. D.; Cummings, B. S. Evidence for Distinct Mechanisms of Uptake and Antitumor Activity of Secretory Phospholipase A 2 Responsive Liposome in Prostate Cancer. *Integr. Biol. Integr. Biol* **2013**, 5, 172–182.
- (243) Grassian, V. H. When Size Really Matters: Size-Dependent Properties and Surface

Chemistry of Metal and Metal Oxide Nanoparticles in Gas and Liquid Phase Environments.

- (244) Buzea, C.; Pacheco, I. I.; Robbie, K. Nanomaterials and Nanoparticles: Sources and Toxicity. *Biointerphases* **2007**, *2*, MR17-R71.
- (245) Hamilton, R. F.; Thakur, S. a.; Holian, A. Silica Binding and Toxicity in Alveolar Macrophages. *Free Radic. Biol. Med.* **2008**, *44*, 1246–1258.
- (246) Rancan, F.; Gao, Q.; Graf, C.; Troppens, S.; Hadam, S.; Hackbarth, S.; Kembuan, C.; Blume-Peytavi, U.; Rü, E.; Rgen Lademann, J.; *et al.* Skin Penetration and Cellular Uptake of Amorphous Silica Nanoparticles with Variable Size, Surface Functionalization, and Colloidal Stability. *ACS Nano* **2012**, *6*, 6829–6842.
- (247) Napierska, D.; Thomassen, L. C. J.; Rabolli, V.; Lison, D.; Gonzalez, L.; Kirsch-Volders, M.; Martens, J. a; Hoet, P. H. Size-Dependent Cytotoxicity of Monodisperse Silica Nanoparticles in Human Endothelial Cells. *Small* **2009**, *5*, 846–853.
- (248) McKim, J. M. Building a Tiered Approach to in Vitro Predictive Toxicity Screening: A Focus on Assays with in Vivo Relevance. *Comb. Chem. High Throughput Screen.* **2010**, *13*, 188–206.
- (249) Hanot, C.; Choi, Y.; Anani, T.; Soundarrajan, D.; David, A. Effects of Iron-Oxide Nanoparticle Surface Chemistry on Uptake Kinetics and Cytotoxicity in CHO-K1 Cells. *Int. J. Mol. Sci.* **2015**, *17*, 54.
- (250) Awasthi, K. K.; Awasthi, A.; Kumar, N.; Roy, P.; Awasthi, K.; John, P. J. Silver Nanoparticle Induced Cytotoxicity, Oxidative Stress, and DNA Damage in CHO Cells. *J. Nanoparticle Res.* **2013**, *15*, 1898.
- (251) Wu, D.; Yotnda, P. Production and Detection of Reactive Oxygen Species (ROS) in Cancers. *J. Vis. Exp* **2011**.
- (252) Lin, I.-C.; Liang, M.; Liu, T.-Y.; Jia, Z.; Monteiro, M. J.; Toth, I. Effect of Polymer Grafting Density on Silica Nanoparticle Toxicity. *Bioorg. Med. Chem.* **2012**, *20*, 6862–6869.
- (253) Sofia, S. J.; Premnath, V.; Merrill, E. W. Poly(ethylene Oxide) Grafted to Silicon Surfaces: Grafting Density and Protein Adsorption. *Macromolecules* **1998**, *31*, 5059–5070.
- (254) Kingshott, P.; Thissen, H.; Griesser, H. J. Effects of Cloud-Point Grafting, Chain Length, and Density of PEG Layers on Competitive Adsorption of Ocular Proteins. *Biomaterials* **2002**, *23*, 2043–2056.
- (255) Pasche, S.; Voros, J.; Griesser, H. J.; Spencer, N. D.; Textor, M. Effects of Ionic Strength and Surface Charge on Protein Adsorption at PEGylated Surfaces. *J. Phys. Chem. B* **2005**, *109*, 17545–17552.

- (256) Cauda, V.; Argyo, C.; Bein, T. Impact of Different PEGylation Patterns on the Long-Term Bio-Stability of Colloidal Mesoporous Silica Nanoparticles. *J. Mater. Chem.* **2010**, *20*, 8693.
- (257) Hellack, B.; Nickel, C.; Albrecht, C.; Kuhlbusch, T. A. J.; Boland, S.; Baeza-Squiban, A.; Wohlleben, W.; Schins, R. P. F. Analytical Methods to Assess the Oxidative Potential of Nanoparticles: A Review. *Environ. Sci. Nano* **2017**, *4*, 1920–1934.
- (258) Li, N.; Sioutas, C.; Cho, A.; Schmitz, D.; Misra, C.; Sempf, J.; Wang, M.; Oberley, T.; Froines, J.; Neel, A. Ultrafine Particulate Pollutants Induce Oxidative Stress and Mitochondrial Damage. *Environ. Health Perspect.* **2003**, *111*.
- (259) Fubini, B.; Hubbard, A. Reactive Oxygen Species (ROS) and Reactive Nitrogen Species (RNS) Generation by Silica in Inflammation and Fibrosis. *Free Radic. Biol. Med.* **2003**, *34*, 1507–1516.
- (260) Yazdani, M. Concerns in the Application of Fluorescent Probes DCDHF-DA, DHR 123 and DHE to Measure Reactive Oxygen Species in Vitro. *Toxicol. Vitro.* **2015**, *30*, 1996–2000.
- (261) Alberts, B.; Bray, D.; Lewis, L.; Raff, M.; Roberts, M.; Watson, J. W. *Molecular Biology of the Cell*; Garland Science, 2002.
- (262) Liu, J.; Stace-Naughton, A.; Jiang, X.; Brinker, C. J. Porous Nanoparticle Supported Lipid Bilayers (Protocells) as Delivery Vehicles. *J. Am. Chem. Soc.* **2009**, *131*, 1354–1355.
- (263) Butler, K. S.; Durfee, P. N.; Theron, C.; Ashley, C. E.; Carnes, E. C.; Brinker, J. C. Protocells: Modular Mesoporous Silica Nanoparticle-Supported Lipid Bilayers for Drug Delivery HHS Public Access. *Small* **2016**, *12*, 2173–2185.
- (264) Cauda, V.; Mühlstein, L.; Onida, B.; Bein, T. Tuning Drug Uptake and Release Rates through Different Morphologies and Pore Diameters of Confined Mesoporous Silica. **2008**.
- (265) Davis, R. W.; Flores, A.; Barrick, T. A.; Cox, J. M.; Brozik, S. M.; Lopez, G. P.; Brozik, J. A. Nanoporous Microbead Supported Bilayers: Stability, Physical Characterization, and Incorporation of Functional Transmembrane Proteins. *Langmuir* **2007**, *23*, 3864–3872.
- (266) Cole, A. J.; David, A. E.; Wang, J.; Galbán, C. J.; Yang, V. C. Magnetic Brain Tumor Targeting and Biodistribution of Long-Circulating PEG-Modified, Cross-Linked Starch-Coated Iron Oxide Nanoparticles. *Biomaterials* **2011**, *32*, 6291–6301.
- (267) Monnier, C. A.; Burnand, D.; Rothen-Rutishauser, B.; Lattuada, M.; Petri-Fink, A. Magnetoliposomes: Opportunities and Challenges. *European Journal of Nanomedicine*, 2014, *6*, 201–215.

- (268) Jain, S.; Hirst, D. G.; O'Sullivan, J. M. Gold Nanoparticles as Novel Agents for Cancer Therapy. *Br. J. Radiol.* **2012**, *85*, 101–113.
- (269) Danhier, F.; Ansorena, E.; Silva, J. M.; Coco, R.; Le Breton, A.; Préat, V. PLGA-Based Nanoparticles: An Overview of Biomedical Applications. *Journal of Controlled Release*, 2012, *161*, 505–522.
- (270) Wang, Y.; Tu, S.; Pinchuk, A. N.; Xiong, M. P. Active Drug Encapsulation and Release Kinetics from Hydrogel-in-Liposome Nanoparticles. *J. Colloid Interface Sci.* **2013**, *406*, 247–255.
- (271) Sommerwerk, A.; Brüßler, J.; Schäfer, J.; Baginski, L.; Bandulik, M.; Bakowsky, U. Lipid Coated Chitosan Microparticles as Protein Carriers. *Phys. status solidi* **2011**, *8*, 1978–1984.
- (272) Jokerst, J. V.; Lobovkina, T.; Zare, R. N.; Gambhir, S. S. Nanoparticle PEGylation for Imaging and Therapy. *Nanomedicine* **2011**, *6*, 715–728.
- (273) Gref, R.; Minamitake, Y.; Peracchia, M.; Trubetskoy, V.; Torchilin, V.; Langer, R. Biodegradable Long-Circulating Polymeric Nanospheres. *Science (80-.)*. **1994**, *263*, 1600–1603.
- (274) Jokerst, J. V.; Lobovkina, T.; Zare, R. N.; Gambhir, S. S. Nanoparticle PEGylation for Imaging and Therapy. *Nanomedicine* **2011**, *6*, 715–728.
- (275) Gref, R.; Lü Ck, M.; Quelled, P.; Marchand, M.; Dellacherie, E.; Harnisch, S.; Blunk, T.; Mü Ller, R. H. “Stealth” Corona-Core Nanoparticles Surface Modified by Polyethylene Glycol (PEG): Influences of the Corona (PEG Chain Length and Surface Density) and of the Core Composition on Phagocytic Uptake and Plasma Protein Adsorption. *Colloids Surfaces B Biointerfaces* **2000**, *18*, 301–313.
- (276) Schöttler, Susanne Becker, Greta Winzen, Svenja Steinbach, Tobias Mohr, K.; Landfester, K.; Mailänder, V.; Wurm, F. R. Protein Adsorption Is Required for Stealth Effect of Poly(ethylene Glycol)- and Poly(phosphoester)-Coated Nanocarriers. *Nat. Nanotechnol.* **2016**, *11*, 372–377.
- (277) Rouhana, L. L.; Jaber, J. A.; Schlenoff, J. B. Aggregation-Resistant Water-Soluble Gold Nanoparticles.
- (278) Muro, E.; Pons, T.; Lequeux, N.; Fragola, A.; Sanson, N.; Lenkei, Z.; Dubertret, B. Small and Stable Sulfobetaine Zwitterionic Quantum Dots for Functional Live-Cell Imaging.
- (279) Wu, J.; Zhang, C.; Xu, S.; Pang, X.; Cai, G.; Wang, J. Preparation of Zwitterionic Polymer-Functionalized Cotton Fabrics and the Performance of Anti-Biofouling and Long-Term Biofilm Resistance. *Colloid Interface Sci. Commun.* **2018**.
- (280) Yousefi, N.; Tufenkji, N. Probing the Interaction between Nanoparticles and Lipid Membranes by Quartz Crystal Microbalance with Dissipation Monitoring. *Front. Chem.* **2016**, *4*, 46.

- (281) Sokolova, V.; Epple, M. Inorganic Nanoparticles as Carriers of Nucleic Acids into Cells. *Angew. Chemie - Int. Ed.* **2008**, *47*, 1382–1395.
- (282) Liberman, A.; Mendez, N.; Trogler, W. C.; Kummel, A. C. Synthesis and Surface Functionalization of Silica Nanoparticles for Nanomedicine. *Surf. Sci. Rep.* **2014**, *69*, 132–158.
- (283) Sang, M. C.; Lee, M.; Kim, W. S. Preparation of Large Monodispersed Spherical Silica Particles Using Seed Particle Growth. *J. Colloid Interface Sci.* **2005**, *286*, 536–542.
- (284) Yu, W. W.; Falkner, J. C.; Yavuz, C. T.; Colvin, V. L. Synthesis of Monodisperse Iron Oxide Nanocrystals by Thermal Decomposition of Iron Carboxylate Salts. *Chem. Commun. (Camb)*. **2004**, 2306–2307.
- (285) Park, J.; Lee, E.; Hwang, N.-M.; Kang, M.; Kim, S. C.; Hwang, Y.; Park, J.-G.; Noh, H.-J.; Kim, J.-Y.; Park, J.-H.; *et al.* One-Nanometer-Scale Size-Controlled Synthesis of Monodisperse Magnetic Iron Oxide Nanoparticles. *Angew. Chemie* **2005**, *44*, 2873–2877.
- (286) Cui, H.; Feng, Y.; Ren, W.; Zeng, T.; Lv, H.; Pan, Y. Strategies of Large Scale Synthesis of Monodisperse Nanoparticles. *Recent Pat. Nanotechnol.* **2009**, *3*, 32–41.

Appendix 1: Silica Particle Production

Silica nanoparticles were produced via the Stöber method.²⁴ This method was chosen over others because of the simplicity of a single pot synthesis. This made translation of results from published literature to the lab bench easier. In addition, the single pot method requires little intervention during the course of silica particle production. Following the work of Stöber, Bogush²³ attempted to develop a correlation that related reagent concentration with desired particle size. Unfortunately, this correlation is rather poor below 200 nm - the range of interest for many nanoparticle drug delivery systems.²³ Thus, we have worked to develop an understanding of particle size with regard to reagent concentration below 200 nm. **Figure 38** demonstrates the differences in turbidity obtained from different size silica particles at the same concentration from 20 to 300 nm.

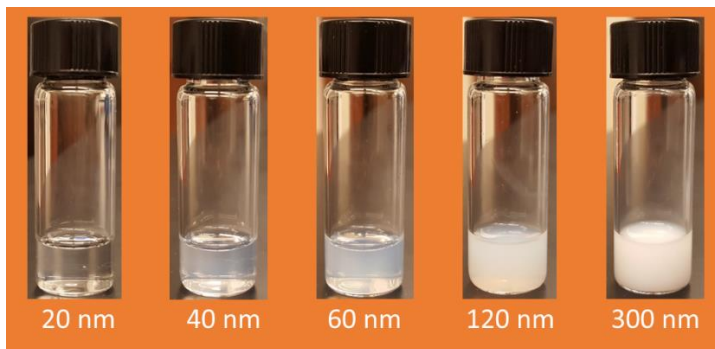


Figure 38. Turbidity effect of different silica particle sizes at identical concentrations.

A.1 Effects of Reagent Concentrations on Size

TEOS, ammonium hydroxide, ethanol and water were mixed together in a round bottom flask and stirred vigorously for 24 hours. Samples were washed with water three times via centrifugation at 14000 RPM for 10 minutes. Tip sonication was used to resuspend the particle dispersions. Reagent concentrations were varied according to trends observed in literature. The results of each reagent variation were examined for trends that showed controllable size. Ethanol was chosen as the solvent species given its low effect on size control. It is worth noting that the ratio of ethanol to TEOS has been implicated in particle size effects and the effect of TEOS concentration has been studied here.²⁸² In some figures below, connecting lines have been drawn between data points to guide the reader's eye. Each data point below represents a single run at those concentration conditions. These experiments were conducted in an exploratory manner and as such limited runs were conducted.

A.1.1 Ammonium Hydroxide Concentration

As the catalyst of the reactions, ammonium hydroxide concentration had a dramatic effect on particle size. From 0.5 to 2 M, each increase in ammonium hydroxide concentration showed nearly a 60% increase in size. However, the 0.5 M steps between each data point in **Figure 39** below are somewhat large. It is believed that at lower concentration steps more control over particle size could be gained.

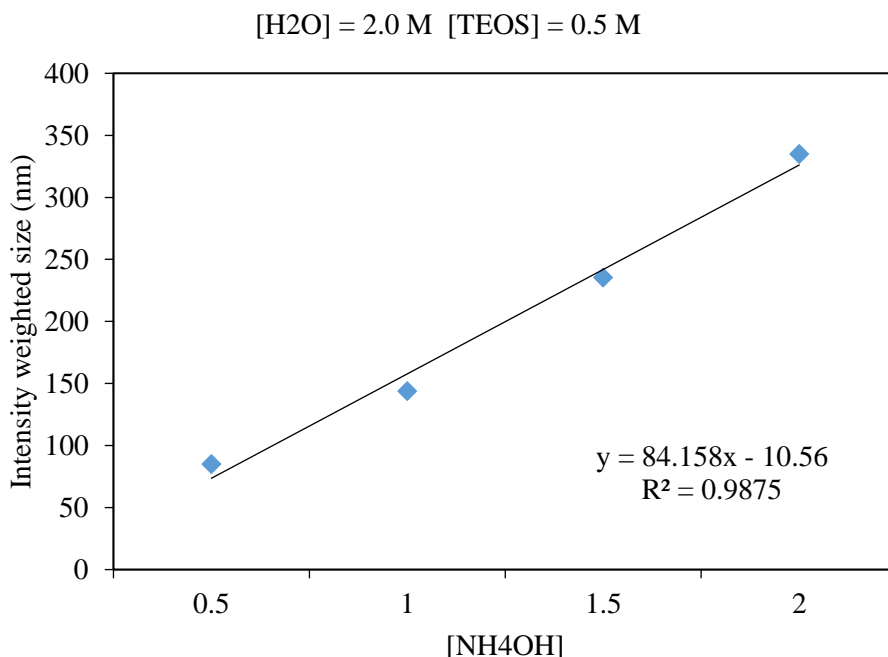


Figure 39. Effect of ammonium hydroxide concentration on particle size.

A.1.2 Water Concentration

Water concentration has shown the greatest stepwise impact on the size of particles produced. **Figure 40** shows the effect of water on particle size from a concentration of 1 to 4 M while keeping NH₄OH and TEOS concentration pinned at 0.5 M. Water concentration is directly related to the rate of hydrolysis in solution and greater water concentration should lead to decreases in diffusion limited effects.²⁵ It is believed that further size increases could be obtained by carrying out reactions at higher concentrations of water, however, other studies suggest that there may be a limit to the size of particles attainable at around 700 nm – depending on concentration of ammonium hydroxide used.²³ The size range obtained below is the size range of interest for nanoparticle work within drug delivery systems. In addition, our data matches similarly to that obtained by Bogush *et al.* What is not shown in **Figure 40** is the polydispersity of the particles obtained from these

syntheses. **Figure 41** shows the polydispersity of the sample obtained at 4 M water concentration. There is clearly at least two populations of particles in this sample and their shape is somewhat irregular rather than spherical. These results are believed to be directly related to TEOS concentration.

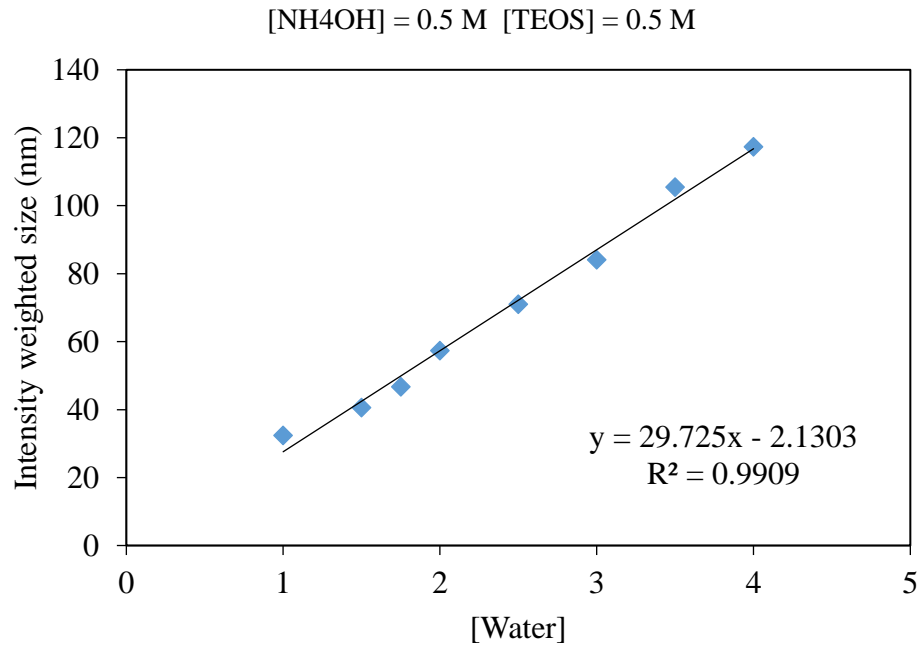


Figure 40. Effect of water concentration on particle size.

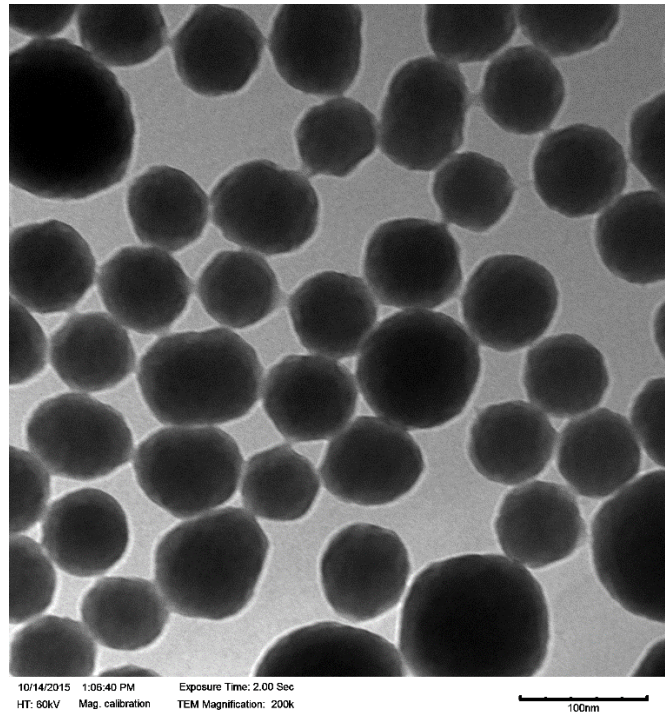


Figure 41. Example of polydispersity obtained while varying water concentration (4 M) and holding NH_4OH and TEOS concentration constant (0.5 M)

A.1.3 TEOS Concentration

The polydispersity of final particle suspensions has been linked to TEOS concentration during Stöber synthesis.²⁸³ Our results indicate a similar effect. **Table 7** below shows a comparison of average size, standard deviation and coefficient of variation (sigma) values for TEOS concentrations from 0.025 to 0.4 M in comparison to that of purchased particles from nanoComposix. The coefficient of variation C_v is calculated by dividing the standard deviation σ by the average of the distribution μ

$$C_v = \frac{\sigma}{\mu} \quad (31)$$

Narrow particle size distributions can be considered for C_v values between 5 and 10 percent and monodisperse samples are often considered below 5 percent.²⁸⁴⁻²⁸⁶ There is a clear trend of decreasing variation with increasing concentration of TEOS molarity. Comparison of the lab produced particles with those purchased from nanoComposix, it appears we are narrowing in on the commercially available size distributions. It should be noted that the differences obtained from TEM image analysis were less pronounced within the DLS measurements. In addition, TEOS concentration has an effect on the number of particles produced. Increasing the TEOS concentration as shown in **Table 7** led to a greater amount of particles produced at each increase in addition to increasing the average size. This result was expected as TEOS is the silica particle precursor. A greater sink of TEOS should correlate with a greater number concentration of particles in the final dispersion.

Table 7. Average size and statistical figures for lab made and purchased silica.

TEOS Molarity	0.025	0.05	0.1	0.2	0.25	0.3	0.35	0.4	nanoComposix
Average Size	99.2	103.9	115.9	133.8	136.0	151.1	150.6	155.8	111.5
Standard Dev	11.7	10.6	13.1	10.7	11.0	13.0	11.2	10.8	6.2
C_v	12%	10%	11%	8%	8%	9%	7%	6.95%	5.52%

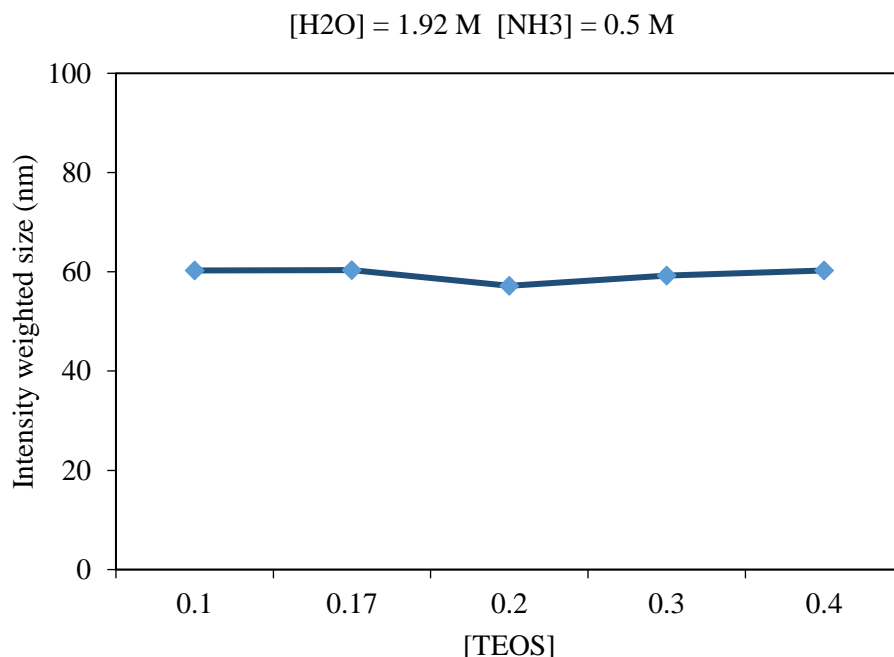


Figure 42. Effect of TEOS concentration on particle size.

A.2 Surface Modification

After production, bare silica particles contain a combination of silanol and ethoxy groups on their surface.³² Utilizing the same chemistry of silica production in which siloxane bonds form between silanol groups, amine groups can be introduced. Introduction of aminosilanes into the reaction medium after silica nanoparticle production has been shown to produce primary amine coatings.³³ (3-Aminopropyl)trimethoxy-silane (APTMS) is a commonly used aminosilane. After the initial 24 hour silica nanoparticle production step, APTMS was introduced into the nanoparticle dispersion. APTMS was allowed to react for an additional 24 hours. A graphical representation of the surface modification with TPMS and subsequent attach of PEG molecules is shown in **Figure 43**. Characterization was carried out with laser Doppler electrophoresis and an amine quantification assay (Fluorescamine).

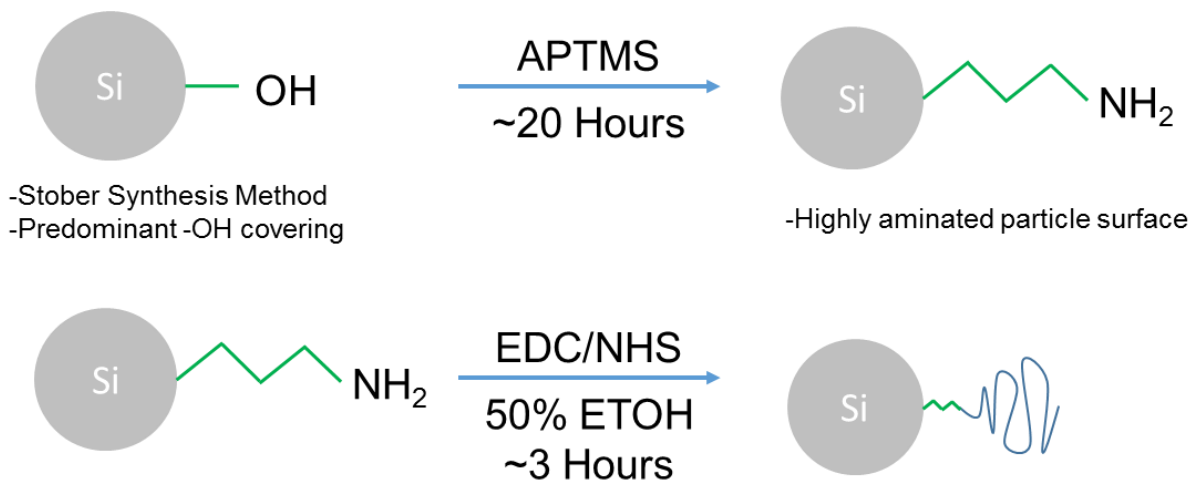


Figure 43. Schematic of reaction conditions for silica particle surface modification with APTMS and PEG.